

AD-A150 741

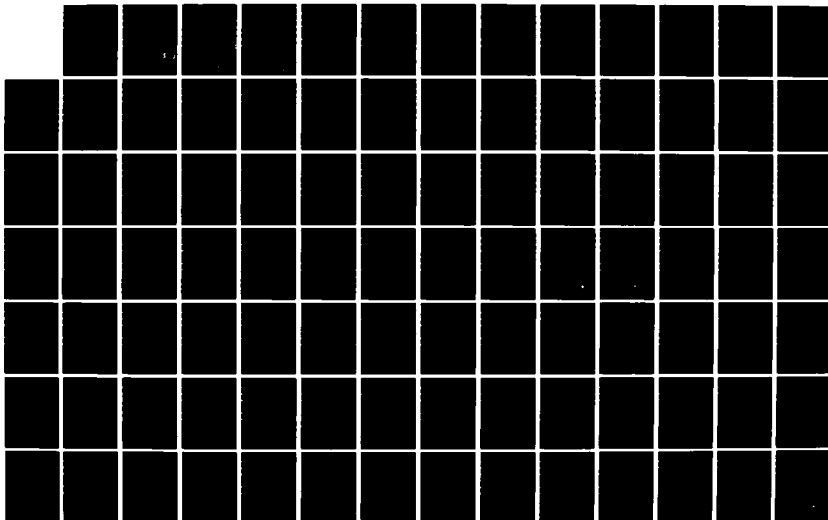
NEAR-FIELD SOURCE CHARACTERIZATIONS OF EXPLOSIONS(U)
SOUTHERN METHODIST UNIV DALLAS TX DEPT OF GEOLOGICAL
SCIENCES 8 W STUMP 20 NOV 84 SMUG-1 AFOSR-RR-84-1279
AFOSR-84-0016

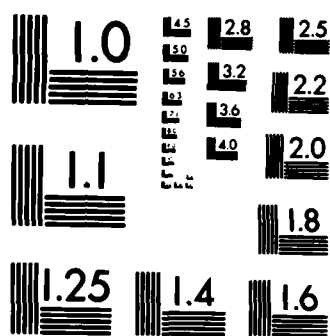
1/2

UNCLASSIFIED

F/G 8/11

NL





MICROCOPY RESOLUTION TEST CHART
NATIONAL BUREAU OF STANDARDS-1963-A

APOSR-TR. 84-1279

(4)

AD-A150 741

DTIC FILE COPY

DTIC
EL
FEB 26 1985
S
A.

Approved for public release
distribution unlimited.

UNCLASSIFIED

AD-A150741

SECURITY CLASSIFICATION OF THIS PAGE

REPORT DOCUMENTATION PAGE

1a. REPORT SECURITY CLASSIFICATION		1b. RESTRICTIVE MARKINGS	
2a. SECURITY CLASSIFICATION AUTHORITY		3. DISTRIBUTION/AVAILABILITY OF REPORT Approved for public release; distribution unlimited.	
2b. DECLASSIFICATION/DOWNGRADING SCHEDULE			
4. PERFORMING ORGANIZATION REPORT NUMBER(S) SMUG-1		5. MONITORING ORGANIZATION REPORT NUMBER(S) AFOSR-TR- 84 - 1279	
6a. NAME OF PERFORMING ORGANIZATION Southern Methodist University Department of Geological Sciences		7a. NAME OF MONITORING ORGANIZATION AFOSR/NP	
6c. ADDRESS (City, State and ZIP Code) Southern Methodist University Department of Geological Sciences Dallas, Texas 75275		7b. ADDRESS (City, State and ZIP Code) AFOSR/NP Building 410 Bolling AFB, DC 20332	
8a. NAME OF FUNDING/SPONSORING ORGANIZATION AFOSR/NP	8b. OFFICE SYMBOL (If applicable)	9. PROCUREMENT INSTRUMENT IDENTIFICATION NUMBER AFOSR-84-6016	
8c. ADDRESS (City, State and ZIP Code) AFOSR/NP Building 410 Bolling AFB, DC 20332		10. SOURCE OF FUNDING NOS.	
11. TITLE (Include Security Classification) Near-field Source Characterizations of Explosions		PROGRAM ELEMENT NO. 61102F	PROJECT NO. 2309
12. PERSONAL AUTHOR(S) Brian W. Stump		TASK NO. A1	WORK UNIT NO.
13a. TYPE OF REPORT Annual	13b. TIME COVERED FROM 15Oct83 to 4Oct84	14. DATE OF REPORT (Yr., Mo., Day) 84 11 20	15. PAGE COUNT
SUPPLEMENTARY NOTATION Seismology, explosion sources, equivalent elastic sources, depth of burial, spall, elastic wave propagation.			
17. COSATI CODES		18. SUBJECT TERMS (Continue on reverse if necessary and identify by block number)	
FIELD	GROUP	SUB. GR.	
19. ABSTRACT (Continue on reverse if necessary and identify by block number) Work in three areas is summarized in this report. The first deals with the quantification of source burial depth effects as observed in the near-field. The interplay of source burial depth effects with other physical processes is discussed. Preliminary data analysis and synthetics are presented. The increase in P wave amplitude and decrease in Rayleigh wave amplitude with increasing source depth is completely modeled with linear models. The second area of work summarizes a set of forward calculational models attempting to include spall in equivalent elastic source models. The study concludes that energy involved in cylindrically symmetric spall can account for 50% of near source waveforms. Finally the subject of inverse studies of small scaled chemical explosions is presented. The utility of small scaled explosion experiments in determining equivalent elastic sources is shown. The resulting source from a (continued)			
20. DISTRIBUTION/AVAILABILITY OF ABSTRACT CLASSIFIED/UNLIMITED <input checked="" type="checkbox"/> SAME AS RPT <input checked="" type="checkbox"/> DTIC USERS <input type="checkbox"/>		21. ABSTRACT SECURITY CLASSIFICATION UNCLASSIFIED	
22a. NAME OF RESPONSIBLE INDIVIDUAL		22b. TELEPHONE NUMBER (Include Area Code)	22c. OFFICE SYMBOL

SECURITY CLASSIFICATION OF THIS PAGE

(c) 253 pound chemical explosion in alluvium illustrates the partition of the explosive energy into spherical and cylindrical components. → cont. page 104

1473

**DVIC
COPY
INSPECTED**

SECURITY CLASSIFICATION OF THIS PAGE

Table of Contents

1. The Effect of Source Burial Depth and Free
Surface Interaction in the Near-Field.
pgs I:1 - 17
2. Constraints on Explosive Sources with Spall
from Near Source Waveforms.
pgs II:1 - 38
3. The Experimental Characterization of
Contained Chemical Explosions
pgs III:1 - 62

AIR FORCE OFFICE OF SCIENTIFIC RESEARCH (AFSC)
NOTICE OF TRANSMITTAL TO DTIC
This technical report has been reviewed and is
approved for distribution under AFM 190-12.
Distribution is unlimited.
MATTHEW J. KERPER
Chief, Technical Information Division

THE EFFECTS OF SOURCE BURIAL DEPTH
AND FREE SURFACE INTERACTION IN THE NEAR-FIELD

Masters Thesis Proposal
submitted by

Beth Flynn
Department of Geological Sciences
Southern Methodist University
October 1984

PROBLEM STATEMENT

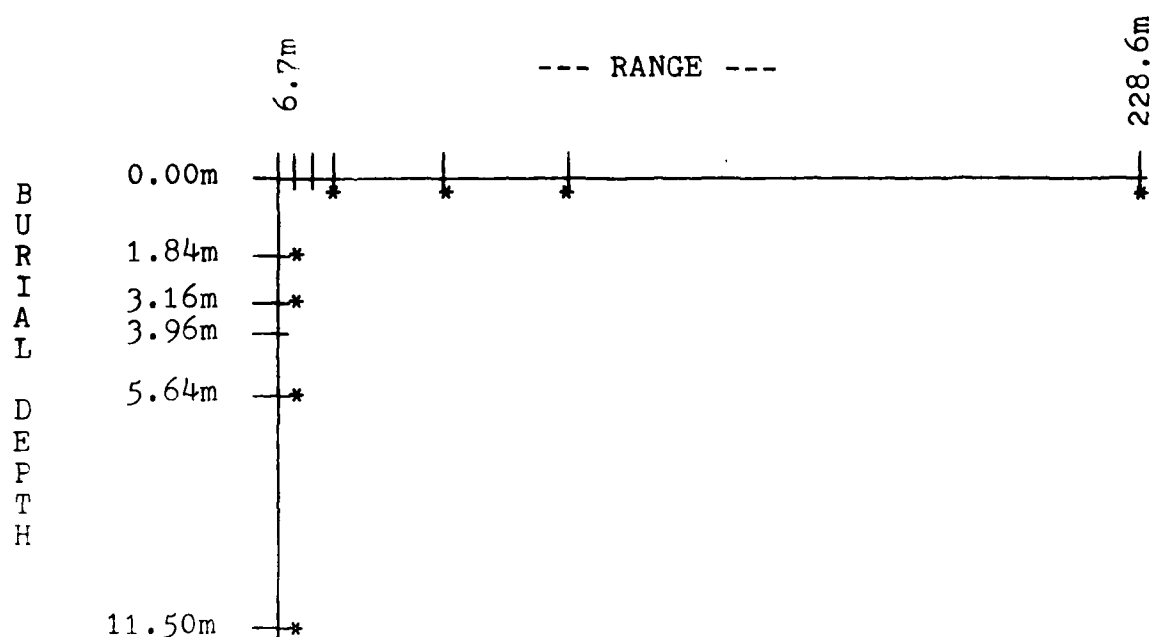
Source depth is one aspect of the more general problem of characterizing a seismic source. The ability to determine the depth of a seismic event is of particular concern to the task of distinguishing explosions from earthquakes, and to the task of more strictly characterizing a seismic event.

An attempt to determine source depth must necessarily deal with the complications that arise with the existence of a free surface. Errors in estimation of such source parameters as depth stem from an incomplete understanding of the various complications the free surface imparts to the seismic source. The free surface is also responsible for a variety of effects on wave propagation, the object of recognizing and defining these effects being their distinction from source effects and, consequently, a more precise definition of the source itself.

The object of this project is a quantitative and theoretical investigation of the physical processes which act as a function of depth in producing nearfield waveforms. Data available for this work consists of paper and digital accelerometer records from 115 kg explosions ranging in burial depth from 0 to 11.5 meters. For each event data was recovered in the range of 6.7 to 228.6 meters (Figure 1). Preliminary analysis of the observational data gave an indication that the dominant features of the waveforms, the P and Rayleigh arrivals, varied as a function of source depth. From this indication it is expected that a study of the relative

P and Rayleigh wave amplitudes in a forward modelling procedure will yield a quantitative relationship between amplitudes and source burial depth.

By extending the results of such a study to greater depths, magnitudes, and ranges they may have implications for studies involving large explosions or earthquakes, and teleseismic recordings. The results of this study may also provide the ground work and constraints to support an inversion of the nearfield data for a characterization of the source, specifically its depth.



* Depths and ranges for which synthetics were calculated

P Velocity	0.920 km/sec
S Velocity	0.350 km/sec
Density	1.900 gm/cc
Poisson's ratio	0.415

FIGURE 1 Burial depths of six explosions (115 kg), and ranges at which data was recovered (6.7, 11.6, 17.4, 37.5, 73.2, 228.6 meters)

PREVIOUS WORK

Free Surface Effects and Source Characterization

Contributions of the free surface to problems in source characterization are recognized in a variety of forms. Scattering mechanisms, interference phenomena, and source depth effects are detectable in both body and surface waves. Though such free surface effects are known to occur and may often be recognized, for the most part they have yet to be quantified, and so can not be precisely accounted for in the estimation of various source parameters.

The presence of a free surface significantly alters the symmetry of the whole space wave propagation problem. As the cylindrical problem for a source at the free surface gives way to the spherical problem for a source at depth, a change in the relative coupling of P and Rayleigh waves is effected. The cylindrical source produces a nearfield waveform rich in SV and Rayleigh energy. A direct product of the free surface, the Rayleigh wave decays, as expected, with source depth. On the other hand, the P wave gains significance with the increased effectiveness of vertical coupling afforded by a larger overburden. At a sufficient depth the source is fully contained and the problem is essentially a spherical one.

In spectral analysis the problem of source characterization is greatly complicated by the interference of direct and reflected arrivals which creates maxima and minima in the

amplitude spectra. Similarly, multiple sources can yield peaked amplitude spectra (Pilant and Knopoff, 1964) so for the purpose of separating the effects of source and propagation path, free surface reflections must be taken into account. Langston (1978) pointed out that a failure to account for the free surface leads to errors in the estimation of moment and corner frequency.

Aside from the commonly recognized pP and sP reflections, the free surface is responsible for a multitude of large amplitude arrivals which, combined with other multipathed arrivals, comprise the P coda and contribute to signal complexity (Douglas, Marshall, Gibbs, Young, and Blamey, 1973). Signal generated noise, the result of direct P waves scattering on free surface or crustal irregularities near the receiver, was detected by Mack (1969). Greenfield (1971) observed high-level codas with characteristics suggestive of the near-source scattering of source-generated Rayleigh waves. From Greenfield's half space scattering model the coda is seen to carry information about the near-source propagation path.

Source characteristics such as rise time, source dimension, and displacement function have manifestations in the amplitude spectra where they may be masked by free surface effects such as P-pP interference phenomena (Douglas, 1981). One such source effect can be attributed to the slapdown following spallation of the ground above an explosive event. With data that had sampled the nonlinear regime of an explosion, Stump (1984) found that, aside from those features already mentioned, the spall time function is an important

factor in the construction of an appropriate source representation. Bakun and Johnson (1973) found that the pF and slap-down arrivals were the only significant contributions to the first part of the P coda at teleseismic distances. Burdick and Helmberger (1979) attributed the amplitude and phase of an observed secondary arrival to the coincidence in time of the pF reflection and the overshoot of direct P, but Douglas and Hudson (1983) demonstrate that, depending on what type of source function is chosen, the secondary arrival may be fully accounted for solely by the surface reflection with no overshoot in the source function. Thus there is a significant degree of uncertainty introduced by the trade-off between source effects and structure effects.

PRELIMINARY RESULTS

To understand what physical processes may influence the relative coupling of P and Rayleigh waves, synthetic waveforms were computed for selected depths, ranges, and material properties of the various observational events. The theoretical problem was simplified to that of a half space model where the interaction of propagating waves with the free surface becomes of primary importance.

Half space Green's functions were calculated and synthetic data compiled for a vertical point force and fully contained double couple source models, using an appropriate instrument response. In the time domain maximum P and Rayleigh wave amplitudes were determined from both the observational (Figure 2) and the theoretical data (Figures 3 and 4), the object being to determine how closely the theoretical models can replicate observed amplitude trends, and to what extent the free surface contributes to those trends.

For the observational data P amplitudes increase with source depth while Rayleigh waves decay, causing the ratios of P to Rayleigh amplitude to increase with depth. Figures 3 and 4 display similar trends for the theoretical data. P and S wave velocities used in the synthetics were appropriate for the material in which the shots were fired and for which Poisson's ratio was found to be 0.418. By also taking Poisson's ratio to be 0.25 the synthetic data were extended to cover other material properties. Overall the amplitude trends remained consistent with those of a material for which Poisson's

ratio is 0.415. The effect of the instrument response is to smooth the waveforms considerably and to de-emphasize the increase with depth of the P amplitude and the decay with depth of the Rayleigh amplitude.

While Figures 2, 3, and 4 display the similarities between the observational and theoretical data sets, there is also a comparison between the two synthetic data sets to be made. While the amplitude decay with range is universal, the P amplitudes display the faster decay rate of a spherical rather than cylindrical wavefront. For the vertical point force source model, the addition of an instrument response caused the P increase with depth to be tentative rather than definite as for the double couple source model. The point force model is a weak generator of P energy at the ranges considered.

There are some physical processes which influence the above observations and are responsible, to varying degrees, for the differences in the trends of the vertical point force and the double couple data sets. An extra spatial differentiation in the calculation of waveforms resulting from the double couple source model gives these waveforms some higher frequency content, and thus contributes more of an increase with depth to the short period P wave. In the vertical point force waveforms the effect of a radiation pattern influences the P wave amplitudes and detracts from the steady trend of increase with depth.

The degree to which the destructive interference of a refracted SP arrival affects direct P amplitudes is also un-

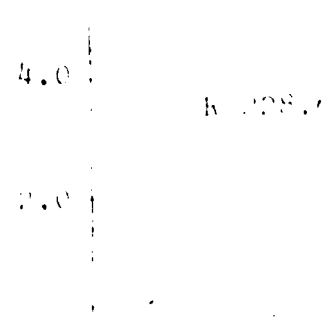
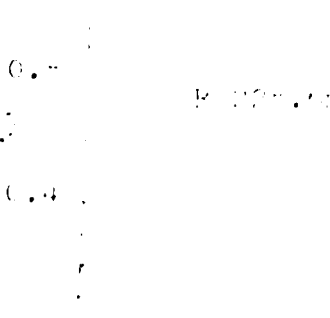
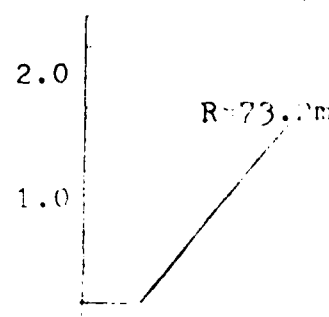
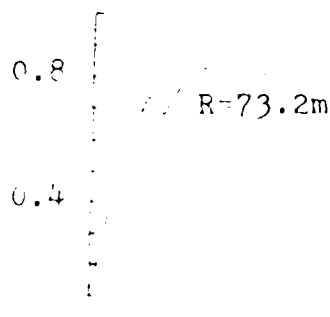
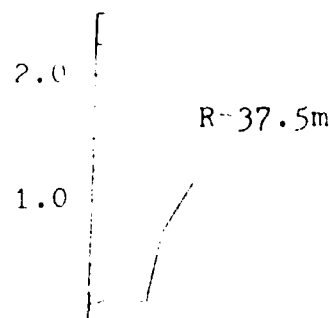
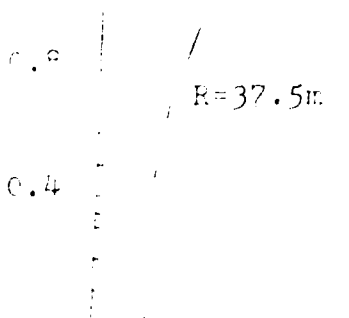
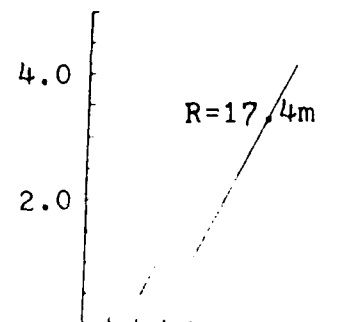
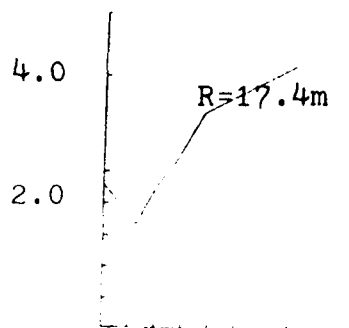
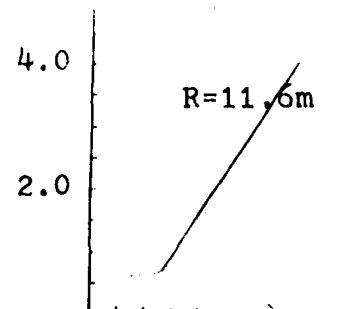
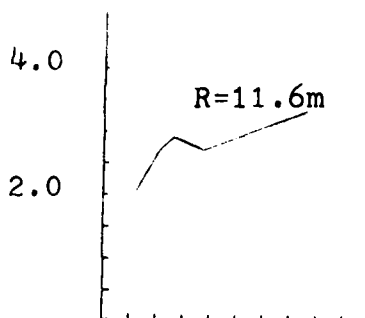
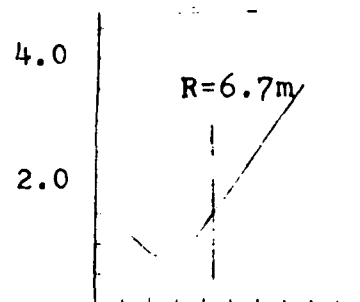
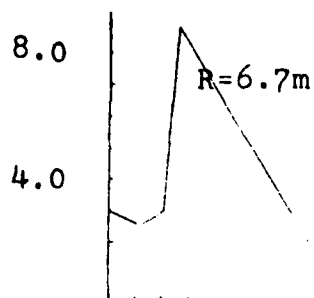
certain. Maximum P wave amplitudes were difficult to determine when the direct and refracted arrivals closely coincided in time. At the shorter ranges, particularly with the smoothing effect of the instrument response, there is apt to be a small amount of error in the values taken to be maximum P amplitudes.

Some preliminary conclusions can be drawn from the results of the time domain studies. The success with which the theoretical models replicated the trends of the observed data suggests that elastic free surface interaction is sufficient to explain the relative P and Rayleigh coupling as a function of source depth.

As an extension of the time domain results, analysis of the digital data in the frequency domain will further define and quantify contributions of the various physical processes discussed above. Full waveform amplitude spectra and windowed P and Rayleigh wave amplitude spectra are to be computed for comparison with spectra of the two half space models.

OBSERVATIONAL DATA Amplitude vs. Depth

Ratio of P to Rayleigh wave amplitude plotted as a function of depth at each of the six recording ranges. Amplitudes were measured from paper records. (velocity amplitudes)



VERTICAL POINT FORCE SYNTHETICS

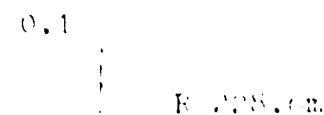
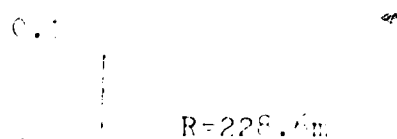
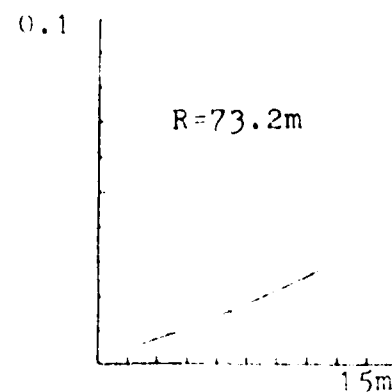
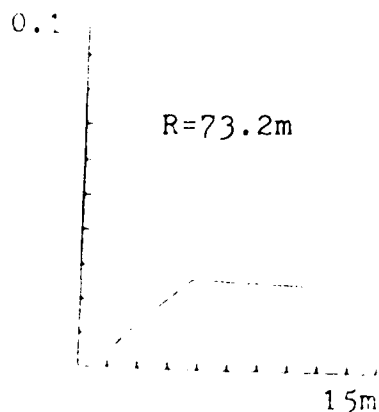
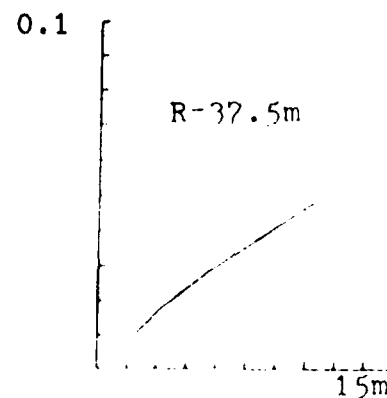
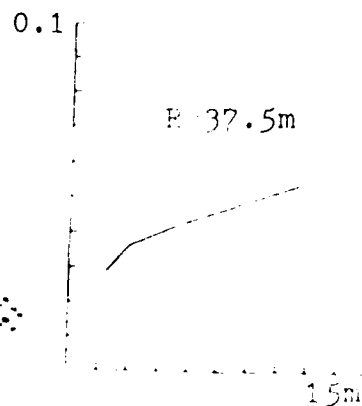
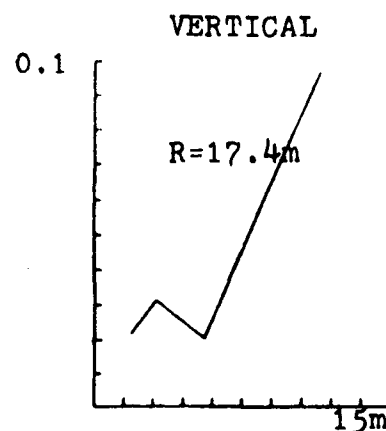
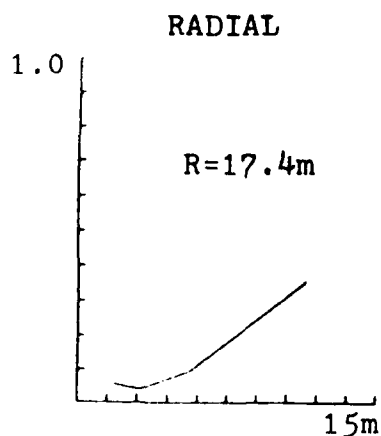
Amplitude vs. Depth

$$V_p = 0.920$$

$$V_s = 0.350$$

$$v = 0.415$$

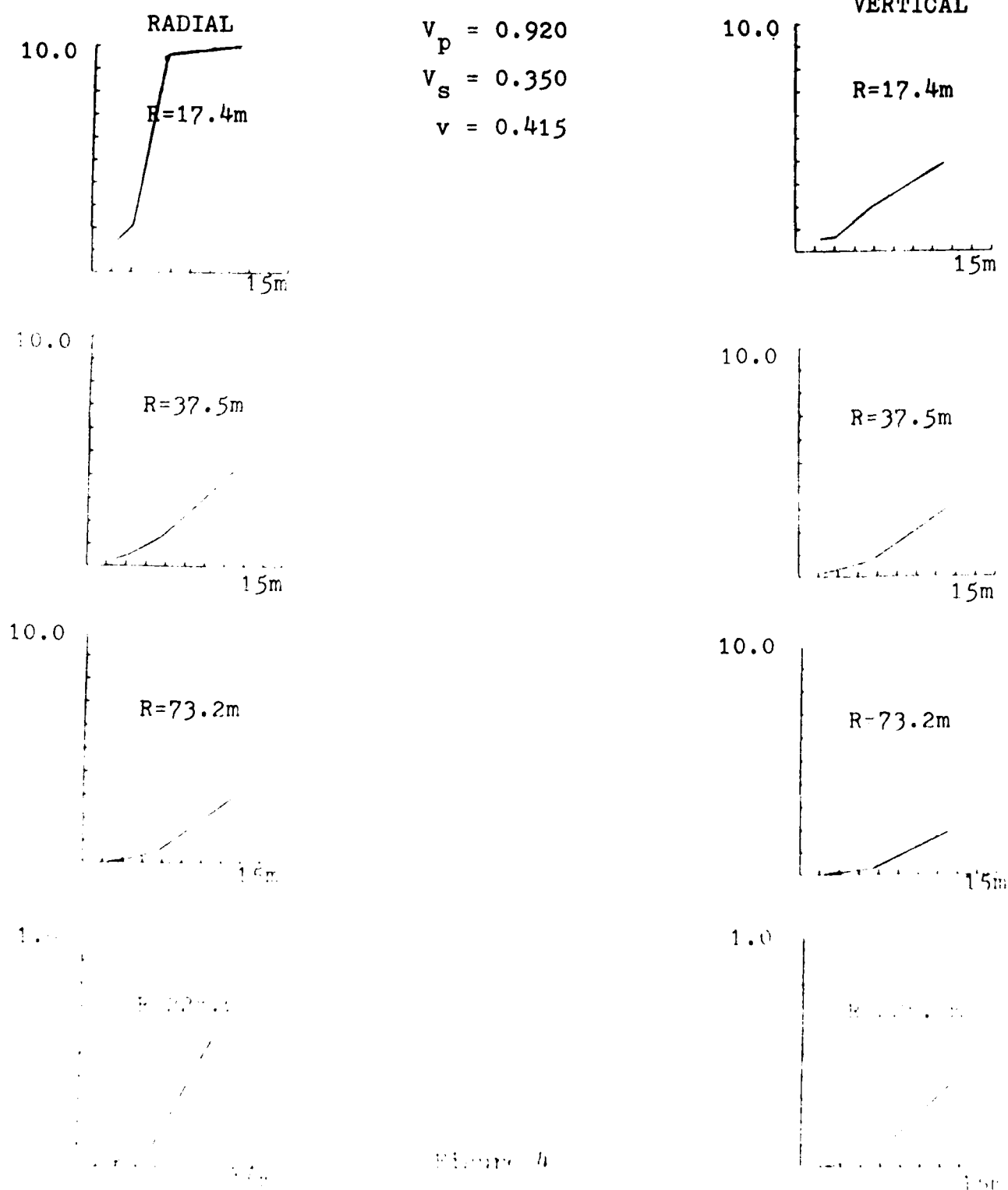
Ratio of P to Rayleigh wave amplitude plotted as a function of depth at four different ranges. Amplitudes were measured from synthetic waveforms calculated for a vertical point force source, with no instrument response included.



DOUBLE COUPLE SYNTHETICS

Amplitude vs. Depth

Ratio of P to Rayleigh wave amplitude plotted as a function of depth at four different ranges. Amplitudes were measured from synthetic waveforms calculated for a double couple source, with an appropriate instrument response.



PROCEDURE

For the modelling involved in this project, programs are available to calculate half-space Green's functions, synthetic waveforms, amplitude spectra, and synthetics for a layered model. In addition some programming tasks such as plotting routines and revisions to existing programs are anticipated. This research is supported under a grant donated to Brian Stump.

The study is approached as a forward modelling problem in the characterization of source depth. Through the work that has already been completed, combined with additional data analysis and synthetic calculations, the following physical processes are to be investigated for their effects on nearfield waveforms:

- 1) P and Rayleigh Coupling
- 2) Multipathing and Scattering
- 3) Surface Reflections
- 4) Explosion Time Functions
- 5) Spall

The theoretical half-space investigation of P and Rayleigh wave amplitudes that was described above contributes quantitative results on the effects of the relative coupling of P and Rayleigh energy. A study of particle motions will yield information that is sensitive to source depth (as well as to the layered velocity structure through which observed

waveforms travelled) and will aid in separation of body and surface waves (Dobrin, Simon, and Lawrence, 1951).

The free surface effects of multipathing and scattering are to be assessed qualitatively from studies published previously in the literature, and quantitatively from the geologic characteristics of the test site as determined from some test site data. These effects will be taken into account in the comparison of observed data with data generated by simplified theoretical models.

The combined time and frequency domain results from the half-space investigation will provide physical constraints to be applied to the development of a layered model. Theoretical wave propagation through a layered velocity structure will give rise to turning rays not accounted for in the half-space models. Therefore, it is expected that the layered model will approximate the structure and processes involved in this particular problem more closely than did the half-space models. The layered model will produce synthetic waveforms and spectra which, in comparison with observed waveforms and spectra, will allow some conclusions to be made about the effects of free surface reflections and source depth.

In addition to the above mentioned propagation path effects, the source time function must be considered when attempting to fit observed and theoretical waveforms. The adequacy of the various theoretical source models used, the differences between them, and the changes in source characteristics from surface to fully contained events must be recognized in doing the forward modelling problem. An evaluation

of the effects of the source function on the resulting waveform not only helps to separate source and propagation path effects, but also lays some foundations for an inverse study (Stump, 1983) which would rely on the results of this project.

The nearfield effects of spall will be considered in the modelling procedure. It must be discerned whether or not the spall contribution is a significant one to this problem. The presence or absence of significant spall effects will have an influence on the type of source representation that is used in the models.

Finally, from the collective results of the above investigations, it is intended that some conclusions will be made on the feasibility of determining source burial depth by inspection of nearfield body and surface waves.

REFERENCES

- Bakun, W.H. and Johnson, L.R. (1973). The Deconvolution of Teleseismic P Waves from Explosions MILROW and CANNIKIN, Geophys. J. R. Astr. Soc., 34, 321-342.
- Baumgardt, D. (1983). Teleseismic P-Coda Stability and Coda Magnitude Yield Estimation, ENSCO, Signal Analysis Systems Division, Springfield, Va.
- Burdick, L.J. and Helmberger, D.V. (1979). Time Functions Appropriate for Nuclear Explosions, Bull. Seism. Soc. Am., 69, 957-973.
- Dobrin, M.B., Simon, R.F. and Lawrence, P.L. (1951). Rayleigh Waves from Small Explosions, Transactions, American Geophysical Union, 32, 6, 822-832.
- Douglas, A. (1981). Seismic Source Identification: A Review of Past and Present Research Efforts, in Identification of Seismic Sources - Earthquake or Underground Explosion, D. Reidel Publishing Co., Boston.
- Douglas, A. and Hudson, J.R. (1983). Letter to the Editor, Bull. Seism. Soc. Am., 73, 4, 1255-1264.
- Douglas, A., Marshall, P.D., and Corbishley, D.J. (1971). Absorption and the Complexity of P Signals, Nature Physical Science, 233, 50-51.
- Douglas, A., Marshall, P.D., Gibbs, P.G., Young, J.B. and Blamey, C. (1973). P Signal Complexity Re-examined, Geophys. J. R. Astr. Soc., 33, 195-221.
- Greenfield, R.J. (1971). Short Period P-Wave Generation by Rayleigh-Wave Scattering at Novaya Zemlya, Journal of Geophysical Research, 76, 7988-8002.
- Langston, C.A. (1978). Moments, Corner Frequencies, and the Free Surface, Journal of Geophysical Research, 83, 3422-3426.
- Mack, H. (1969). Nature of Short Period P-Wave Signal Variations at LASA, Journal of Geophysical Research, 74, 3161-3170.

Pilant, W.L. and Knopoff, L. (1964). Observations of Multiple Seismic Events, Bull. Seism. Soc. Am., 54, 19-39.

Stump, B.W. (1983). Source Characterization of Bermed Surface Bursts, Bull. Seism. Soc. Am., 73, 4, 979-1003.

Stump, B.W. (1984). Constraints on Explosive Sources with Spall from Near Source Waveforms, accepted for publication, Bull. Seism. Soc. Am.

CONSTRAINTS ON EXPLOSIVE SOURCES WITH SPALL FROM NEAR SOURCE WAVEFORMS

**Brian W. Stump
Southern Methodist University
Department of Geological Sciences
Dallas, Texas 75275**

ABSTRACT

Spall, the tensile failure of a material due to high stress loading has been observed in a number of contained and surface explosions. The phenomenon results in a repartition of the initial spherical explosion energy source, yielding a second energy source which is cylindrical and delayed in time. Recent spall models by Day et al (1983) demanding conservation of momentum have shown the phenomenon to have little contribution to twenty second surface waves. These models are extended to include the effect of the process on near source seismograms. The spall model is constrained by observations within the nonlinear regime of the source which bound the mass, momentum, and timing of the process. Comparison of these forward models with the inverse vertical point force source inferred from seismic recordings of a bermed surface explosion yields excellent agreement. The spall model developed from the contained explosion, Cheat, is used to create synthetic seismograms. Comparisons of these waveforms with those from a Mueller-Murphy contained explosion indicate that the waveform contribution from spall is similar in size to the spherical explosion waveform. The complete synthetic composed of the spall and explosion contribution compares favorably with observational data from the Cheat experiment in both amplitude and energy distribution.

INTRODUCTION

Spall, which is defined as the tensile failure of near surface layers, has often been observed in soil and rock excited by explosive sources. In the case of contained explosions the initial compressive wave leaves the source, reflects as a tensile wave at the free surface, and then travels back into the material. At some depth below the free surface the strength of this stress wave overcomes the tensile strength of the material, the overburden stress, and the tail of the remaining upgoing compressive wave. The material fails in tension imparting momentum to the surficial layers. These layers are sent into ballistic free fall, are acted on with the force of gravity, and eventually reimpact upon the surrounding soil. Spall caused by this mechanism has been studied by a number of individuals (Rinehart, 1959; Chilton et al., 1966; Eisler et al., 1966)

In the case of surface bursts with observed spall the simple free surface tensile reflection cannot be called upon as a mechanism leading to tensile failure (Melzer, 1981; Stump and Reinke, 1982). One possible explanation for spall from such sources is that the shear and Rayleigh energy generated from surface explosions may be strong enough to fail the material (Stump, 1983).

Whatever the mechanisms leading to spall, it is observed from explosions in a variety of geometries. When characterizing the explosion source from observed seismic radiation, it may become necessary to include the effects of spall in addition to that of the initial explosion. The symmetry of the explosion source will not be retained when spall is introduced and the phase of the resulting source function will also be shifted.

The purpose of this study is the quantification of the effects of the spall model on near source observations of explosions. This study is motivated by the existence of a high quality, densely sampled data set from a collection of

contained, partially buried, and surface explosions (Babcock,1980 ; Stump and Reinke,1982). These data sampled both the nonlinear and linear regime surrounding the source. The data from within the nonlinear regime will be used to build the equivalent elastic representation of the source. This model will then be utilized in the calculation of near source seismograms which can be compared for validation against seismic observations in the linear regime.

PREVIOUS WORK

Spall from contained explosions was first documented by Rinehart, 1959. Extensive studies were completed from contained nuclear explosions at the Nevada Test Site (Eisler and Chilton, 1964; Chilton et al., 1966; Eisler et al., 1966). These studies attempted to quantify the spatial extent of spall, its timing, and its strength with limited data. The conclusion of these primarily observational investigations was that spall in competent material from contained explosions was a result of the tensile reflection at the free surface of the outgoing explosive compressive wave. Since these early works were completed, additional observational data have been obtained and analyses of spall waveforms completed by Perret (1976,1978). These more extensive data support many of the early conclusions about the process.

With the acquisition of many observations of the spall phenomenon in the nonlinear regime it was natural to investigate spall effects on the linear elastic motions observed in the near source, regional, and teleseismic distance ranges. ViCELLI (1973) estimated the spall mass from contained explosions and then along with the velocity of the spalled material calculated the total momentum. This momentum was then introduced as a single vertical point force source at the free surface of an elastic half-space in order to generate synthetic seismograms. These calculations indicated that in the distance range of 10-1000km, the calculated amplitudes were large enough to explain the observational data base. As a further check of the significance of spall, ViCELLI ran two nonlinear numerical calculations of the explosion. The first calculation included no tensile strength so spallation was allowed. The second calculation introduced material tensile strength sufficient to stop spallation. The model with spall contained Rayleigh wave amplitudes 2.7 times larger than the model with no spall in the 10-20km range. The author went on to extrapolate that spall may have significant effects on

teleseismic surface waves.

Springer (1974) investigated the nonlinear data from nuclear explosions and tabulated the expected delay times between the compressive wave from the explosion and that resulting from spall closure or slapdown. It was his suggestion that these time delays would allow spall to appear as a secondary source in the explosion. Other workers have also suggested spall slapdown as a source of teleseismic P waves (Frasier, 1972 and Bakun and Johnson, 1973).

Sobel (1978) examined a much larger observational data base involving nonlinear spall observations. Scaling relations were developed and the effect of the phenomenon on teleseismic m/M estimates studied. The author concludes that spall would yield little or no effect on these measurements.

Most recently, Day et al (1983) have taken a closer look at both the numerical and analytical models of spall as they apply to teleseismic surface wave observations. The authors point out that previous spall models have not required momentum to be conserved. They develop a model which conserves momentum and then calculate teleseismic surface waves using the equivalent body force representation. It is their conclusion that when momentum is conserved spall has little contribution to 20 sec surface wave energy.

A number of investigators have begun to use near source waveforms from nuclear explosions to develop seismic source functions for explosions. These waveforms have been chosen since it is generally believed that they are least contaminated by propagation path effects including attenuation. These source functions are then used to make teleseismic synthetics for analysis purposes or are used to define the source and act as measurements of relative or absolute source strength. Studies to date have taken two approaches: (1) that of assuming a spherical explosion or reduced displacement potential (Mueller and Murphy, 1971; von Seggern and Blandford, 1972; Hadley and Helmburger, 1981; Burdick, 1983); or (2) utilizing the second order moment tensor which includes the effects of tectonic stress release and the spherical

explosion (Toksoz and Kehrner, 1972; Stump and Johnson, 1983). These studies have not explicitly considered the effect of spall on the source characterization.

The purpose of this work is to numerically and observationally explore the effects of spall on near source waveforms from explosions. In light of Viacelli's near source calculations at 15km and the analytic and numerical models of Day et al (1983) spall may be a significant source of short period Rayleigh wave energy.

SPALL MODEL

The early equivalent body force representations of near surface spallation have followed the work of Viacelli (1973) and modeled the source as a vertical point force at the earth's free surface. There are several problems with this representation. First, momentum is not conserved by this source model and as Day et al., (1983) have pointed out, this may lead to serious problems in long period ground motion estimation. Second, the spalled material may be near the free surface but it does extend to depth (Perret, 1978). The model must take this depth effect into account. Third, spall is not a point phenomena but is distributed in both range and depth (Eisler, 1964). The range of spallation typically reaches twice the depth of source burial. Fourth, the phenomena is not always cylindrically symmetric. Video recordings of ground motion surrounding ground zero of contained nuclear tests at the Nevada Test Site indicate that spall closure patterns are complex, possibly related to subsurface geology (Walker, 1982). Finally, spallation does not occur simultaneously everywhere. Spall initiation from contained explosions occurs when the propagating stress wave from the explosion overcomes the material tensile strength and the overburden stress. Since this condition occurs at different times in the material, the initiation of spall has an apparent velocity. Observational studies indicate that spall initiation for contained explosion occurs first near the free surface at ground zero and propagates outward and downward from this point. The termination of spall occurs first at depth and range and propagates back to near the ground zero initiation point.

In the development of a spall model for near source modeling the work of Day et al., (1983) has been followed. This model which conserves momentum consists of three contributions: (1) that loading related to the momentum imparted to the material when spall occurs; (2) that loading related to the unloading of the unspalled material when the spalled material is in free fall; and (3) that loading which occurs when the spalled material rejoins with the rest of the earth.

Assuming the spalled material has mass, m_s , and spalls simultaneously everywhere with constant upward escape velocity V_0 , then one can make a point force representation of the spall initiation:

$$f_1 = m_s V_0 \delta(t - t_{si}) \quad (1)$$

where t_{si} is the spall initiation time. This approximation will be adequate for this study where the wave lengths of interest are long compared to the source dimensions.

The relaxation due to the unloading of the spalled body is:

$$f_2 = -m_s g [H(t - t_{si}) - H(t - t_{si} - T_s)] \quad (2)$$

T_s is the spall dwell time which is equal to $2V_0/g$ where g is the acceleration due to gravity.

Finally there is the force which occurs when the spalled material rejoins:

$$f_3 = m_s V_0 \delta(t - t_{si} - T_s) \quad (3)$$

This last term, f_3 , is the only one present in Viicelli's early model. We assume that the observations are such that the wave lengths are long compared to the source dimension. To extend this study would require the inclusion of all finite source effects. This subject is intended for future study.

In reality the spall initiation and rejoin have rise times associated with them. The time of spall initiation, t_{si} , is not the same for all points and thus $m_s(t)$ is not the true step function that led to the delta function f_1 and f_3 . For the long period teleseismic surface waves the difference between the idealized model and a more physically realistic one may be small. In the near source regime this distinction is more

important. We therefore introduce a smooth time function to replicate the finite time required for the total mass to spall. Since we wish to model accelerograms which are observationally smooth we impose a continuous first and second order derivative on the time function.

$$M_s(t) = m_T \left(\frac{6t^5}{T_{SR}^5} - \frac{15t^4}{T_{SR}^4} + \frac{10t^3}{T_{SR}^3} \right) (H(t) - H(t - T_{SR})) \quad (4)$$

m_T is the total spalled mass and T_{SR} is the spall rise time which is a complicated function of material strength, source strength, source burial depth, and seismic velocity. This time function follows closely the work of Litehiser (1976) in modeling earthquake sources with time functions that are continuous.

The resulting equivalent body forces which conserve momentum are:

$$f_1(t) = \left[\left(\frac{30t^4}{T_{SR}^5} - \frac{60t^3}{T_{SR}^4} + \frac{30t^2}{T_{SR}^3} \right) m_T V_0 (H(t) - H(t - T_{SR})) \right] \quad (5)$$

$$f_2(t) = -m_T g \left[\left\{ \left(\frac{6t^5}{T_{SR}^5} - \frac{15t^4}{T_{SR}^4} + \frac{10t^3}{T_{SR}^3} \right) \cdot (H(t) - H(t - T_{SR})) \right\} + \{ H(t - T_{SR}) - H(t - T_s) \} + \left\{ \left(1 - \left(\frac{6(t - T_s)^5}{T_{SR}^5} - \frac{15(t - T_s)^4}{T_{SR}^4} + \frac{10(t - T_s)^3}{T_{SR}^3} \right) \right) \cdot (H(t - T_s) - H(t - T_s - T_{SR})) \right\} \right] \quad (6)$$

$$f_3(t) = \left[\left(\frac{30(t - T_s)^4}{T_{SR}^5} - \frac{60(t - T_s)^3}{T_{SR}^4} + \frac{30(t - T_s)^2}{T_{SR}^3} \right) m_T V_0 (H(t - T_s) - H(t - T_s - T_{SR})) \right] \quad (7)$$

and $T_s = 2V_0/g$ as before.

These source models can then be included in the normal moment tensor representation of the explosion. Past models for earthquakes and explosions have assumed the first order moment is zero and have written (Stump and Johnson, 1977)

$$u_k(x', t') = G_{kij}(x', t'; \underline{Q}, 0) \otimes M_{ij}(\underline{Q}, t') \quad (8)$$

In order to include the effects of the spall model just developed we write:

$$u_k(x', t') = G_{k3}(x', t'; x_s, 0) \otimes f_3(x_s, t') + G_{kij}(x', t'; \underline{Q}, 0) \otimes M_{ij}(\underline{Q}, t') \quad (9)$$

Equation 9 can be used in the forward sense for calculating synthetic seismograms. Alternatively the equation given a set of observations, U_k , synthetic Green's functions for point forces and couples, G_{k3} and G_{kij} can be inverted to determine the sources, $f_3(x_3, t)$ and $M_{ij}(0, t)$. This source representation will include the spherical explosion, tectonic stress release, and spall.

Inversions for only the second order moment tensor from contained explosions have been completed for a number of events at the Nevada Test Site (Stump and Johnson, 1984).

In a previous study of buried surface explosions the following source representation was utilized in source inversions (Stump, 1983)

$$U_k(x', t') = G_{k3}(x', t'; 0, 0) \otimes f_3(0, t') + G_{k1}(x', t'; 0, 0) \otimes f_1(0, t') \quad (10)$$

The source in this case was represented as vertical and radial point forces. One can see that the new source model is really a combination of the spherical source model plus any double couple component (equation 8) and the vertical component of the surface source model (equation 10) previously published.

OBSERVATIONS

In order to quantify the relative effects of the spherical explosion and spall models on the synthetic seismograms a robust data set must be available. The best instrumented explosion to date is a chemical explosion (CHEAT) detonated in alluvium (Stump and Reinke, 1983). This experiment consisted of the detonation of 253 lbs of TNT at a depth of 11.5m. A total of 48 gages were fielded within the nonlinear region of the source (Fig 1). This array was designed to characterize the two dimensional (r,z) aspects of the explosion with secondary emphasis on its three dimensional properties. An additional 33 gages were placed in the linear near source region for typical seismic source characterization studies (50-150m range).

It is the intention of this study to use the nonlinear data to build the spall and spherical explosion source models. These models will be used to compute synthetic seismograms which can be compared to the near source linear data. Ultimately a simultaneous inversion for both the spherical and cylindrical source models is anticipated.

The nonlinear spall zone was characterized using the method of Stump and Reinke (1982). The criteria for delineating a gage that had spalled are:

- a. Primary Criteria
 - (1) Minus 1g (-0.5 to -2.0) vertical acceleration dwell
 - (2) Impulsive rejoin signal on all components
 - (3) No acceleration dwells on horizontal
- b. Secondary Criteria
 - (1) Dwell times
 - (2) Amplitudes of rejoin

The gages that spalled in one, two-dimensional plane (actual measurement) of the test bed are given in Figure 2. The spall zone for CHEAT extends to a depth between 4.3 and 7.5m directly above the source and radially out to a range beyond 10.85m. The azimuthal symmetry of the process is illustrated by the strong coherence of observed waveforms at the 3m range and 60,

180 and 300 azimuths. As a result of this data, all further spall modeling for CHEAT will assume that the process is azimuthally symmetric. The propagation of the initial compressive wave, spall initiation, and spall rejoin in the vertical direction can be observed in the 1m range data which vary in depth from 7.5m to the free surface (Figure 3). The initial compressive wave can be seen to propagate from depth to the free surface, reflect as a tensile wave, and then fail the soil as it propagates away from the free surface. The apparent velocity of spall initiation is given in Figure 2 as 180 m/s which is much slower than either the P or S wave velocities. It is this slow propagation which is responsible for the rise time placed on the equivalent body force source model of spall.

Using the spall zone defined by the accelerometer array, estimates of the spall mass were made. The upper and lower bounds of the spall zone in two dimensions are given in Figure 4. The resulting limits on spall mass are 2.73 to 4.20×10^9 gm. The lower bound mass estimate includes the deepest spalled gage at each range. Beyond 10.85m the spall region was estimated by linear extrapolation of the spall zone to the free surface. Since gage density left a large gap between the last spalled gage and the first unspalled gage at each range, a maximum spall mass was estimated by placing the upper bound of the spall zone half way between the spalled and unspalled gages at ranges of 1.00m and 10.85m and then extrapolating the zone to the free surface at the same point as the lower bound curve. The resulting spall mass can be compared to the scaling relations suggested by Viecelli and Sobel:

$$m_s = 1.6 \times 10^9 W \text{ kg} \quad (\text{Viecelli})$$

$$m_s = 9.6 \times 10^9 W \text{ kg} \quad (\text{Sobel})$$

W: Kiloton

For CHEAT we have $M = 0.128 \times 10^{-3}$ kton. The estimated spall mass becomes:

$$M(V) = 2.08 \times 10^5 \text{ kg}$$

$$M(S) = 1.25 \times 10^6 \text{ kg}$$

$$M(\text{obs}) = 2.73 \text{ to } 4.20 \times 10^6 \text{ kg}$$

The observed spall mass is 2-3 times greater than the Sobel estimate and 12-15 times greater than the Viecelli model. The improvement of the Sobel model reflects a model based upon a larger data base covering a wider range of explosive yields.

The spall separation velocity was determined from all the nonlinear zone data. The spall failure velocity throughout the test bed is given in Figure 4. An arithmetic mean of these velocities is 0.53 m/s. This failure velocity in alluvium compares to values in the range of 10 m/s for hard rock sites. One can speculate that the separation velocity of the spalled layer is a strong function of the materials strength. The stronger the material the greater the velocity gradient needed prior to failure. The total mass estimates from the Viecelli and Sobel models which were based on events from NTS in harder or stronger materials suggest that although the spalled mass and its velocity may vary from material to material the total momentum captured by the process may be only a function of explosive yield. A comprehensive study of spall data from a variety of sources would be needed to validate these highly speculative suggestions.

Once the mass and escape velocity have been determined, one can calculate the spall dwell time. For CHEAT the estimate becomes:

$$T_s = 2V_0/g = 108 \text{ ms}$$

The spall dwell times measured in the observational data are given in Figure 4. Taking into account the spatial average of these measurements good agreement is found with the dwell time calculated from the average escape velocity.

Utilizing equations 5,6, and 7 and the observational model constraints just reviewed (Table 1), a set of synthetic source models were calculated. The primary variable in these models was the source rise time indicative of the finite time for spall initiation. The total force and its integral for two rise times (28,108ms) and maximum mass are given in Figure 5. The total mass has no effect on the time function but acts as a scalar multiplier so these results can be generalized to any spall mass. The integral of the source functions indicates the previously discussed result that momentum is conserved.

The interplay between source rise time and spall dwell time is well defined in these samples. The peak of the total force decreases as the spall rise time increases from 28 to 108ms (from 1.2×10^{13} dynes to 0.22×10^{13} dynes). The longer periods of the source spectra are not as drastically affected, as indicated by the change in the integral of the force over the same range of spall rise times (8.8×10^{10} dynes-sec to 4.7×10^{10} dynes-sec). As one goes from a source rise time short compared to the dwell time to one which is comparable to the dwell time, the time function changes from one which has a sharp delta like pulse, a long flat dwell, and a second sharp delta pulse to a time function which has a periodicity equal to approximately 1.5 times the source rise time or spall dwell time.

A check upon the spall model can be made by comparison of a predicted spall source against the past analysis of a set of sand bermed explosion sources (Stump, 1983). In this study utilizing equation 10 and observed ground motion data from the detonation of a chemical explosion bermed with sand (denoted PHGI-06), the radial and vertical equivalent elastic point forces - f_r and f_z - were determined. The radial point force was found to be approximately twice the strength of the vertical point force. The radial source function rise time was found to

be controlled by the time the sand berm constrained the explosive by-products. The primary energy in the vertical force was delayed in time with respect to the radial source and was longer period. At the time of the inverse study the experimentally determined vertical force was hypothesized to be due to spall as its timing and period corresponded to spall observations within the nonlinear regime of the source.

The spall model developed in this paper does not discriminate between surface or buried explosions and thus can be applied to the bermed surface burst data and compared to f_3 determined from the inversion of bermed surface burst data. This result is independent of the physical mechanism leading to failure.

The depth and range of spall, its initiation velocity, and dwell time for the PHGI-06 experiment are given in Figure 6. The resulting spall model is given in Table 2. Comparison of the time functions for the spall model and that determined by the inversion of the observational near source data is given in Figure 7.

The spall model dwell times compare very well with the observed test bed dwell times. The spall mass used in the source calculation was the upperbound of that delineated by the nonlinear acceleration data and assuming azimuthal spall symmetry. The spall initiation velocity in the model (0.29 m/s) is higher than the average of the velocities observed at gages in the test bed. Spall velocities were not recorded in the test bed nearer than 5.4m of the charge. There is an indication in the data that the spall velocities increase as one moves closer to the charge. One can also calculate the spall velocity from the observed dwell time:

$$V_0 = T_s g/2 = 0.29 \text{ m/s}$$

The spall velocity used in our model is in good agreement with the average dwell time in the test bed. The final spall rise time used in the theoretical spall model is a factor of 2 longer than that predicted by utilizing the spall initiation

velocity of 180 m/s on a vertical gage array. The spall rise time will be longer than this estimate since it is a two dimensional rather than a one dimensional phenomenon. The PHGI-06 results suggest that spall rise time is close to spall dwell time. As one can see in the CHEAT spall models, this near equality leads to smooth time functions which avoid the delta like beginning and end introduced by the Day et al, 1983 models.

The comparison of the calculated and predicted vertical point force spall models for PHGI-06 (Figure 7) show good agreement between the forward and inverse techniques in an absolute sense. The negative dwell period and amplitude are nearly exact. The greatest discrepancy in the model occurs during the first 35ms where the predicted upward force is not replicated in the PHGI-06 inversion model. It is during this time period that the directly coupled energy from the explosion will be acting in the negative direction. Our model in this paper does not include at this point the directly coupled energy and as such would not be expected to match the inversion model during this time period.

SYNTHETIC SEISMOGRAMS

In order to compute complete seismograms for the fully contained explosion a spherical explosion model must be added to the spall model previously derived. The model followed is that of Mueller and Murphy (1971) and was chosen because of its ability to easily accomodate the effects of various source materials and explosive yields. A second aspect of this model which is satisfying is its beginnings from an analytic approximation to a pressure pulse on a spherical cavity. The solution for the reduced displacement potential in the frequency domain becomes:

$$\psi(\omega) = \frac{r_{el} c^2}{4\mu} \left[\left\{ \frac{P_0 (1.5c/r_{el})}{\frac{2.25c^2}{r_{el}^2} + \omega^2} + P_0 \pi \delta(\omega) \right\} - i \left\{ \frac{P_0 \omega}{\frac{2.25c^2}{r_{el}^2} + \omega^2} - \frac{P_{oc}}{\omega} \right\} \right] \frac{1}{(\frac{c}{r_{el}})^2 - \beta \omega^2 + i \frac{c}{r_{el}} \omega} \quad (11)$$

λ, μ : Lamé's constants

ρ : density

P_{os} : $1.5 \rho g h$

P_{oc} : $\frac{4\mu}{3} (r_c/r_{el})^3$

r_{el} : $1000 W^{1/3} h^{-0.42}$

r_c : $28.7 W^{0.29} h^{-0.11}$

P_0 : $P_{os} - P_{oc}$

c : P wave velocity

h : burial depth

W : explosive yield

β : $(\lambda + 2\mu)/4\mu$

For the CHEAT source function the following parameters were used:

$h = 11.5\text{m}$
 $\rho = 1.9 \text{ gm/cm}$
 $C = 920 \text{ m/s}$
 $v_s = 350 \text{ m/s}$
 $W = 0.128 \times 10 \text{ kt}$

The synthetic seismograms for the spherical explosive source were calculated using equation 8. The Greens functions were for an elastic half-space for source media: $C = 920\text{m/s}$, $v_s = 350\text{m/s}$, $\rho = 1.9\text{gm/cc}$, $h=11.5\text{m}$. The velocity waveforms from this source at the 50m and 100m ranges are given in Figure 8. At 50m the radial velocity is dominated by the P wave while the vertical velocity has body waves which are of equal amplitude to the surface waves. At 100m the Raleigh wave is equal in amplitude to the P wave on the radial component and bigger than the P wave on the vertical component of velocity. The peak amplitudes are tabulated in Table 3.

Using the three CHEAT spall sources (Figure 5) with rise times of 28,56,and 108 ms, three sets of synthetic seismograms were created for the 50 and 100m ranges. The Green's functions used the same material properties as those for the spherical synthetic except the source depth was set at 3m to replicate the observed phenomena (Figure 2). The waveforms are given in Figure 15 while the peak velocity amplitudes are in Table 3. As expected the peak amplitudes decay as the rise time of the source is lengthened while the spikiness of the synthetic is greatly reduced. It is at the longest rise time that the spall amplitudes are equal to or slightly less than the explosion amplitudes. At the shortest rise time the spall synthetics are as much as 7 times larger than the explosion amplitudes.

Some observed data from the CHEAT experiment at 50 and 100m are given in Figure 10. These waveforms are not as spikey or high frequency in nature as the 28 and 56 ms rise-time spall synthetics. The amplitudes observed in the experiment are much smaller than those of the 28 and 56 ms rise-time spall synthetics but comparable to the spherical explosion and spall

RT=108ms synthetics. As found in the case of the surface burst spall source, the CHEAT data argues for a spall source whose rise time (T_{sp}) is comparable in size to its dwell time (T_S).

Complete explosion synthetics were calculated by summing the spherical and spall waveforms. Comparison to the CHEAT data at the 50 and 100m ranges is given in Figure 10. The spall waveforms were those from the 108ms source rise time (Figure 5b). These waveforms were delayed by 65ms with respect to the explosion to replicate the timing of spall with respect to the explosion. In addition the spall synthetics were multiplied by a factor of 2 to yield better agreement with the observational data. This upper bound spall mass does not violate the nonlinear observations in Figure 4. In light of the simple propagation model and the source models the comparisons are remarkably good.

CONCLUSIONS

The utility of data from the nonlinear regime in constraining equivalent elastic body force models of explosions has been shown. The nonlinear data from both contained and surface burst (bermed with sand) explosions leads one to conclude that significant energy is contained within the spall process. The nonlinear data, forward source modeling, and the surface source inversions all argue for relatively smooth spall models in which the spall rise time is close to the spall dwell time.

Synthetic waveforms from the spall model are comparable in size to the waveforms of the purely spherical source. This ratio is a strong function of the rise time given to the spall model. This analysis points to the need for inclusion of spall models when modeling near source data, determining equivalent elastic sources, and estimating yield.

Finally, comparison of the various spall mass and initiation velocity procedures indicates that material strength may be a controlling factor for total spall mass and escape velocity. Comparison of low tensile strength alluvium to hard rock data indicate that total spalled mass in alluvium is greater than that predicted by experimental scaling relations while spall escape velocity in alluvium is much smaller than in hard rock. The counterbalance of these two phenomena may lead to a strength independent scaling relationship for total momentum.

TABLE 1
CHEAT

Sample interval	$\Delta t = 0.005 \text{ s}$
Number of Samples	$N = 35$
Spall initiation velocity	$V_0 = 0.53 \text{ m/s}$
Spall mass	$M_T = 2.7 \text{ to } 4.2 \times 10 \text{ kg}$
Spall dwell time	$T_s = 108 \text{ ms}$
Spall rise time	$T_{sr} = 28, 56, 108 \text{ ms}$

TABLE 2
PHGI-06

Spall initiation velocity	$V_0 = 0.29 \text{ m/s}$
Spall mass	$M_T = 3.2 \times 10 \text{ kg}$
Spall dwell time	$T_s = 60 \text{ ms}$
Spall rise time	$T_{sr} = 55 \text{ ms}$

TABLE 3

DATA TYPE	Radial (cm/s)	Vertical (cm/s)
Explosive Source (50m)	4.2	3.1
Explosive Source (100m)	1.0	1.6
Spall Source RT=28ms (50m)	11.3	20.0
Spall Source RT=56ms (50m)	3.3	5.00
Spall Source RT=108ms (50m)	2.3	1.2
Spall Source RT=28ms (100m)	8.8	14.2
Spall Source RT=56ms (100m)	2.0	3.6
Spall Source RT=108ms(100m)	0.59	0.88

REFERENCES

- Babcock, S., 1980. Pre-HYBRID Gust Phase I Quick Look Report, Engineering Research Institute, University of New Mexico, CERF-AF-26, 1980.
- Bakun, W.H. and L.R. Johnson, 1973. The deconvolution of teleseismic P waves from explosions Milrow and Cannikin, Geophys. J. Roy. Astr. Soc. 34, 321-342.
- Chilton, F., J. Eisler, and H. Henback, 1966. Dynamics of spalling of the earth's surface caused by underground explosions, J. Geophys. Res., 71 5911.
- Day, S. D., M. Rimer, and J. T. Cherry, 1983. Surface waves from underground explosions with spall: analysis of elastic and nonlinear source models, Bull. Seism. Soc. Am. 73, 247-264.
- Eisler, J. and F. Chilton, 1964. Spalling of the earth's surface caused by underground nuclear explosions, J. Geophys. Res., 69, 5285.
- Eisler, J., F. Chilton, and F. Sauer, 1966. Multiple subsurface spalling by underground nuclear explosions, J. Geophys. Res, 71, 3923.
- Frasier, C. W., 1972. Observations of pP in the short-period phases of NTS explosions recorded at Norway, Geophys. J. Roy. Astr. Soc., 31, 99-110.
- Litehiser, J., 1976. Near-field seismograms from two-dimensional propagating dislocation, Ph.D. Thesis, University of California, Berkeley.
- Melzer, L. S., 1981. "Typical Spall from Near-Surface High Explosive Events," Minutes of the DNA Spall workshop held on 12-13 September 1979, Dasiac, Kaman Tempo, Santa Barbara, California, February 1981.
- Mueller, R. A. and J. R. Murphy, 1971. Seismic characteristics of underground nuclear detonations: Part I, seismic scaling law of underground nuclear detonations, Bull. Seism. Soc. Am. ,61, 1675-1692.
- Perret, W. R., 1971. "Free-Field and Surface Motion from a

- Nuclear Explosion in Alluvium: Merlin Event," SC-RR-69-334, Sandia National Laboratories, Albuquerque, New Mexico.
- Perret, W. R., 1978. "Surface Motion Near Underground Explosions in Desert Alluvium-Operation NOUGAT 1, Area 3, Nevada Test Site," SAND77-1435, Sandia National Laboratories, Albuquerque, New Mexico.
- Rinehart, J. S., 1959. "Spalling and Large Blasts", Proceedings of the 2nd Plov Share Symposium, San Francisco, May 13-15, 1959, Part I, 135-155, UCRL-5675.
- Sobel, P. A., 1978. The effect of spall on mb and Ms, Teledyne Geotech Report SDAC-TR-77-12, Dallas, Texas.
- Springer, D., 1974. Secondary sources of seismic waves from underground nuclear explosions, Bull. Seism. Soc. Am., 64, 581-594.
- Stump, B. W., and L. R. Johnson, 1977. the determination of source properties by the linear inversion of seismograms, Bull. Seism. Soc. Am. 67, 1489-1502.
- Stump, B. W. and R. E. Reinke, 1982. "Spall-Like Waveforms Observed in High-Explosive Testing in Alluvium," AFWL-TR-82-15, Air Force Weapons Laboratory, Kirtland AFB, New Mexico, 122p.
- Stump, B. W., 1983. Source characterization of bermed surface bursts, Bull. Seism. Soc. Am., 73, 979-1003.
- Stump, B. W. and R. E. Reinke, 1984. Spall observations and mechanisms in alluvium, Journal of Geophysical Research
- Stump, B. W. and L. R. Johnson, 1984. Near-field source characterization of contained nuclear explosions in tuff, Bull. Seism. Soc. Am. 74, 1-26.
- Toksoz, M. M. and H. H. Kehrner, 1972. Tectonic strain release by underground nuclear explosions and its effect on seismic discrimination, Geophys J. 31, 141-161
- von Seggern, D. H. and R. R. Blandford, 1972. Source time functions and spectra for underground nuclear explosions, Geophys. J. 31, 83-97.
- Walker, J. J., 1982. "Analysis of TV Records for Ground Motion Characterization," DARPA/AFOSR Symposium on the

**Physics of Nonisotropic Source Effects from Underground
Nuclear Explosions, DARPA-GSD-8203 and AFOSR-MP-8201,
Dec 1982.**

Acknowledgements

Thanks to S. Day and J. Hannon for critical review of the manuscript. This work was supported under Grant AFOSR-84-0016.

FIGURE CAPTIONS

Figure 1: Nonlinear gage array on the 2531b Cheat explosion.

Figure 2: Two dimensional spall delineation from the Cheat explosion.

Figure 3: Accelerations at 1m radial range from the Cheat explosion. The depths of the gages vary from 0.23 to 7.50m. The solid line is representative of the initial compressive wave, the dashed line is spall initiation, and the long dashed line is spall rejoin.

Figure 4: At each gage location is marked the spall dwell time (ms) and in parentheses the spall initiation velocity (cm/s) for the Cheat explosion.

Figure 5: Cheat spall model for equivalent body forces (solid circles $\times 10^{13}$ dynes) and their integrals (open circles 10^{11} dynes-sec) for rise times of (a) 28ms (b) 108ms.

Figure 6: Spall dwell time in ms and spall initiation velocity in cm/s (in parentheses) for the PHGI-06 explosion.

Figure 7: The integral of the vertical source function for PHGI-06 (open circles) and the spall model prediction for PHGI-06 (closed circles). All values need to be multiplied by 10^{11} to yield dynes.

Figure 8: Cheat predicted velocities for the spherical explosion source.

Figure 9a: Cheat spall synthetics at the 50m range.

Figure 9b: Cheat spall synthetics at the 100m range.

Figure 10: Two characteristic observations from the Cheat experiment at 50 and 100m are given. Synthetic seismograms consisting of the explosion source in Figure 9 and the spall source in Figure 5b delayed by 65ms and multiplied by 2 are also given.

AFWL CLOSE-IN STATIONS CHEAT

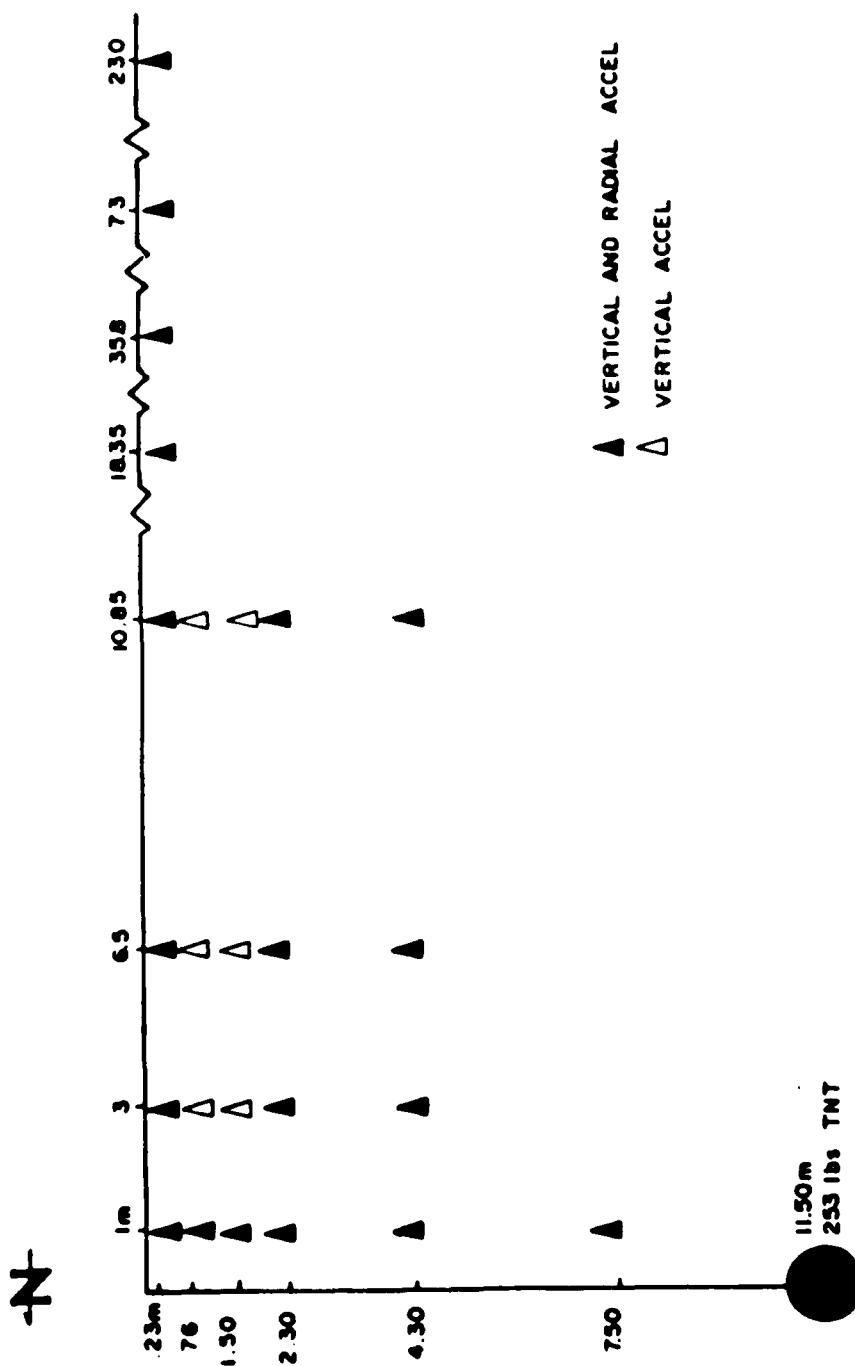


Figure 1

SPALL IN CHEAT

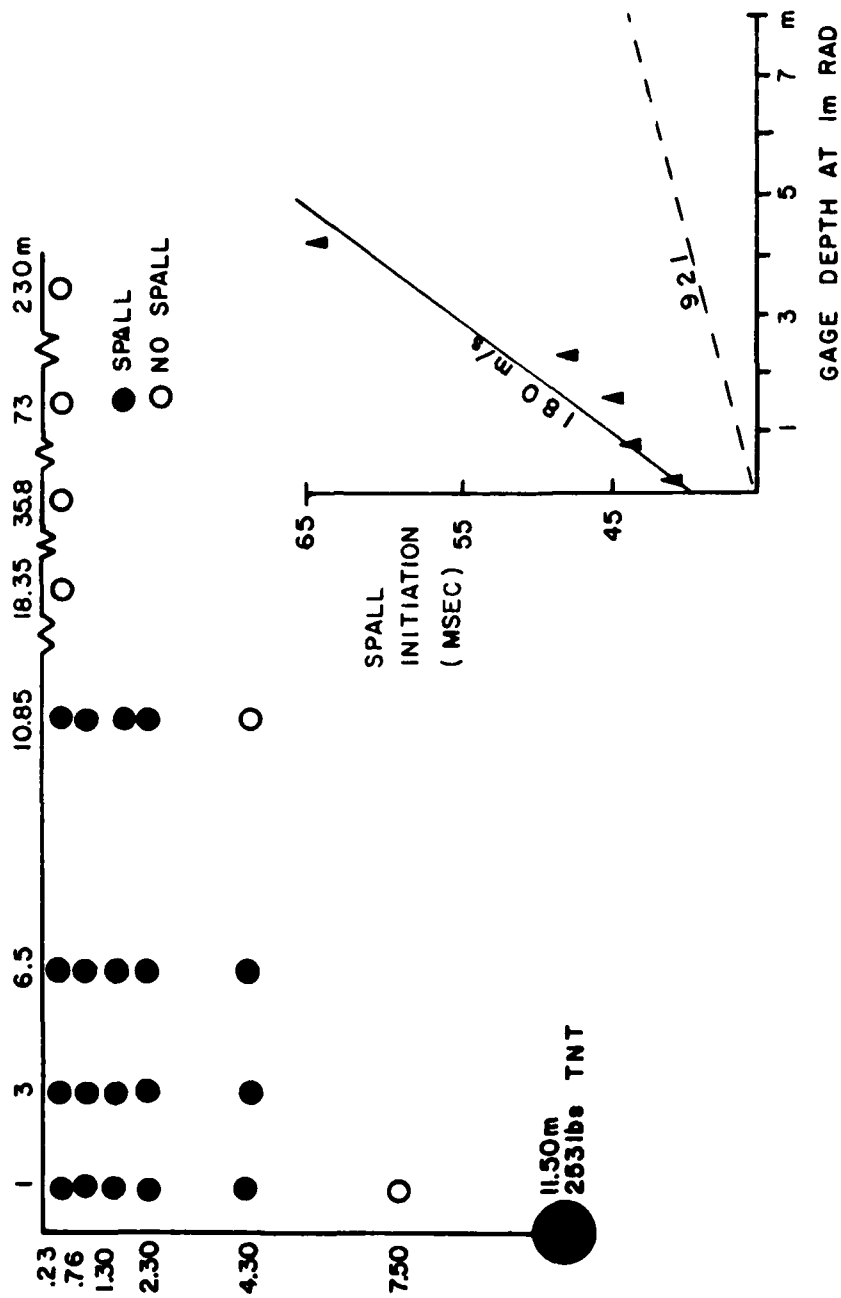


Figure 2

CHEAT SPALL RECORDS $r=1m$

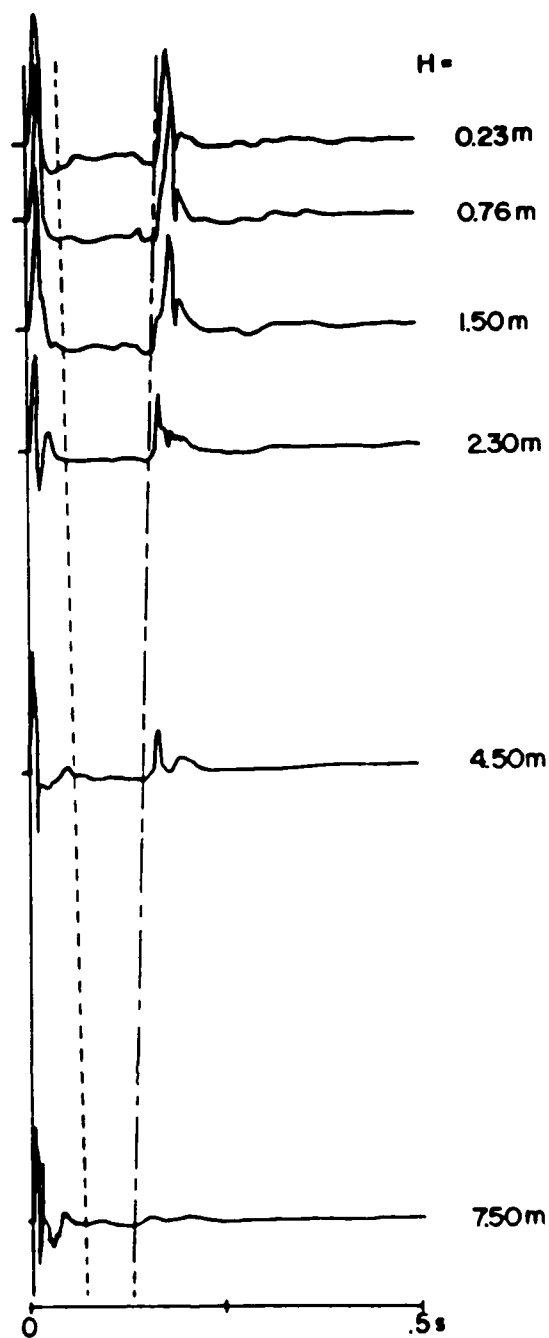


Figure 3

CHEAT SPALL RANGE, TIME, and ESCAPE VELOCITY

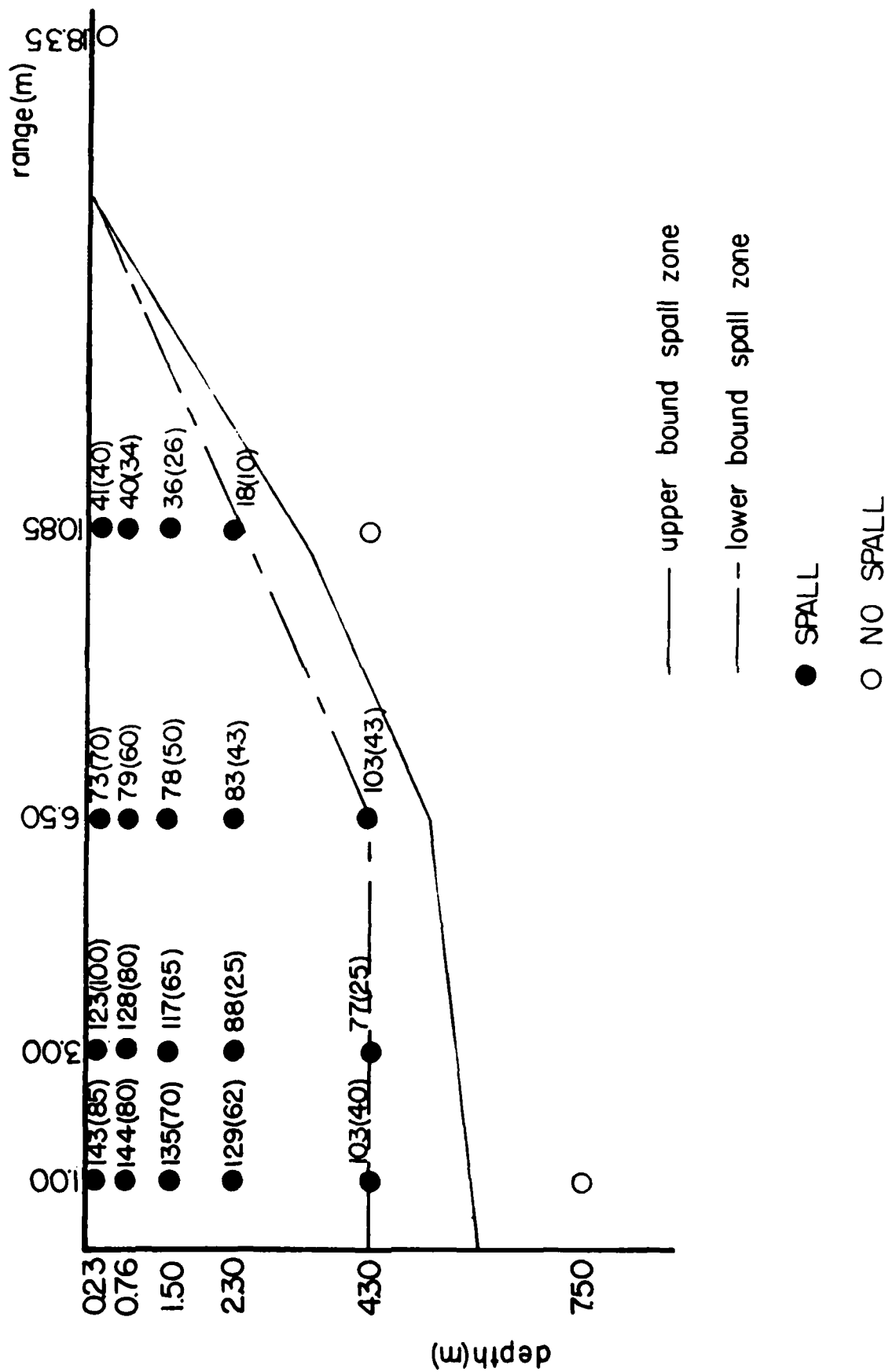


Figure 4

CHEAT SPALL RISE TIME = 28ms

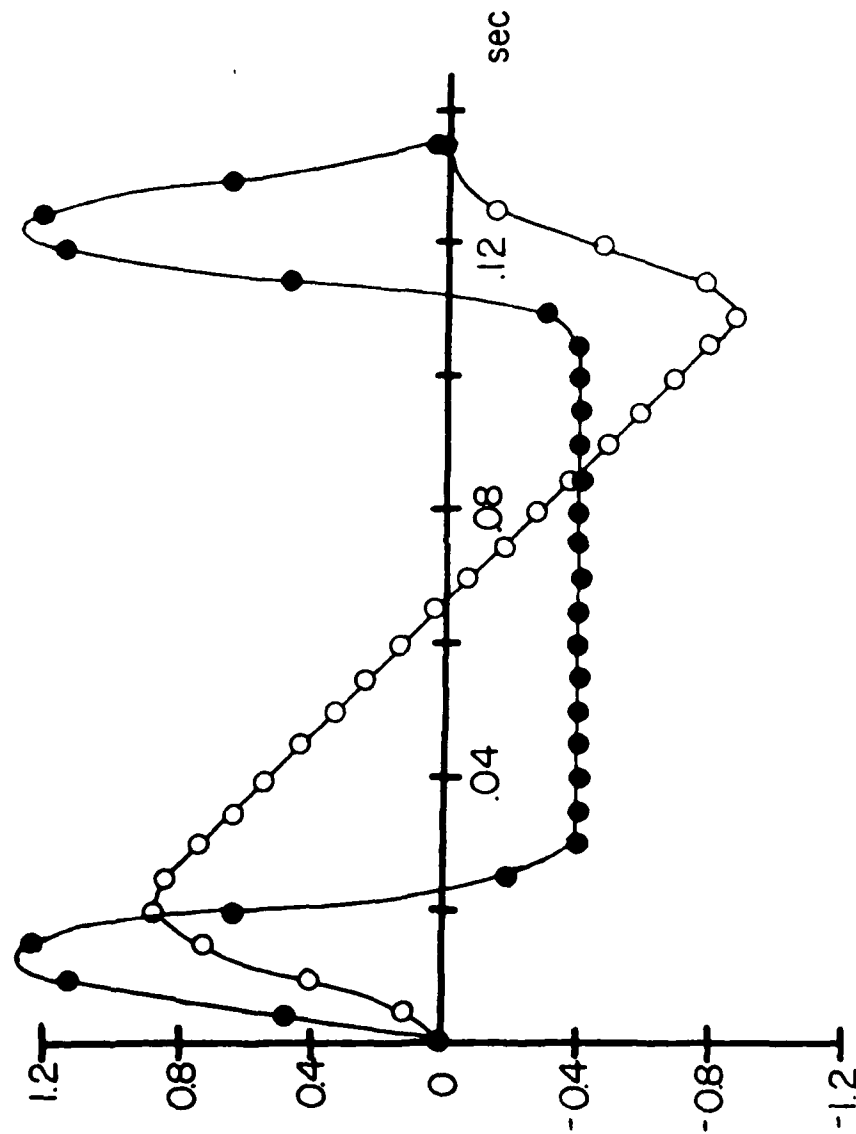


Figure 5a

CHEAT SPALL RISE TIME = 108ms

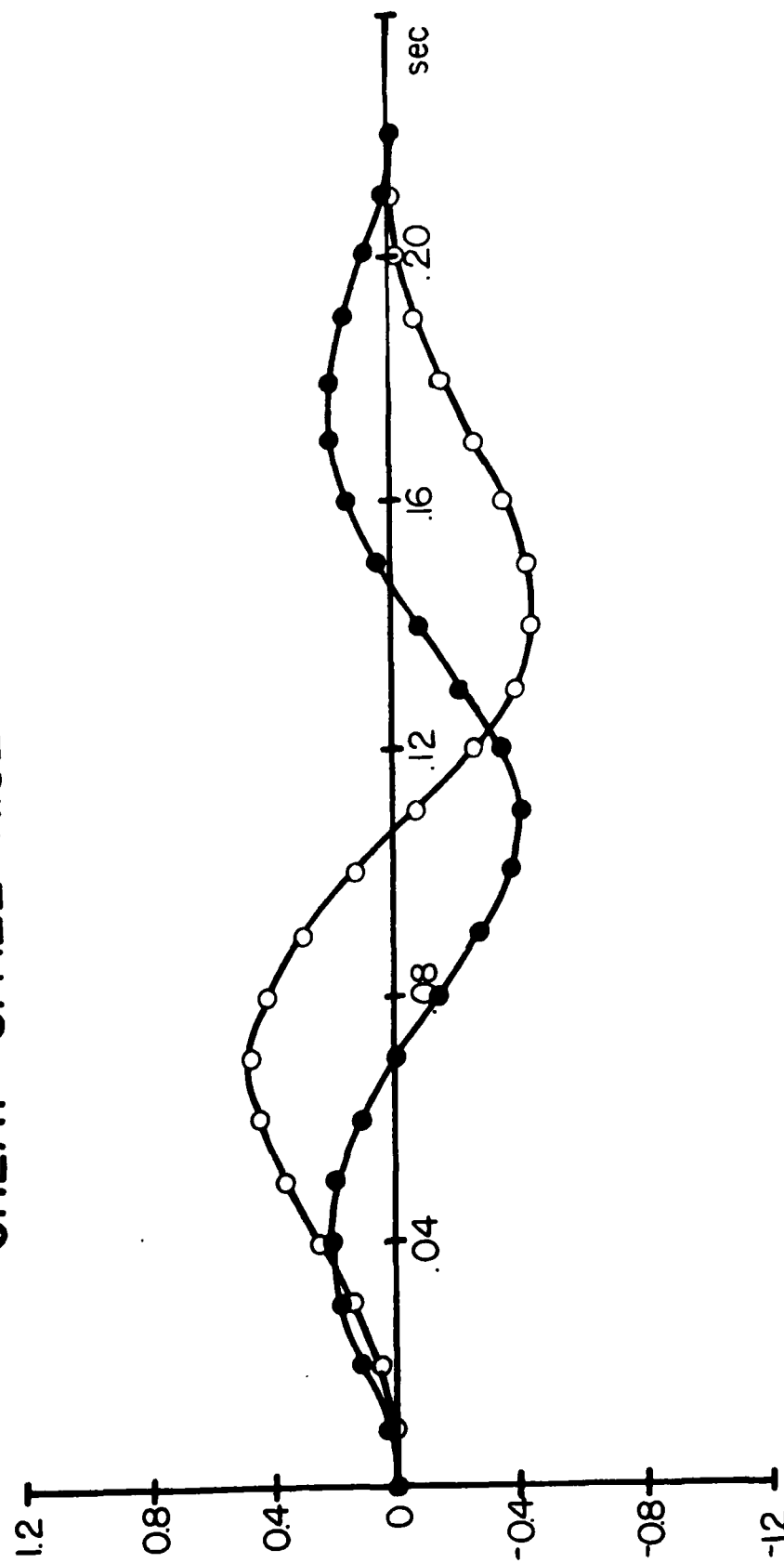


Figure 5b

PHG I-06 SPALL RANGE, TIME, and ESCAPE VELOCITY

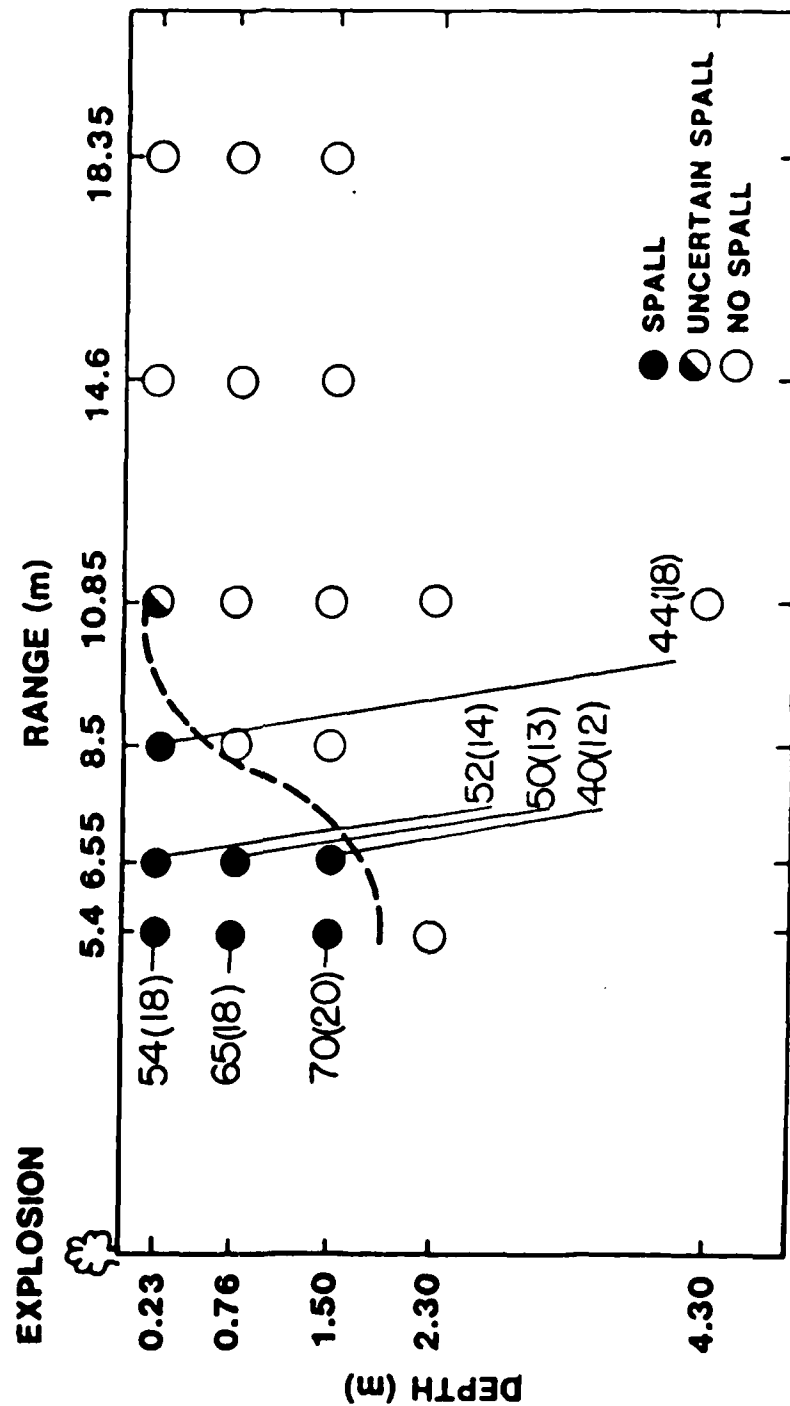


Figure 6

PHG 1-06 FORWARD and INVERSE SPALL MODELS

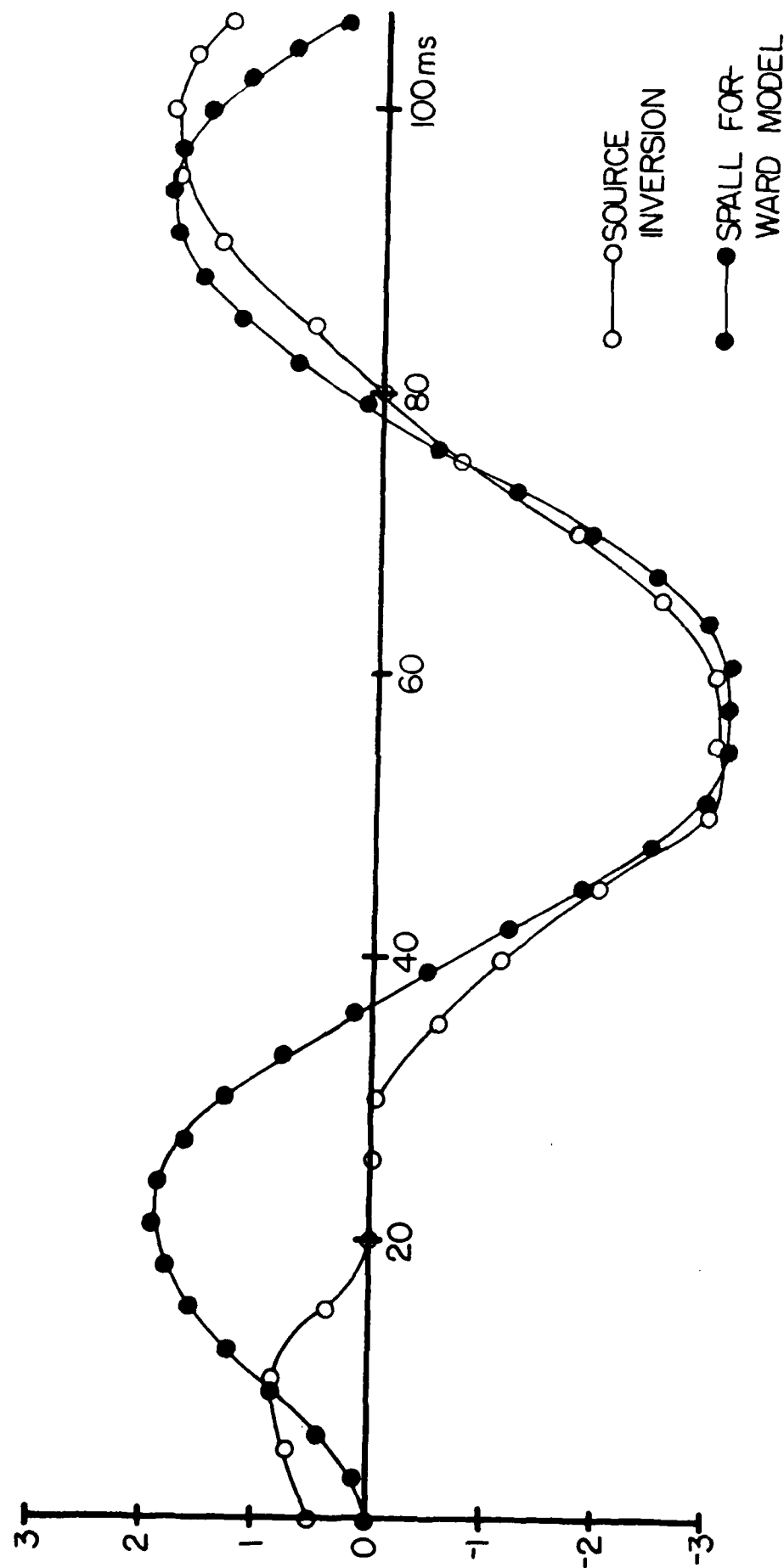


Figure 7

SPHERICAL EXPLOSION SYNTHETICS HS

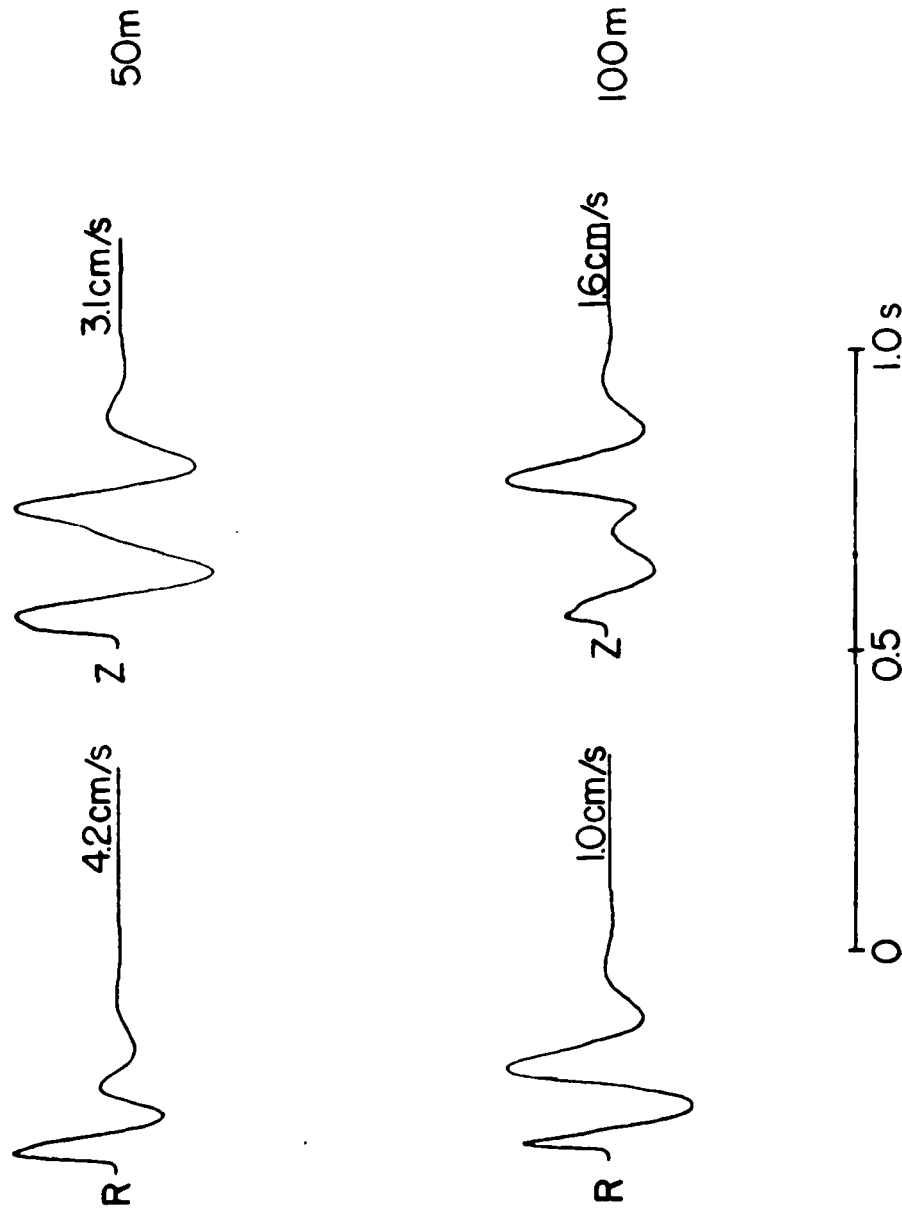


Figure 8

SPALL SYNTHETICS

(R = 50m, H = 3m)

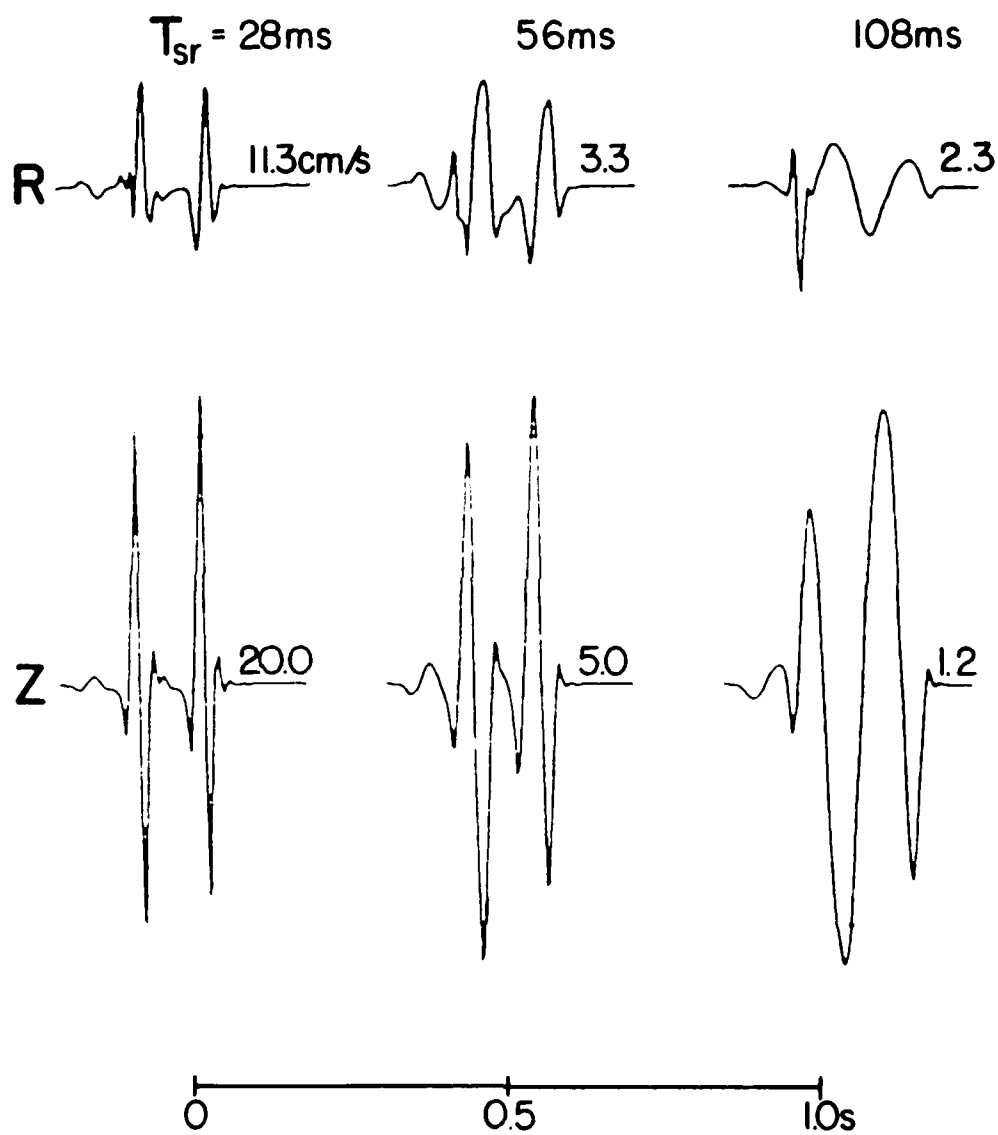


Figure 9a

SPALL SYNTHETICS

(R=100m, H=3m)

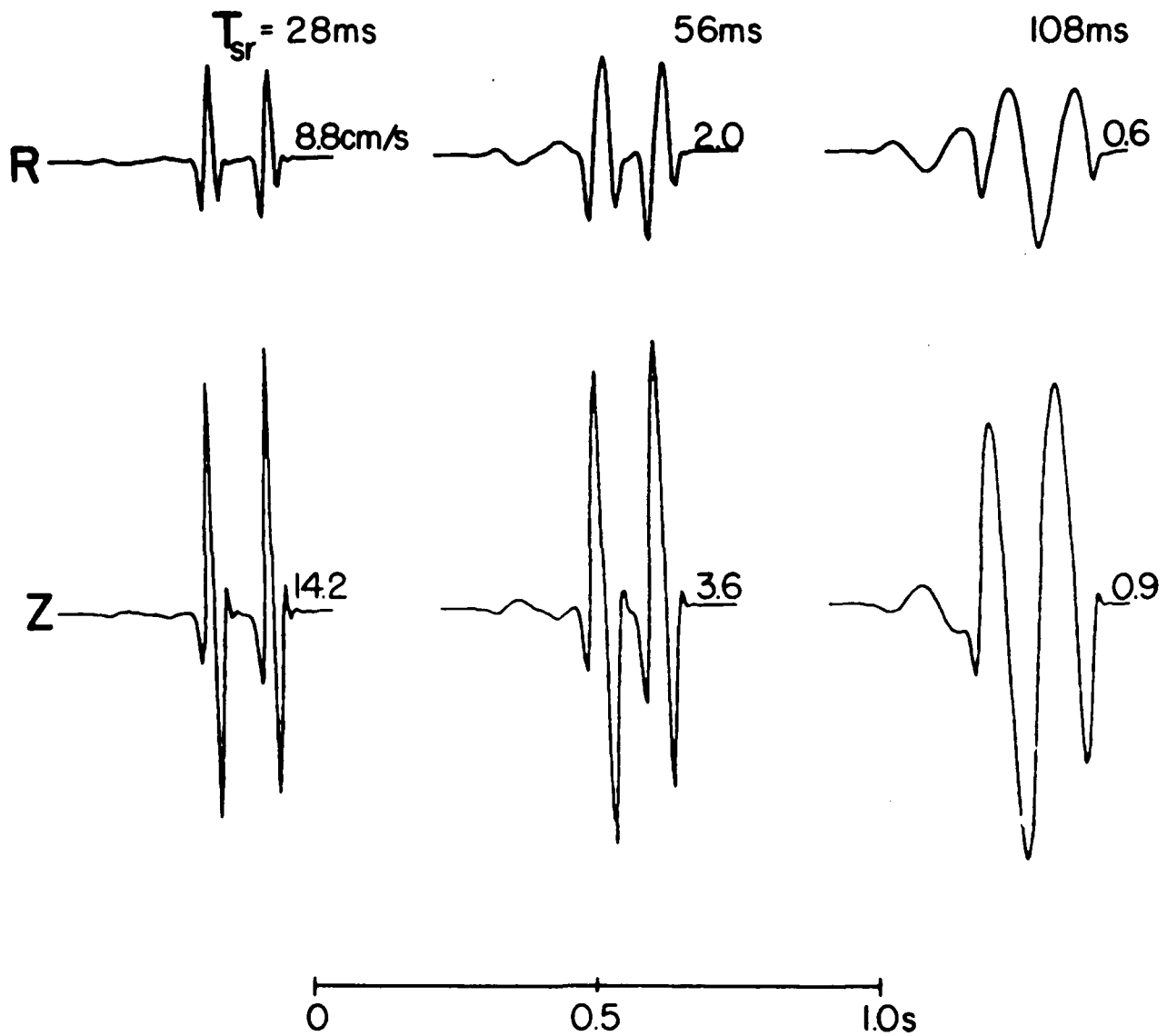


Figure 9b

EXPLOSION & SPALL - OBSERVATIONS & SYNTHETICS

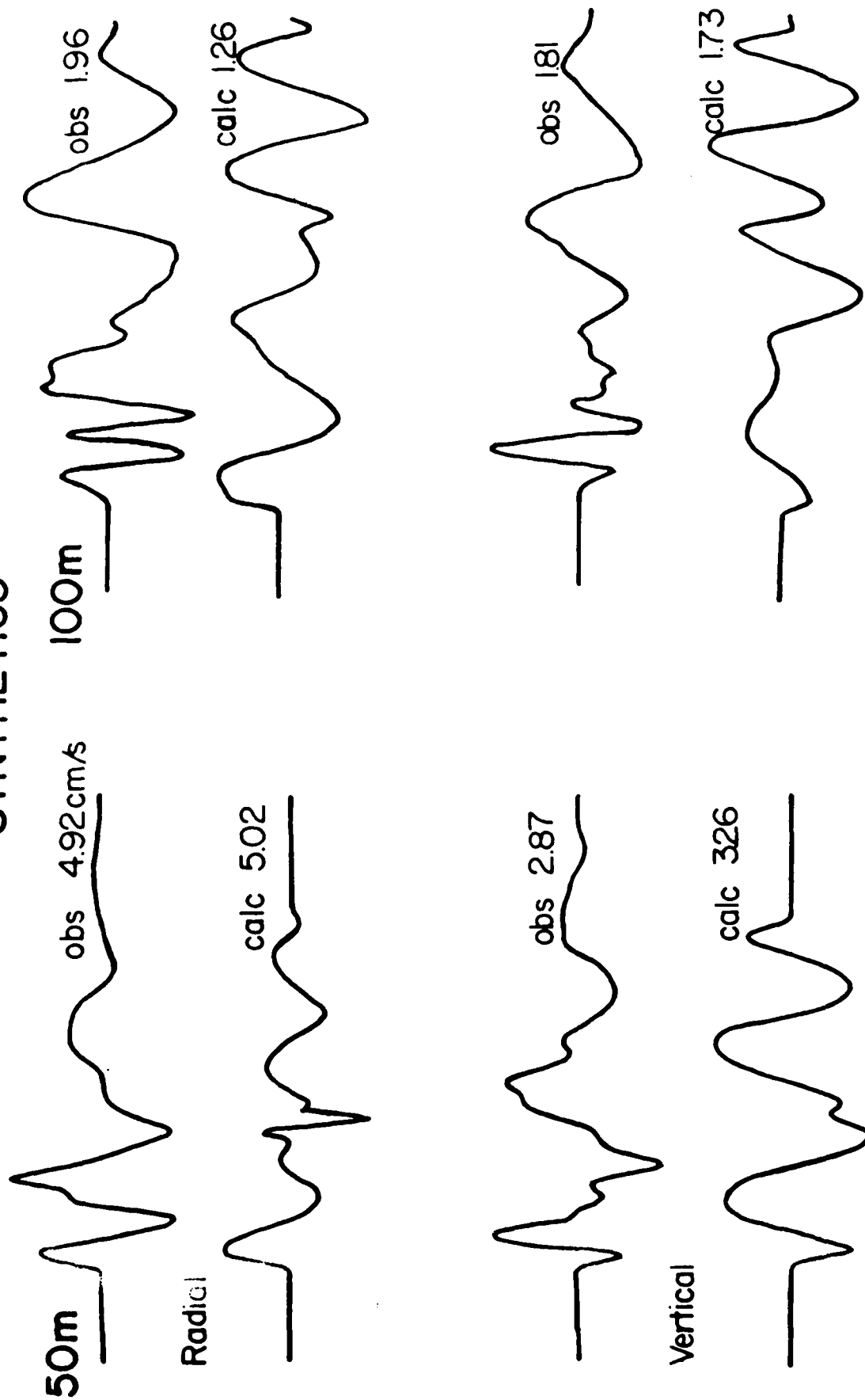


Figure 10

**The Experimental Characterization
of Contained Chemical Explosions**

**Brian W. Stump
Department of Geological Sciences
Southern Methodist University
Dallas, Texas 75275**

Abstract

The utility of small scaled chemical explosion experiments for the purpose of seismic source characterization is explored. A 253 lb TNT source at 11.5m depth of burial was instrumented in the nonlinear and linear regime. The nonlinear data is utilized in the parameterization of the equivalent elastic source. The linear data is inverted to determine these source parameters and then validated against the nonlinear data. The results of this study are that (1) the applicability of the moment tensor representation is shown (2) useful source results can be obtained from relatively simple propagation path models and (3) the resulting source is composed of two parts --- the initially spherical explosion and the cylindrically symmetric spall. The spherical explosion is higher frequency (50-80 ms) than the spall source (200 ms) which is delayed in time. The initial explosion can be modeled by the isotropic moment tensor while the spall source is represented as the moment tensor elements with the ratio: $M_{11} = 1$, $M_{22} = 1$, $M_{33} = 2$.

1. INTRODUCTION

The determination of the explosion source functions in geological materials has remained a problem that has not been completely quantified. Questions still remain concerning source overshoot (Burdick et al, 1984, Douglas and Hudson, 1983), corner frequency scaling (Mueller and Murphy, 1971), high frequency roll-off (Stump and Johnson, 1984, Peppin, 1977, von Seggern and Blandford, 1972), quantification of nonlinear source processes such as spall (Day et al, 1983, Stump, 1985, Viacelli, 1973, Bakun and Johnson, 1973) and nonisotropic source processes (Lay et al, 1984; Aki and Tsai, 1972). The inability to resolve these aspects of the explosion source has resulted from observational data which are inadequate for source quantification. Explosion studies have primarily relied upon teleseismic and to a lesser degree near-field data from the explosions.

In no case has a complete experiment been designed with the primary goal being the characterization of the three dimensional motion field beginning in the nonlinear regime and extending to the near source linear zone. Such a data set can be used to illustrate the growth of the source pulse and then its elastic propagation. If this experiment is to be successful, one additional problem encountered in other studies must be overcome, that of unknown propagation path effects. Even if instruments are placed throughout the experimental test bed, the source will be unresolved if the propagation path is not known.

In the case of nuclear experiments the scale of the experiment precludes (at least initially) adequate gage placement to characterize both near source and nonlinear motion in three

dimensions. Small scale chemical explosions offer an experimental basis in which one can instrument the motion field. Such experiments also offer a choice of test medium.

Comparison of the chemical and nuclear source indicates that differences in source coupling exist. In the case of chemical explosions it is the explosive by-products from the explosion which raise the cavity pressure and then couple energy into the surrounding material. Nuclear explosions generate great temperatures and x-rays both of which when deposited into the surrounding material lead to the generation of cavity pressure and ground motion. Both these processes occur in the first few micro seconds of the experiment. After this initial deposition the processes are comparable.

In order to characterize the explosion source in a controlled environment, a contained chemical explosion test has been designed. The emplacement media was chosen to be alluvium as an initial test. The test site was chosen with a well constrained velocity P structure so that source and propagation trade offs could be minimized. Experiments such as the one reported here could be completed in a variety of materials.

The observational nonlinear data will be used in the creation of the appropriate parameterization for the equivalent elastic seismic source. Once the proper source parameterization has been constructed, the robust near source data set will be inverted for the source parameters. Forward models from the nonlinear data will be compared to the sources determined from the inversion scheme.

2. EXPERIMENTAL SET-UP

As indicated in the experimental design philosophy, instrumentation for the test was divided into two distinct arrays. The first consisted of close-in, radial array of accelerometers (Figure 1). At the three meter range gages were placed at three azimuths to constrain the azimuthal symmetry of the source (Figure 2). The total nonlinear gage array was designed to yield good spatial control on the nonlinear processes and then provide a transition into the near source linear instrumentation.

Each solid triangle in Figure 1 consists of a horizontal (radial to the source) and vertical accelerometer. The open triangle sites consisted of a single vertical accelerometer. The placement of the gages within drill holes is a process that has been studied by many other authors. Within the alluvium environment, at the relatively low accelerations, it has been found that gages placed by raining sand into the hole respond the same as gages grouted with material matching grout (Ake, J. , 1980). The raining technique yields densities which closely match the surrounding material. Based upon these results the rained sand gage emplacement technique was used for all gages in the nonlinear zone. The waveforms were recorded on analog tape and later digitized. The FM tape drives were run at a high rate of speed since the shot time was known resulting in good signal to noise ratios. The nonlinear data was digitized at 5000 samples per second after application of a 5 pole Butterworth filter at 1250 Hz.

The gage array in the linear regime (50-150m) is diagrammed

in Figure 3. Each solid triangle in this diagram represents a three component force balance accelerometer. This array was designed to give both azimuthal and range data for the purpose of characterizing the equivalent elastic source. The instruments in this part of the experiment were force-balanced accelerometers with flat response between 0.02 to 50 Hz. The gages were placed in 6" holes and then back filled with native material. The data was sampled at 200 samples per second with 5 pole Butterworth filter applied at 50 Hz. Unlike the nonlinear data, all seismograms in this set were recorded digitally. In processing the near source data the acceleration waveforms were integrated to yield velocity. During this integration procedure the accelerations were corrected for a static offset which would appear as a ramp in velocity. No additional post processing was necessary.

The two gage arrays gave a total of 81 possible motion measurements from the experiment. It was felt that as an initial test of controlled source studies that this set of data would be adequate to characterize the source.

The source in this experiment was a 253 lb TNT sphere with a measured diameter of 0.51m. The burn rate of TNT is approximately 6097m/s giving an estimated detonation time of 42 μ s. In order to check this estimate a number of similar TNT spheres were instrumented with time of arrival (TOA) crystals which break when the explosive front reaches them. The data from these crystals for a 1000 lb TNT sphere are given in Figure 4. Assuming it takes 8.7 μ s to break the TOA crystal (supported by experimental evidence), the predicted burn time for the sphere was 55.8 s with a 2 μ s variation across the sphere. This empirical data translates into a 34.5 μ s burn time for the 253 lb

sphere. The explosive was placed at 11.5 m depth and then the emplacement hole was backfilled with rained sand just as the nonlinear array accelerometers were placed.

3. Observational Data

An overview of the complete observational data can give one a qualitative sense of the various physical processes occurring in the explosion source. The nonlinear array data is particularly instructive in separating the various aspects of the source contributing to the elastic data. Of the 48 gages fielded in this region, data was recovered from 45.

The initial P pulse from the explosion is illustrated at the gage closest to the explosion in Figure 5. The acceleration, velocity, and displacement are shown prior to any corrections being applied to the data. The surface reflection should arrive 10-20 msec following the direct P pulse. The displacement rise time is approximately 25 ms with an apparent overshoot in the source although the free surface reflection is included in the data.

The vertical propagation of the initial P pulse, its surface reflection and the ultimate tensile failure of near surface layers are illustrated in Figure 6. Prior to this test there was some question as to the tensile failure of near source layers from the reflected P pulse (Stump and Reinke, 1984). One can see in this figure that the spall occurs first nearest the free surface and then propagates down into the material as expected from the free surface tensile reflection. The characteristic minus one g dwell is hard to discern at the scale of Figure 6 so the shallowest gage is reproduced in Figure 7. At this range the material is in free fall for 130-150ms. Spall rejoin is seen to

occur first at depth and propagate to the free surface as expected from the increased overburden stress with depth (figure 6). One can also see the initial P wave pulse growth as it propagates vertically. This pulse widening is due to the nonlinear response of the material.

Utilizing the criteria of Stump and Reinke (1984) the spall zone surrounding the explosion was delineated. The gages that spalled are given by the solid circles in Figure 8. The primary criteria for spall in an accelerometer record are: (1) minus 1 g (-0.5 to -2.0 g) dwell on vertical records; (2) impulsive rejoin signals on all components; and, (3) no horizontal acceleration dwell ($< 0.2g$). With these criteria the spall zone is found to extend radially to between 10.85 and 18.35m while the depth of the process stops between 4.30 and 7.50 meters. The average dwell times measured from the velocity records are given in Figure 8 along with the peak velocity prior to tensile failure (in parenthesis, cm/s). The dwell times are maximum directly above the explosion near the free surface and decay as one moves away from this point in range and depth. Similarly the related escape velocity is also maximized directly above the explosion. This observational data has been used to constrain the mass and momentum captured by the spall processes (Stump, 1985a). The resulting estimates are:

$$M_{oes} = 2.73 \text{ to } 4.20 \times 10^6 \text{ kg}$$

$$I = M_{oes} V_{av} = 1.45 \text{ to } 2.23 \times 10^{11} \text{ dyne-sec}$$

The nonlinear data allow the quantification of one aspect of the

seismic source, spall. The actual importance of the processes is found to depend on the source rise time which is controlled by the propagation velocity of spall initiation and termination.

The estimates of spall mass and momentum are dependent upon an assumption of azimuthal symmetry. The three vertical records at the 3m range support this symmetry assumption (Figure 9). At this range the P wave peak accelerations are 9.3, 9.1, 9.1 g's. The P pulse widths are 19, 16, 15 ms as measured on the accelerograms. The spall dwell times are measured to be 123, 126, 121 ms. The spall initiation times are 38, 33, 32 ms.

The velocity and displacement records allow one to observe the growth of the explosion pulse as it moves away from the explosion. The proximity of the accelerometers to the free surface means that these pulses will include interactions of the explosion stress wave with the free surface including spall. The velocity and displacement records for the vertical and radial gages at the 1, 3, 6.5, and 10.85 m ranges are given in Figure 10. No corrections have been made to the data prior or during the integration procedure thus accounting for the long period drift observed in several displacement records.

The dotted lines on each vertical record indicated the estimated spall dwell time. At the 1m range we have the maximum spall dwell time with a displacement pulse width of 180-190 ms. This displacement pulse is controlled by the total time material was in freefall anywhere in the test bed. This point is substantiated by the fact that the displacement pulse width remains constant as one moves radially away from ground zero and down in depth despite the fact that the dwell time of spall decreases. At the 1m range and 7.5m depth no spall occurs but the pulse width of displacement remains at 190 ms. Similar results

hold for the 18.35m range data.

The vertical velocity records are characterized by the initial rise time from the P pulse, followed by free fall, ending with rejoin. As one moves out of the spall zone the velocity field is characterized by a P pulse with a width near 50 msec followed by a negative dwell equal to approximately 150 msec. This simple interpretation then leads to an initial P pulse from the source with a 50 msec rise time followed by a much longer period phenomena reflective of the energy imparted to the material from spall (Figure 11). This pulse construction clearly illustrates the role of the initial compressive wave and the spall phenomena in the energy leaving the equivalent elastic source. This interpretation is further strengthened later when a comparison of the velocity pulse at 18.3 m is made with the far field source function determined from the inversion of the observational data from 50-150m.

Moving into the linear regime the elastic array data portrayed in Figure 3 is summarized. Of the 33 instruments in this array, data was recovered from 28. All data was lost at Station 9 while vertical records were not recorded at Stations 4 and 6.

The symmetry of the motion field is illustrated in Figure 12. The radial and vertical accelerograms for the three stations at a range of 50m are given. Both the peak accelerations and the waveforms at the three azimuths argue for at least a cylindrically symmetric source. The accelerograms on both the radial and vertical components appear to be dominated by the P waves. Similar symmetries can be observed in the vertical and radial motions at increasing ranges. The pattern observed at 3m in the nonlinear regime has continued into the elastic region.

The motion field is not completely symmetric as shown by the existence of transverse accelerations (Figure 13). The occurrence of transverse motions from contained explosions has been noted previously (McLaughlin et al, 1983). In the case of nuclear explosions transverse near-field motions have been observed to be as large as the radial and vertical. Unlike the nuclear data the transverse motions for this chemical explosion are between 3 and 35% of the radial (Figure 14). No coherent radiation pattern from the transverse motions was determined. There is a wide variability in the waveforms given in Figure 13.

The change in the waveform over the 50-150m range is given in Figure 14. A discussion of the appropriate velocity structure will follow but one can see in this figure the high frequency body waves are followed by the relatively longer period surface waves. At 50m the body waves dominate both the radial and vertical velocities. Between 75-100m the surface waves become the biggest contribution.

A characteristic displacement spectra of one radial acceleration record is given in Figure 15. The noise, dotted line, intersects the data at between 1 and 2 Hz at the low frequency end and at 60-70 Hz at the high frequencies. We shall confine our source study to this band, 2Hz to 60 Hz. As the figure illustrates the data exhibits a corner frequency in this band with the hint of some overshoot.

4. Velocity Structure and Synthetics

The alluvial test site was chosen because of intensive site characterization work that had been completed. (Stump and Reinke, 1982). In addition a number of depth of burial experiments had been conducted near by. The alluvial test site in combination with the chemical explosive led to the test acronym, Contained High Explosive Alluvium Test (CHEAT).

The results of several refraction surveys of the test area are summarized in Figure 16a. The near surface P wave velocities begin at 400 m/s and increase to nearly 900 m/s. The interpretation of this data led to the velocity model given in Figure 16b consisting of 3 layers over a half-space. The layer P wave velocities are 366, 671, 823 m/s with the half space at 23m with a velocity of 1120 m/s.

The first arrival data from the CHEAT experiment itself is in agreement with the earlier refraction data. The P velocity structure for the test bed is thus well resolved. Unfortunately, like many geologic site characterization studies, the shear velocity structure has little constraint. Cross hole shear surveys were conducted but led to results with a good deal of scatter. The results do indicate, though, shear wave velocities beginning near 200m/s at the free surface followed by a positive gradient with depth. The shear velocity may reach 400 m/s or more near shot depth.

The utilization of this site characterization information comes in the form of the computation of synthetic seismograms. The approach to this part of the study was done in two ways. The

first was to compute the simplest possible path effects for each distance range. In view of the simple observational seismograms (Figures 12 and 14) the first set of models were for an elastic half-space. An average velocity model was chosen which led to the best overall fit to the slope of the refraction data and the S-P times on the Cheat data at all ranges. This model was $\alpha = 920 \text{ m/s}$, $\beta = 350 \text{ m/s}$, $\rho = 1.90 \text{ gm/cc}$ and is summarized in Table 1. The second iteration on this half-space modeling was to pick a P and S velocity at each range in order to better model the time of arrival data. In this case the P time of arrival data was from the depth corrected refraction data and the S-P times measured from the Cheat data. The resulting models yielded a P velocity which began at 558 m/s (50 m range) and increased to 788 m/s at the 150 m range. Poissons ratio began at 0.325 and decreased to 0.255 at the 150 m range.

In order to explicitly account for the layered structure developed in the refraction work reflectivity seismograms were calculated for the velocity structure diagramed in Figure 17. The reflectivity technique for synthetic computation was employed so that both the body and surface wave contribution to the near source seismograms could be included. A variety of iterations in modeling were attempted prior to the model in Figure 17. The primary variable in these trials was the shear structure since it was the least resolved. The final acceptance of the low shear wave gradient was supported by a desire to reduce trapped energy in the model that led to long ringing seismograms quite unlike those observed (Figures 12 and 13).

These three sets of Green's functions were developed for the study since they span the range of possible models for matching the observational data. Source inversions will be completed with all three models. The adequacy of simple propagation models will be tested. Figure 18 illustrates the synthetics from the layered structure . The major differences between the layered and half-space models are the development of a complex P wave signature beyond 75 m in the reflectivity seismograms and the dispersion of the surface wave trains in particular the Love waves.

5. First Degree Modeling

The primary purpose of the CHEAT experiment was the determination of the equivalent elastic source function and then the relation to physical source processes as constrained by the nonlinear motion data. The first step in achieving the equivalent elastic source function is a parameterization of the forward problem. Previous studies have utilized the first degree moment tensor representation (Stump and Johnson, 1984) for explosions:

$$u_k(x',t') = G_{ki,j}(x',t';0,0) \otimes M_{ij}(0,t') \quad (1)$$

The isotropic part of the moment tensor is taken to be proportional to volume changes in the source region and thus the explosion component of the source. The deviatoric part of the moment tensor is then taken as the source component not accounted for by a symmetric explosion.

The nonlinear motion data has illustrated the importance of spall. In an attempt to explicitly include the effect of spall in the source parameterization Day et al (1983) added a set of vertical point forces such that total momentum is conserved. Equation (1) then must include the zeroth order moment:

$$u_k(x',t') = G_{k3}(x',t';x_3,0) \otimes f_3(x_3,t') + G_{ki,j}(x',t';0,0) \otimes M_{ij}(0,t') \quad (2)$$

Where x_3 indicates that the spall source may be at a different depth than the explosion. Stump (1985a) studied Equation 2 in a forward calculational procedure and determined that the zeroth order moment contribution could account for 50% of observed near-field waveforms from explosions. In light of these results

the CHEAT data was designed to be used in an inversion procedure to determine the complete source. Equation (2) transformed into the frequency domain then yields the needed set of linear equations

$$u_k(x', \omega) = G_{k3}(x', \omega; x_3, 0) \cdot f_3(x_3, \omega) + G_{kij}(x', \omega; 0, 0) \cdot M_{ij}(0, \omega) \quad (3)$$

$u_k(x', \omega)$ are the observed near source seismograms from Cheat, G_{k3} and G_{kij} are the material Green's functions discussed in Section 4, and f_3 and M_{ij} are the source characterization we wish to determine.

The application of the inverse procedure for the determination of f_3 and M_{ij} is dependent upon the linear independence of the Green's functions from these sources. Unfortunately in the near source region these terms are not independent. This result is discussed in Stump, 1985b. In that paper the following equivalence is shown

$$\frac{\partial}{\partial t} G_{k3} = A (G_{k1,1} + G_{k2,2} + 2 G_{k3,3}) \quad (4)$$

This linear dependence leads to a condition which cannot uniquely determine both the zero and first order moments. Even though the forward modeling of the spall procedure indicated the importance of the zeroth order moment in our inversion study we are forced to use only the first order moment, Equation (1). Vertical asymmetries in the resulting first order moment tensor can then be interpreted in terms of the spall contribution utilizing equation (4).

The three velocity models discussed in Section 4 were each used in the inversions. Two separate inversions were completed for each velocity model. One inversion included all near source data totalling 28 seismograms. The second inversion was completed with data from the 50, 60, 75 m range excluding all 100 and 150 m data (15 seismograms). These two sets were used to investigate the importance of station distribution in resolving the source function.

In all inversions the data modeled were velocity records. The degree of fit for all radial and vertical components was good. In general the transverse motions were not adequately modeled. The observed and calculated seismograms from the range varying half-space Green's functions at Station 3 are given in Figure 19. These observations and synthetics are for the 50 m range and illustrate the good fits to the radial and vertical records and the poor fit to the transverse. The average correlation coefficients for the R, T, Z components in the six inversions are given in Table 2. As the Table illustrates, the layered velocity model led to the best fits although the significance of the difference is small. The most marked change in the correlation coefficients occurs for the vertical seismograms when the data at the 100 and 150 m ranges are deleted. One vertical record at 150 m range is very poorly modeled, correlation coefficient of .01, accounting for a large portion of this discrepancy. The choice of one velocity model and resulting Green's functions over another is difficult to make based on Table 2. The layered structure may be chosen in light of

its small improvement in fits to the observational data.

The isotropic moment tensors (far-field and near-field) from the inversion utilizing all the data (50-150 m) and the three sets of Green's functions are given in Figure 20. The comparison of the three time functions are remarkably similar in light of the differences in the Green's functions. In each inversion the source appears to consist of an initial pulse with a duration of 80 msec followed by a second pulse with a duration near 200 msec.

The spectral characterization of the isotropic source function is given in Figure 21. The spectra of the source shows a corner frequency near 20Hz followed by a high frequency roll off with a slope of 3. The high frequency roll off is comparable to that observed in the data. A second peak in the spectra occurs near 200 ms indicative of the second pulse seen in the source function. The increase in spectral level beyond 60Hz indicates the frequency at which the variances in the moment tensor begin to be as large as the estimate itself.

The interpretation of the isotropic component of the CHEAT explosive source is that the initial part of the explosion consists of a pulse with a duration of between 50-80 ms, followed by a secondary source with a 200 ms duration. This representation follows directly from the nonlinear data discussed in Section 3 and illustrated pictorially in Figure 11. The first pulse results from the spherically symmetric explosion followed by the longer period cylindrically symmetric, spall source. The validation of this source model comes in a comparison of the source from the moment tensor inversion and the velocity record close to the

source. A general representation equation for seismic sources can be written as:

$$\begin{aligned}
 u_n(\underline{x}', t') = & \int_{V_0} \int_{-\infty}^{\infty} G_{ni;j}(\underline{x}', t'; \underline{x}, t) M_{ij}(\underline{x}, t) dt dV + \\
 & \int_V (G_{ni}(\underline{x}', t'; \underline{x}, 0) \rho(\underline{x}) \dot{u}_i(\underline{x}) - \frac{\partial}{\partial t} G_{ni}(\underline{x}', t'; \underline{x}, 0) \rho(\underline{x}) u_i(\underline{x})) dV + \\
 & \int_{\partial V} \int_{-\infty}^{\infty} (G_{ni}(\underline{x}', t'; \underline{x}, t) T_i(\underline{x}, t) - \frac{\partial}{\partial x_j} G_{ni}(\underline{x}', t'; \underline{x}, t) C_{ijkl}(\underline{x}) U_k(\underline{x}, t) n_l) dt dA
 \end{aligned}
 \tag{5}$$

The first integral represents the body forces in terms of the moment tensor, the second integral deals with the initial conditions while the third term includes the boundary conditions. Thus a source can be represented as a boundary condition, body force, or initial condition. The inversions utilizing equation (1) yields $M_{ij}(0, t)$. An equally valid representation of the source in terms of the displacements and stresses is:

$$\begin{aligned}
 u_n(\underline{x}', t') = & \int_{\partial V} \int_{-\infty}^{\infty} (G_{ni}(\underline{x}', t'; \underline{x}, t) T_i(\underline{x}, t) - \\
 & G_{ni;j}(\underline{x}', t'; \underline{x}, t) C_{ijkl}(\underline{x}) U_k(\underline{x}, t) n_l) dt dA
 \end{aligned}
 \tag{6}$$

Comparing equations (1) and (6) we see that one should be able to qualitatively compare \dot{M}_{ij} to the near source velocities. In Figure 22 a comparison of wave shapes between the far field moment tensor as determined from observational data at the 50, 60, 75, 100, 150m ranges to the near source velocity at 18.35m. The comparison is excellent including the initial p wave with a pulse width between 50-80 ms followed by the second pulse, earlier attributed to spall, with a pulse width of 200 ms.

In all the inversions the off diagonal elements of the moment tensor were at least a factor of 2 smaller than the three diagonal elements of the moment tensor. The far-field and near-field moment tensors from the range varying half-space Green's functions with all data are given in Figures 23a and b. The initial source pulse is approximately symmetric on the M_{11} , M_{22} , and M_{33} components. The second part of the source pulse, attributable to spall because of the trade off given in Equation (4), is two times larger on the M_{33} component than the M_{22} and M_{11} components.

The far and near-field peak moment tensors for the six inversions completed in this study are given in Table 3. Since both the P and S velocities vary widely between the three velocity models utilized, there is an order of magnitude variation in the moment estimation. Our best velocity models, range varying half-space and layered, only yield a factor of 2-3

variation. It is this variation which we believe is more representative of the possible scatter in source size introduced by the propagation path unknowns. The primary reason for this variation is the unresolved shear structure. The primary difference between the two models is that the layered structure can return down going energy back to the free surface while the half-space model cannot.

In all the inversions summarized in Table 3 the M_{33} component is larger than the nearly equal M_{22} , and M_{11} . This fact is shown in the time series given in Figure 23b. The initial pulse is nearly symmetric on the M_{11} , M_{22} , M_{33} components but it is the longer period secondary pulse which introduces the asymmetry. This frequency shift yields a far-field moment tensor with peak amplitudes nearly symmetric and a near-field moment tensor with a M_{33} component as much as two times larger than M_{22} and M_{11} . Such a long period asymmetry matches the spall source model.

Conclusions

The utility of carefully designed seismic experiments in characterizing explosive sources has been illustrated. This experiment, a small scaled chemical explosion, has allowed the seismic source as determined by an inversion procedure to be related to observed physical processes in the source region. The nonlinear motion data from within the source burial depth has shown the growth of the source pulse. The new result that has been supported by this unique data set is the quantification of the spall process as a contribution to the equivalent elastic seismic source. The potential for quantifying effects such as source size and emplacement material is great in similar experiments.

The utilization of the moment tensor source representation in an inversion procedure has also been validated by the analysis of this new data base. The selection of the appropriate velocity model for synthetic seismogram calculation introduces a factor of 2 to 3 variation in moment when comparing the best homogeneous half-space Green's function to a complete plane layered model. These moments are stable as subsets of the complete data set are inverted.

The explosion source model which has resulted from this study consists of two distinct parts. The first, relative high frequency, source is the initial spherical explosion. This component dominates the far-field moment tensor and is between 50-80 ms in duration. The second part of source is the cylindrical energy which results from the interaction of the initially spherical compressive wave with the free surface. Through the inversion and the analysis of the nonlinear data this spall process creates a cylindrically symmetric source delayed in time from the initial compressive wave. In addition, the spall process results in a longer period component to the source, in our case 200 ms. This frequency shift is controlled by the time near surface layers remain in free fall once tensile failure has occurred. The amount of frequency shift will then be dependent upon the tensile strength of near surface layers. The spall part of the explosion is characterized by the diagonal moment tensor elements $M_{11} = 1$, $M_{22} = 1$, $M_{33} = 2$. This secondary source because of its longer period component is maximized on the near-field moment tensor.

Similar results have been observed in inversions of nuclear data although the timing and duration of the phenomena is different. Figure 2, contains the moment tensors from the nuclear explosion Farm. This source has an initial pulse followed 1-2 second by the cyclic longer period energy. The interpretation one can now place upon the source is that the initial pulse is the spherical explosion followed by the cylindrical spall contribution.

References

- Aki, K. and Y.. B. Tsai (1972). Mechanism of Love-wave excitation by explosive sources, J. Geophys. Res. **77**, 1452-1475.
- Ake, J. P.11 (1980). Letter Report and Preliminary Data Analysis, "Ground Motion in a Non-Airblast Environment." Engineering Research Institute, University of New Mexico, Albuquerque, New Mexico 87131.
- Bakun, W. H. and L. R. Johnson (1973). The deconvolution of teleseismic P waves from explosions Milrow and Cannikin, Geophys. J. Roy. astr. Soc., **34**, 321-342.
- Burdick, L. J., T. Wallace, T. Lay (1984). Modeling near-field and teleseismic observations from the Amchitka test site, J. Geophys. Res. **89**, 4373-4388.
- Day, S. D., N. Rimer, and J. T. Cherry (1983). Surface waves from underground explosions with spall: analysis of elastic and nonlinear source models, Bull. Seism. Soc. Am. **73**, 247-264.
- Douglas, A. and J. A. Hudson (1983). Comments on "Time Functions Appropriate for Nuclear Explosions," by L. J. Burdick and D. V. Helmberger and "Seismic Source Functions and Attenuation from Local and Teleseismic Observations of the NTS Events Jorum and Handley," by D. V. Helmberger and D. M. Hadley, Bull. Seism. Soc. Am. **73**, 1255-1264.
- Lay, T., T. C. Wallace, and D. V. Helmberger (1984). The effects of tectonic release on short-period P waves from NTS explosions, Bull. Seism. Soc. Am., **74**, 819-842.
- Mueller, R. A. and J. R. Murphy (1971). Seismic characteristics of underground nuclear detonations, Part I. Seismic spectrum scaling, Bull. Seism. Soc. Am. **61**, 1675-1692.
- McLaughlin, K. L., L. R. Johnson, T. V. McEvelly (1983). Two-dimensional array measurements of near-source ground accelerations, Bull. Seism. Soc. Am. **73**, 349-375.
- Peppin, W. A. (1977). A near-regional explosion source model for tuff, Geophys. J. Roy. astr. Soc. **48**, 331-349.
- Stump, B. W. and R. E. Reinke (1982). "Spall-Like Waveforms

Observed in High-Explosive Testing in Alluvium,"
AFWL-TR-82-15, Air Force Weapons Laboratory, Kirtland
AFB, New Mexico, 122 p.

Stump, B. W. and L. R. Johnson (1984). Near-field source
characterization of contained nuclear explosions in
tuff, Bull. Seism. Soc. Am., 74, 1-26.

Stump, B. W. and R. E. Reinke (1984). Spall observations and
mechanisms in alluvium, accepted J. Geophys. Res.

Stump, B. W. (1985a). Constraints on explosive sources with
spall from near source waveforms, accepted Bull. Seism.
Soc. Am.

Stump, B. W. (1985b). Trade-offs in point force and force couple
representations in seismology, in preparation.

Viecelli, J. A. (1973). Spallation and the generation of surface
waves by an underground explosion, J. Geophys. Res.
78, 2475-2487.

von Seggern, D. and R. Blandford (1972). Source time functions
and spectra for underground nuclear explosions, Geophys.
J. Roy. astr. Soc. 31, 83-97.

Acknowledgements

The experimental program involved the following people Paul Minto, Al Leverette, Joe Repichowski, Tony Taglioferro. Special thanks to Lane Johnson and Tom McEvilly for support in fielding the linear array. Finally Robert Reinke was involved in all aspects of the program. The success of experiment is directly attributable to him. This work supported under Grant AFOSR-84-0016.

Table 1

All ranges	920 m/s	350 m/s	1.9 gm/cc
------------	---------	---------	-----------

Each range

50	558	284	1.9
60	582	312	1.9
75	617	343	1.9
100	689	390	1.9
150	788	452	1.9

Table 2:
Correlation Coeffiecents

		<u>R</u>	<u>T</u>	<u>Z</u>
Single Half-Space Model	50-75m			
	50-150m	.8122	.2503	.6402
Range Varying Half Space Model	50-75m	.7560	.2672	.6452
	50-150m	.8884	.3740	.8910
Layered Velocity Model	50-75m	.8494	.2812	.6008
	50-150m	.9360	.3797	.8675

Table 3

Moment From CHEAT Inversions
 Nearfield - 10^{16} dyne-cm
 (Farfield - 10^{17} dyne-cm/s)

INVERSION	M ₁₁	M ₁₂	M ₁₃	M ₂₂	M ₂₃	M ₃₃	M _{TR}	ψ (m ³)
50-60m Single Half- Space	13.6 (47.4)	0.279 (0.312)	1.44 (1.21)	13.3 (47.2)	0.798 (0.733)	19.2 (50.0)	15.3 (48.2)	.757
50-150m Single Half- Space	11.3 (56.2)	0.506 (0.515)	0.654 (0.889)	10.9 (55.7)	0.326 (0.628)	17.1 (57.4)	13.1 (56.4)	.649
50-75m Varying Half-Space	2.78 (7.80)	0.426 (0.299)	0.484 (0.827)	2.89 (0.836)	0.249 (0.224)	4.51 (9.59)	2.88 (8.35)	.354
50-150m Varying Half-Space	2.76 (8.23)	0.384 (0.296)	0.474 (8.54)	2.85 (8.54)	0.310 (0.402)	5.10 (10.4)	2.87 (8.68)	.288
50-75m Layered	1.11 (2.54)	0.479 (0.259)	0.519 (0.424)	1.20 (2.56)	0.135 (6.19)	1.75 (3.17)	1.35 (2.76)	.106
50-150m Layered	0.851 (2.41)	0.144 (0.137)	0.175 (0.187)	0.928 (2.31)	0.1012 (0.147)	1.03 (2.57)	0.936 (2.42)	.0733

Figure Captions

- Figure 1: Side view of the nonlinear gage array for the CHEAT experiment.
- Figure 2: Surface view of the nonlinear gage array for the CHEAT experiment.
- Figure 3: The linear gage array for the CHEAT experiment.
- Figure 4: Observed arrival times of the explosive front in a 1000 lb TNT sphere.
- Figure 5: Observed acceleration, velocity, and displacement at the gage closest to the CHEAT source.
- Figure 6: The vertical propagation of the initial P pulse, its free surface reflection, and spall of near surface layers as observed on vertical accelerometers directly above the explosion.
- Figure 7: The vertical acceleration at the free surface directly above the explosion. The initial P pulse, spall (-1g dwell), and spall rejoin can be observed.
- Figure 8: The depth and range of spall in one two dimensional plane. The first number next to each gage is the spall dwell time in ms and the number in parenthesis is the escape velocity in cm/s.

Figure 9: The three vertical accelerations from the 3m range at azimuths of 0 , 120 , 240 .

Figure 10: The radial (R) and vertical (Z) velocity (light line) and displacement (heavy line) at the 1m, 3m, 6.5m, 10.85m, 18.35m ranges, all observed depths. The dotted lines next to the vertical velocity records are representative of spall dwell times.

Figure 11: The model representative of the source pulse growth in the nonlinear region. The dotted lines represent spall dwell times at each range.

Figure 12: The azimuthal symmetry of the vertical and radial accelerations observed at the 50m range.

Figure 13: The observed transverse accelerations in the linear regime.

Figure 14: The radial and vertical velocity records from the CHEAT experiment between the 50 and 150m ranges.

Figure 15: The radial acceleration and displacement spectra for the 50m range. The noise dominates the spectra below 1Hz and above 60Hz.

Figure 16a: The sample refraction result from the test area.

b: The model developed from the refraction data.

Figure 17: The final layered model for calculation of reflectively seismograms.

Figure 18: The reflectively Green's functions convolved with the CHEAT instrument response. The radial (R) and vertical (Z) explosion (Ex) Green's functions as well as the transverse (T) dip-slip (DS) Green's functions are given.

Figure 19: The observed and calculated velocity records at Station 3 (50m range) from the inversion utilizing all the data and the range varying Green's functions.

Figure 20: The isotropic moment rate tensor (\dot{M}_{12}) and moment tensor (M_{12}) from the CHEAT inversions utilizing all data between 50-150m along with the single half-space, range varying half-space, and reflectively Green's functions.

Figure 21: The spectral characterization of the isotropic moment tensor from the single half-space, all data inversion.

Figure 22: Comparison between the isotropic moment rate tensor and the velocity record observed at the 18.35m range.

Figure 23: The moment rate tensor (a) and moment tensor (b) from the inversion of all the linear data utilizing the range varying half-space Green's functions. All moments are relative to the M_{33} component which has the peak amplitude of 10.4×10^{17} dyne-cm/s in (a) and 5.10×10^{16} dyne-cm in (b).

Figure 24: The moment tensors, including the isotropic component, for the nuclear explosion FARM. The numbers above the traces should be multiplied by 10^{23} to yield dyne-cm.

AFWL CLOSE-IN STATIONS CHEAT

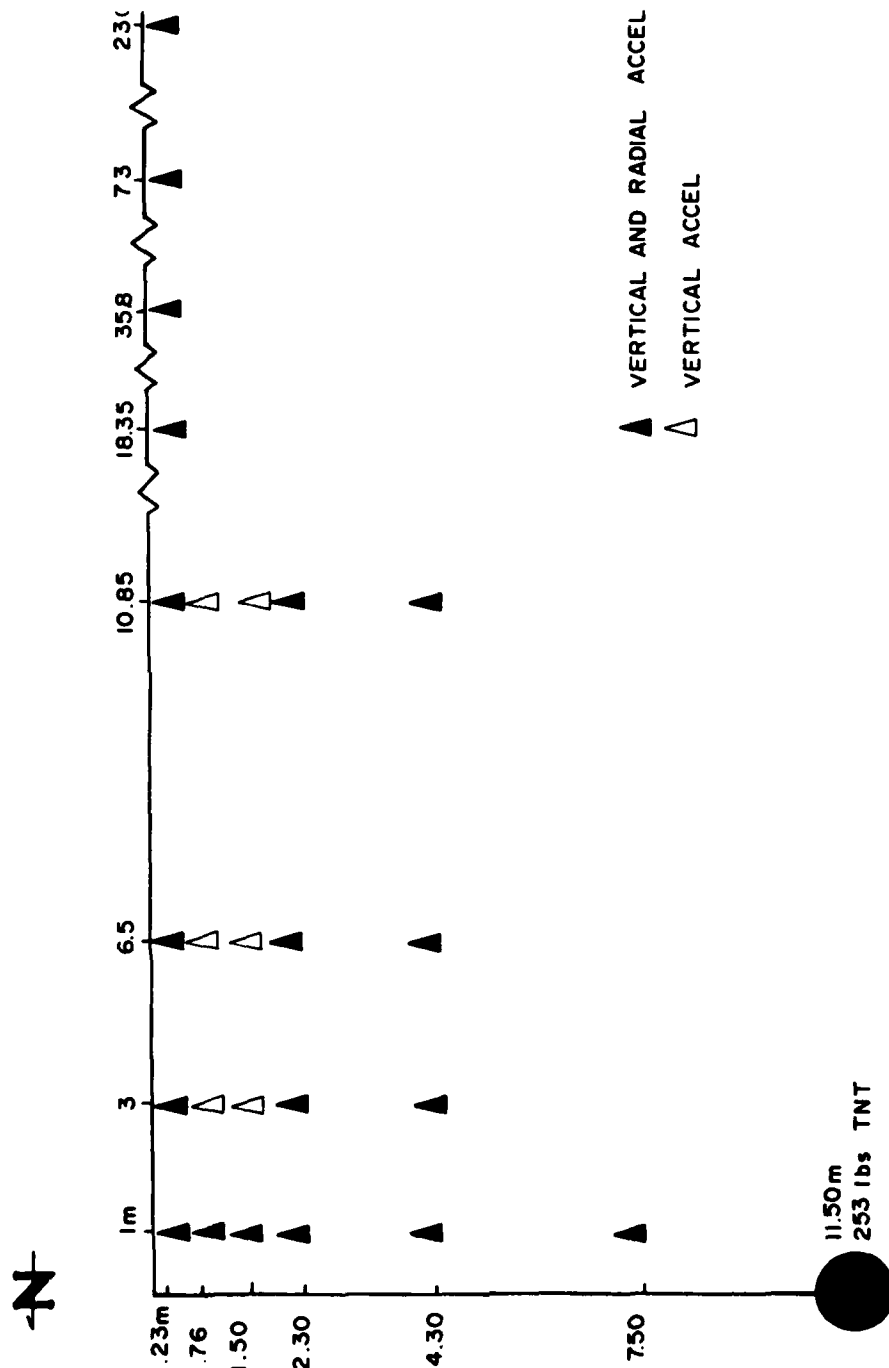


Figure 1

AD-A150 741

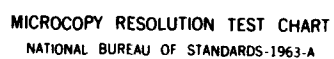
NEAR-FIELD SOURCE CHARACTERIZATIONS OF EXPLOSIONS(U)
SOUTHERN METHODIST UNIV DALLAS TX DEPT OF GEOLOGICAL
SCIENCES B W STUMP 20 NOV 84 SMUG-1 AFOSR-RR-84-1279
AFOSR-84-0016 F/G 8/11

2/2

UNCLASSIFIED

NL

		END											
		FILED											
		DTIC											



MICROCOPY RESOLUTION TEST CHART
NATIONAL BUREAU OF STANDARDS-1963-A

AFWL CLOSE-IN STATION PLANS
CHEAT

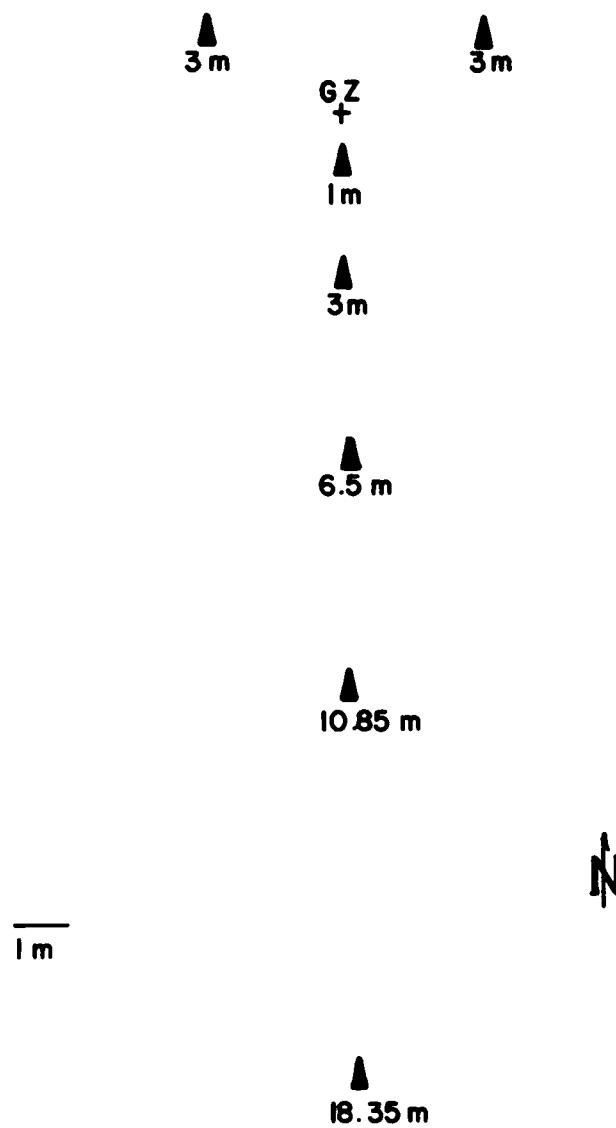


Figure 2

CHEAT DISTANT STATIONS

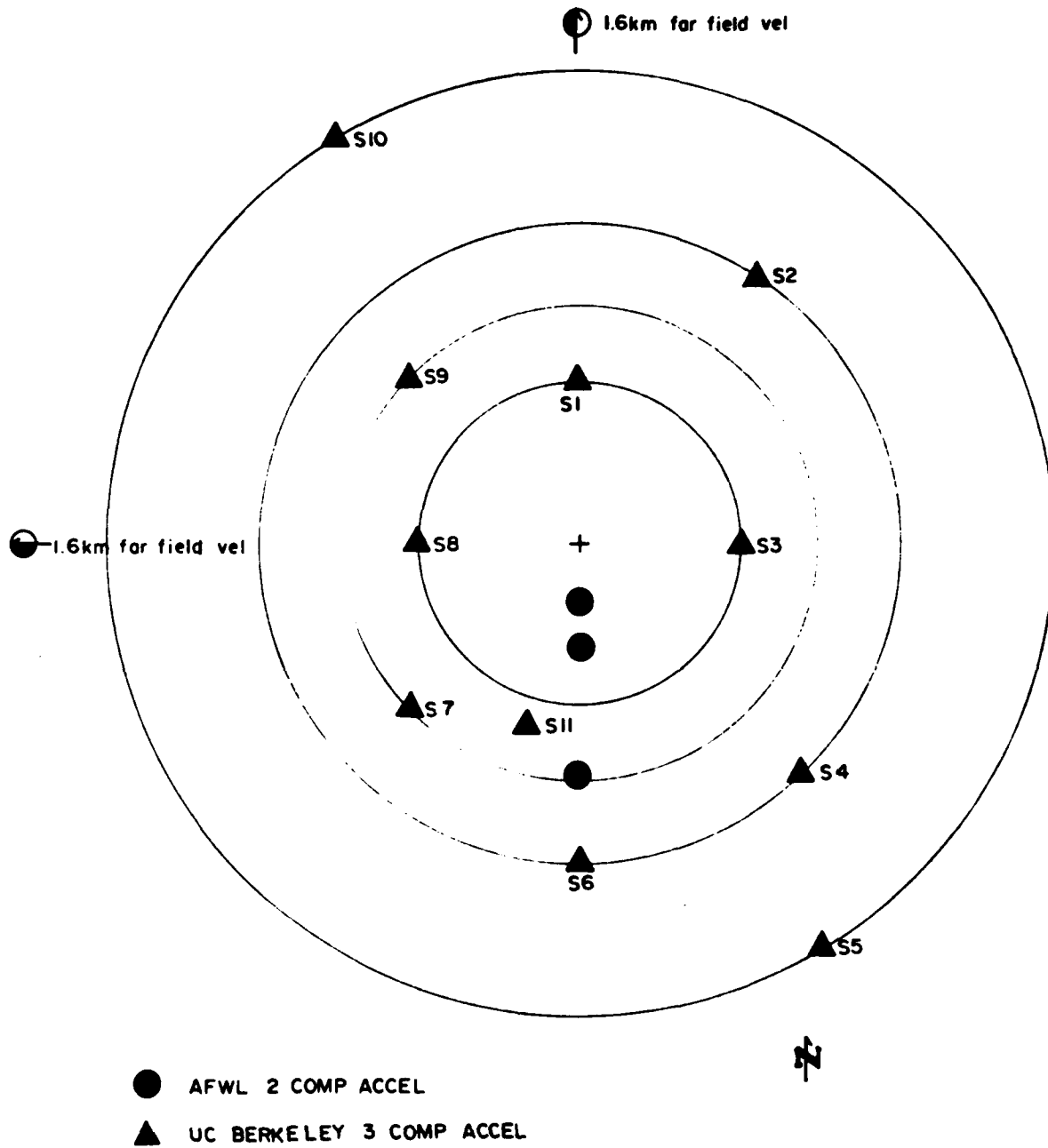


Figure 3

DETONATION TIMES
of TNT SPHERE

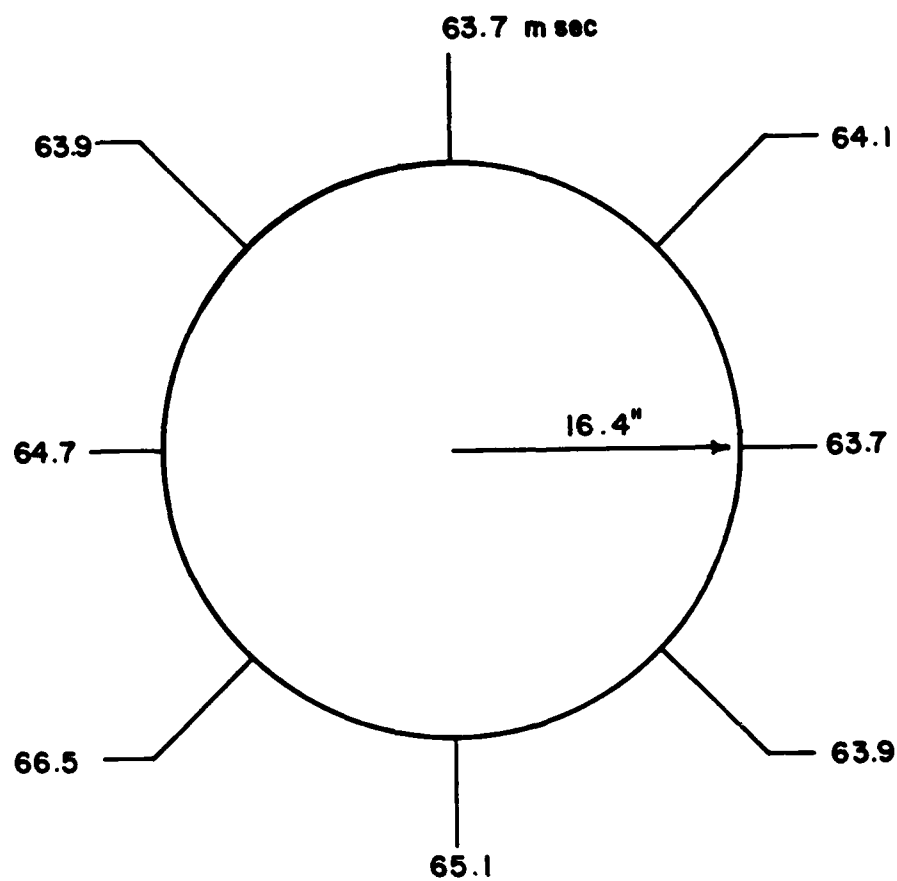


Figure 4

CHEAT CLOSE-IN OBSERVATIONS

R=1.0m DEPTH=7.5m RADIAL

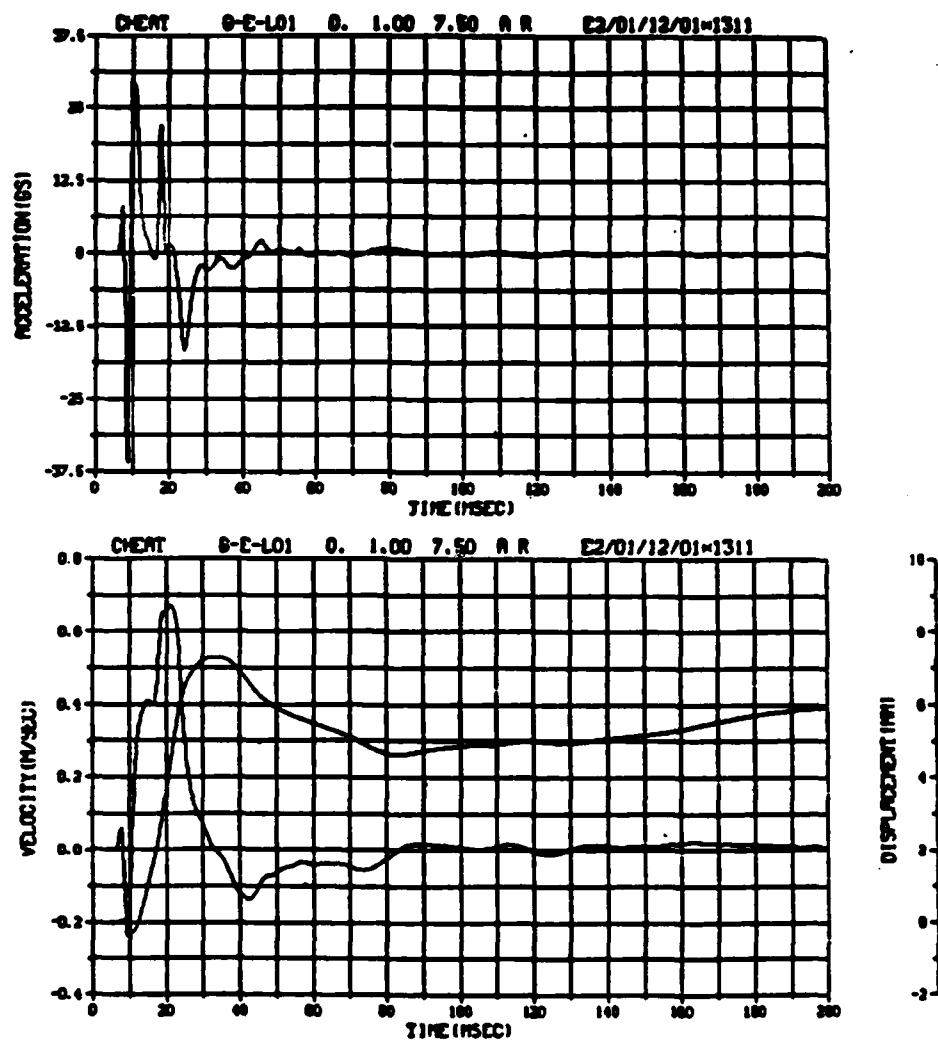


Figure 5

CHEAT SPALL RECORDS $r=1m$

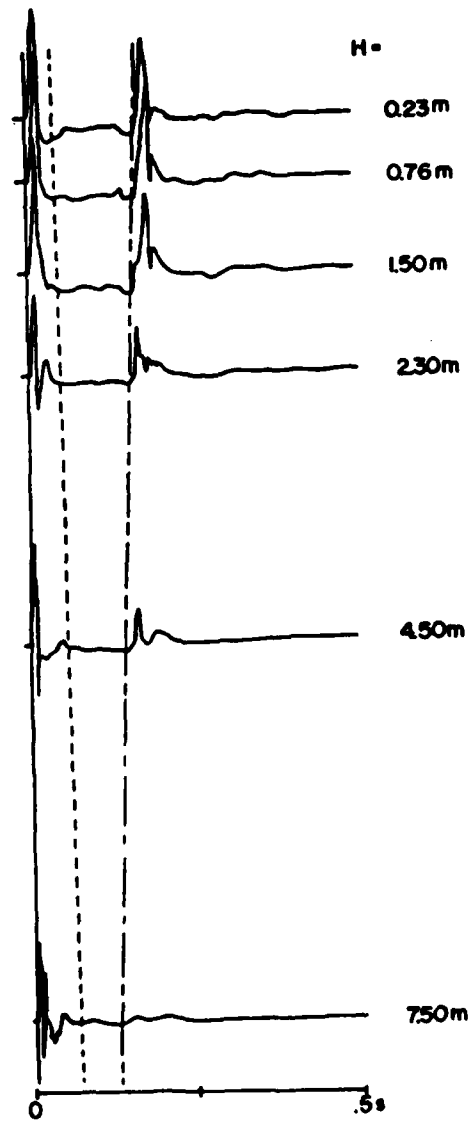


Figure 6

CHEAT CLOSE IN 1m radius, .23m depth

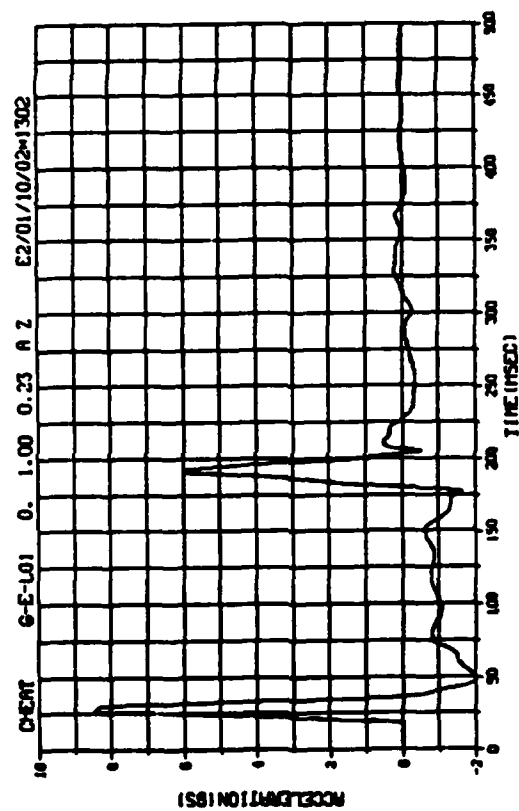


Figure 7

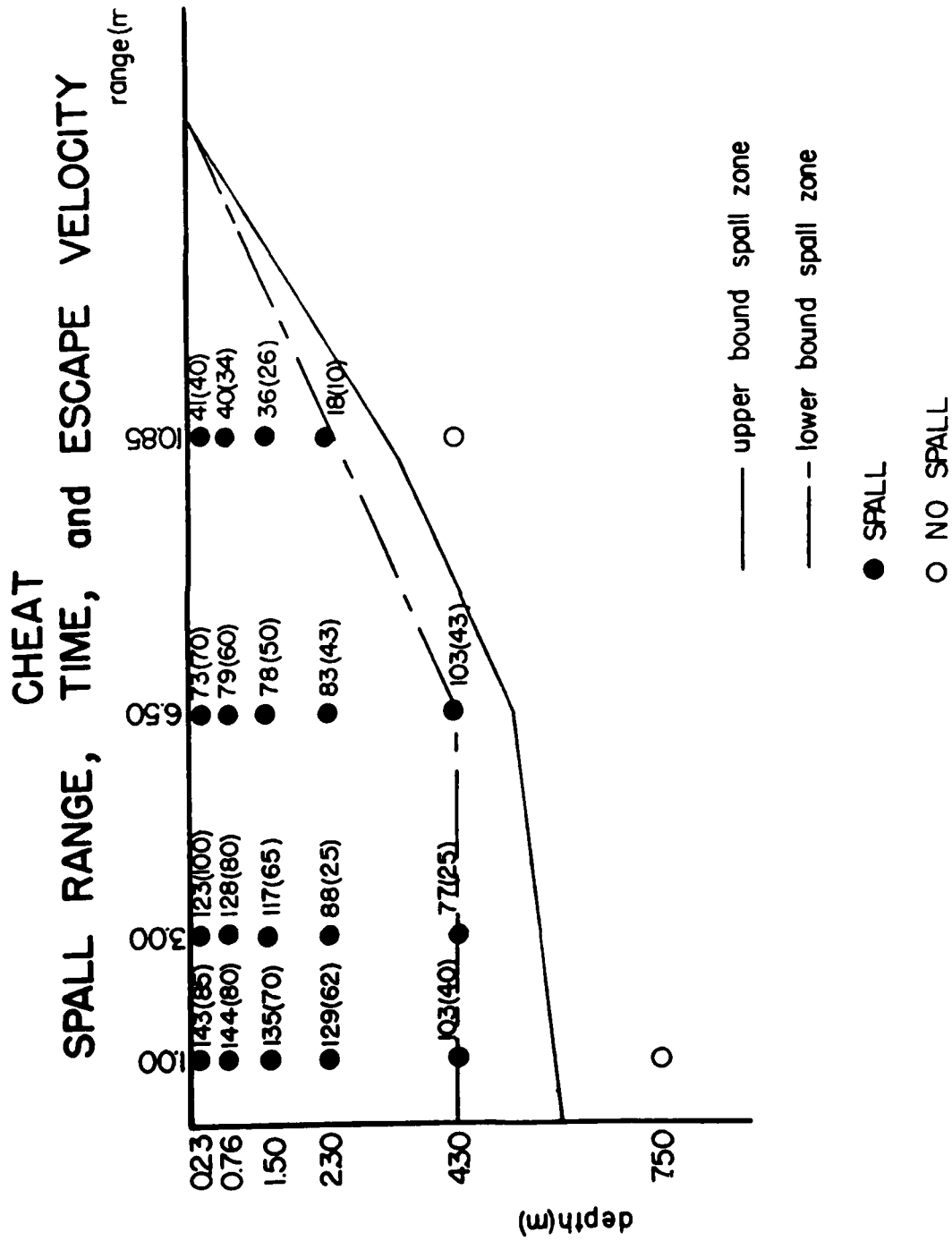


Figure 8

SPALL SYMMETRY
 $r=30m$ $h=0.23m$

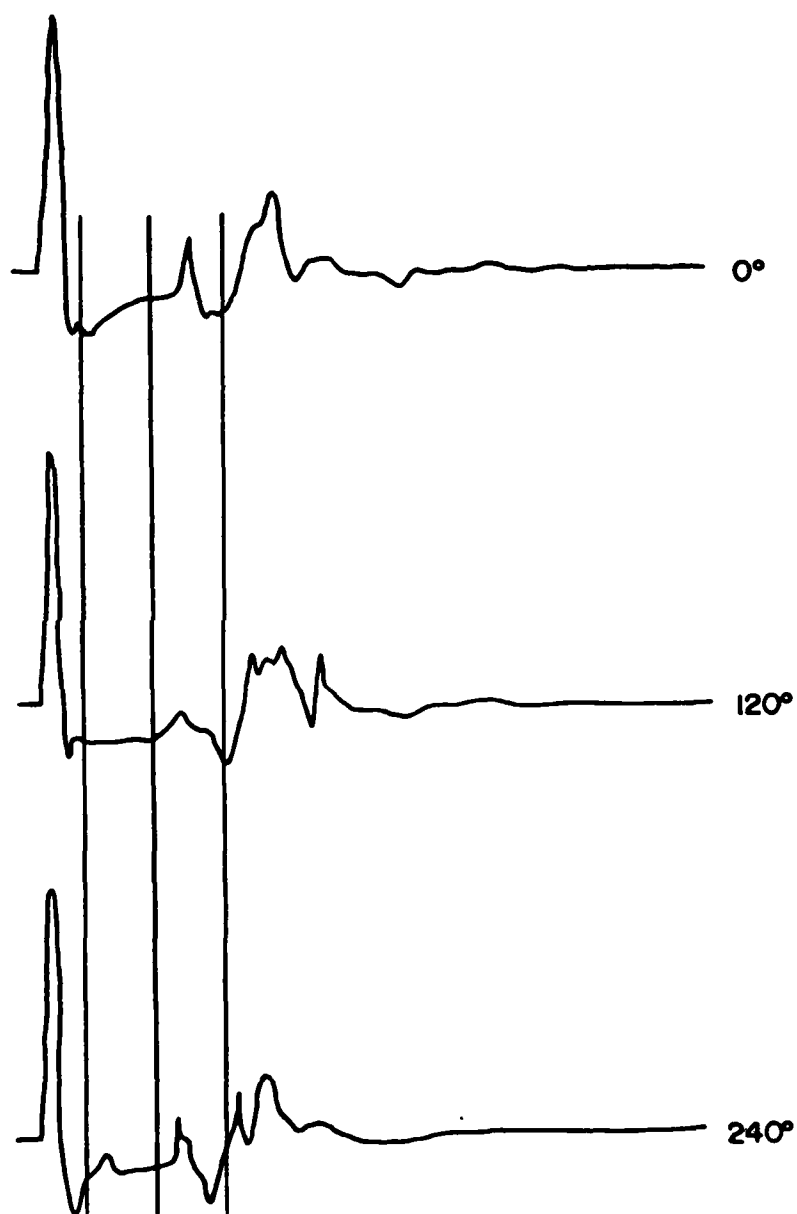


Figure 9

CHEAT 1m range

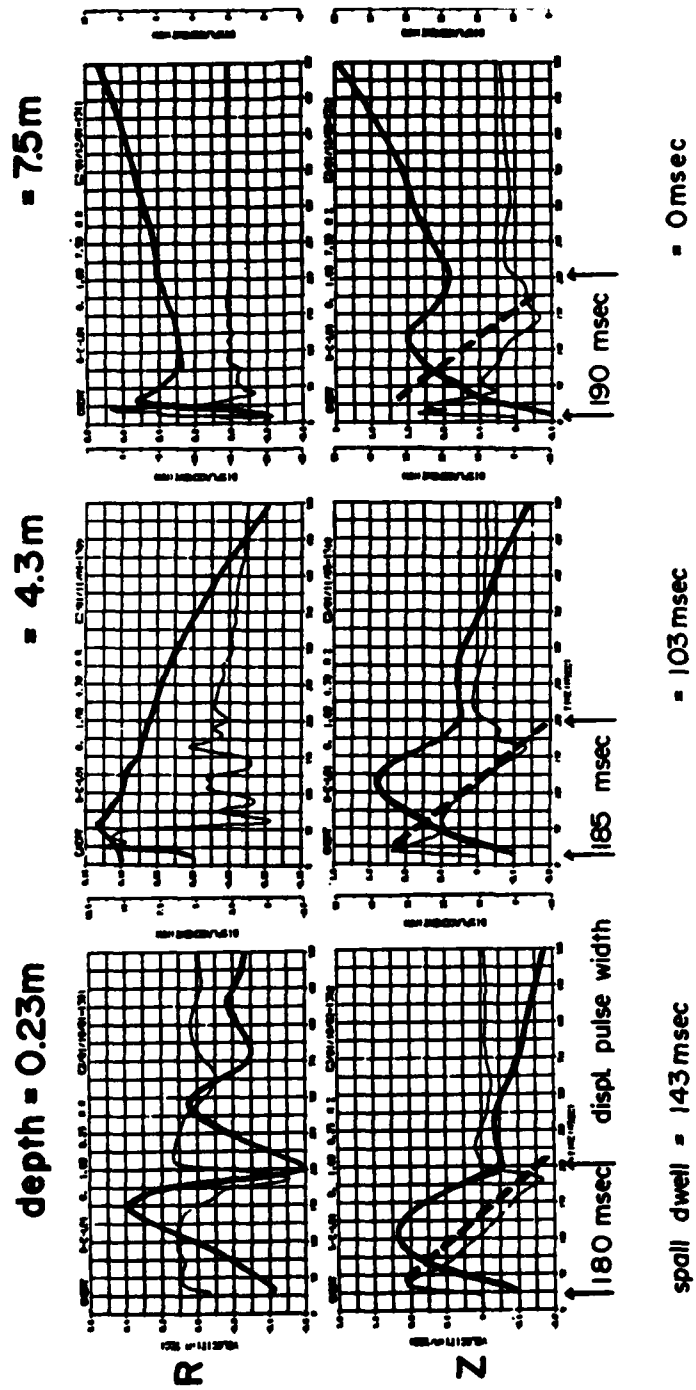


Figure 10a

CHEAT 3m range

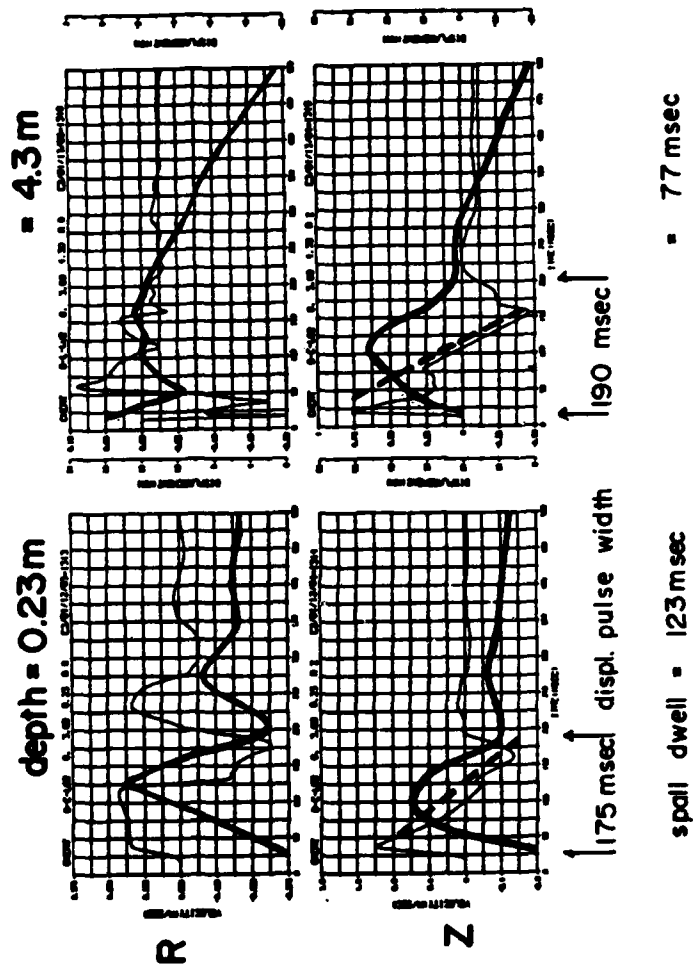


Figure 10b

CHEAT 6.5m range

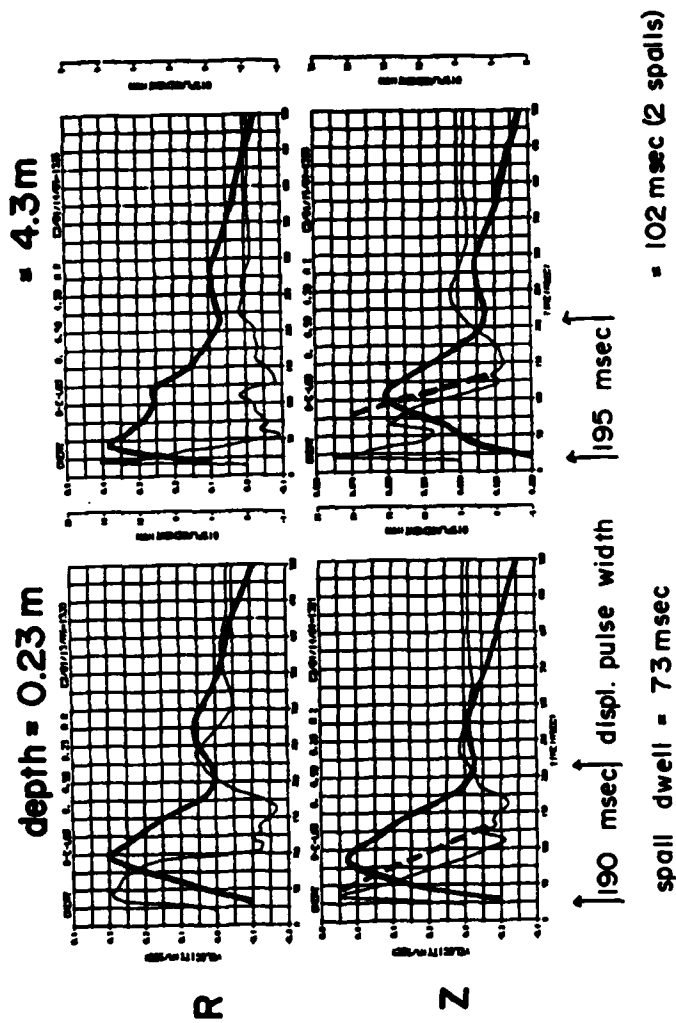
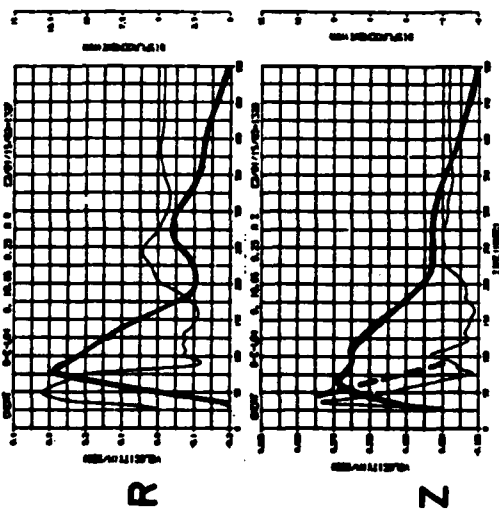


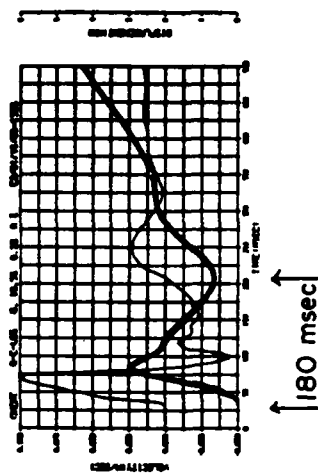
Figure 10c

CHEAT 10.85 m range

depth = 0.23m



1835m range
depth = 0.23m



spill dwell = 41msec

= 0 msec

Figure 10d

PULSE GROWTH IN THE NONLINEAR REGIME (VELOCITY)

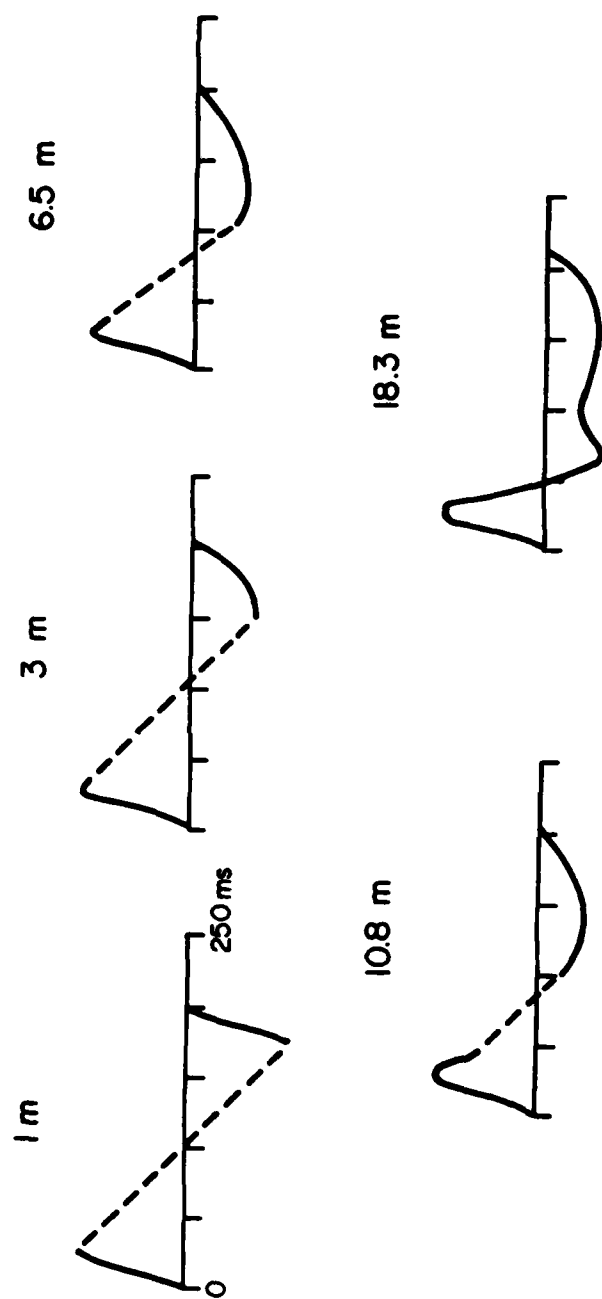


Figure 11

CHEAT 50m ACCELERATION

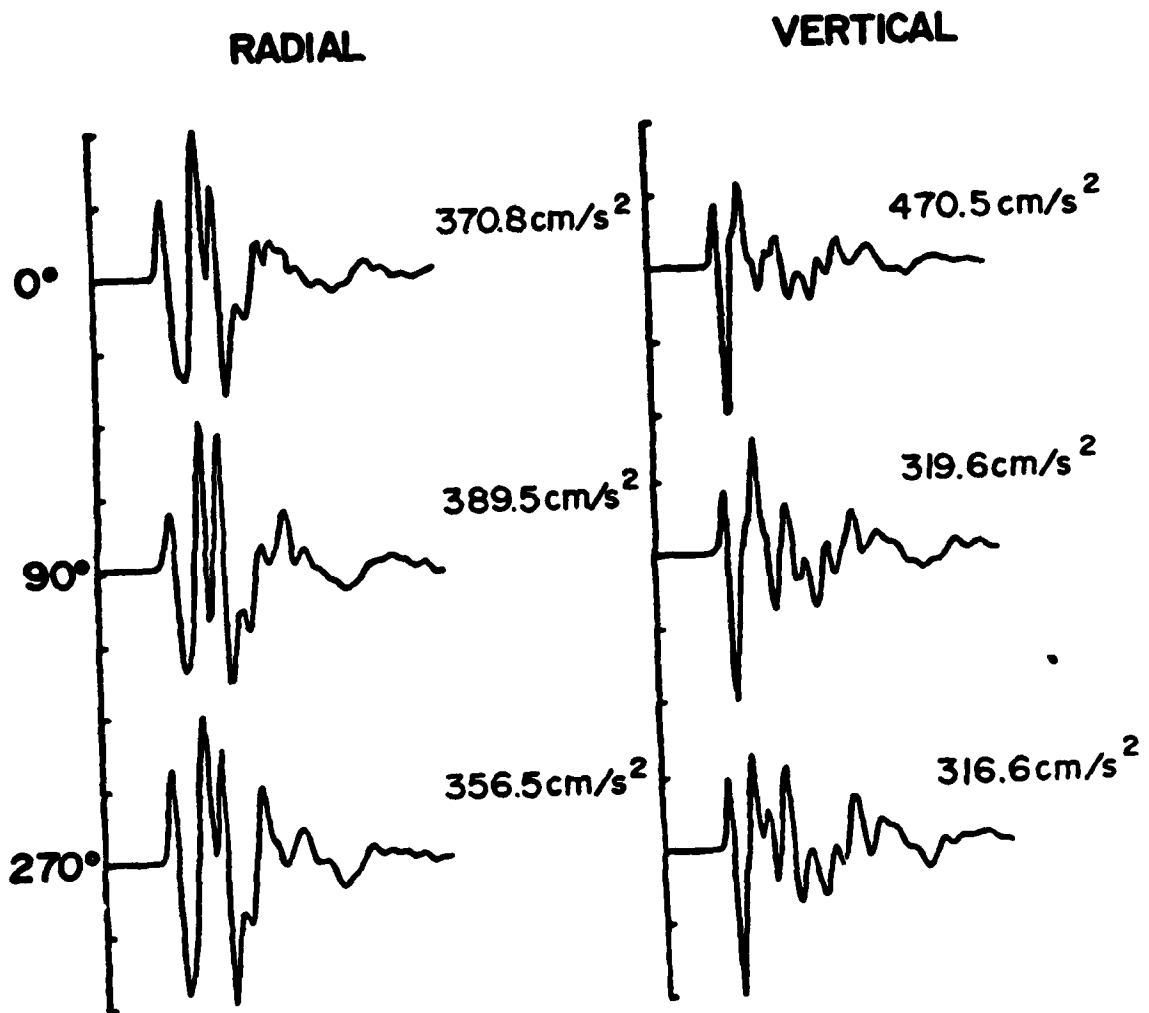
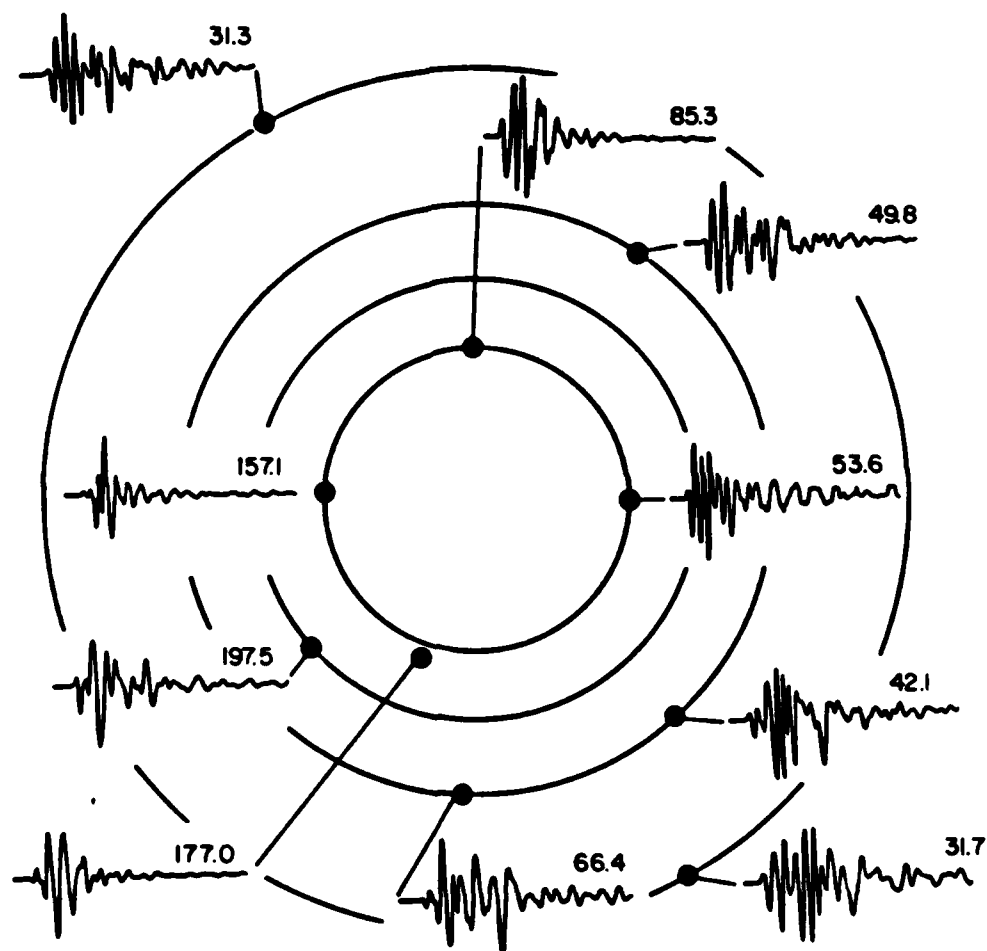


Figure 12

CHEAT TRANSVERSE



all angles are 2

Figure 13

CHEAT RECORDS

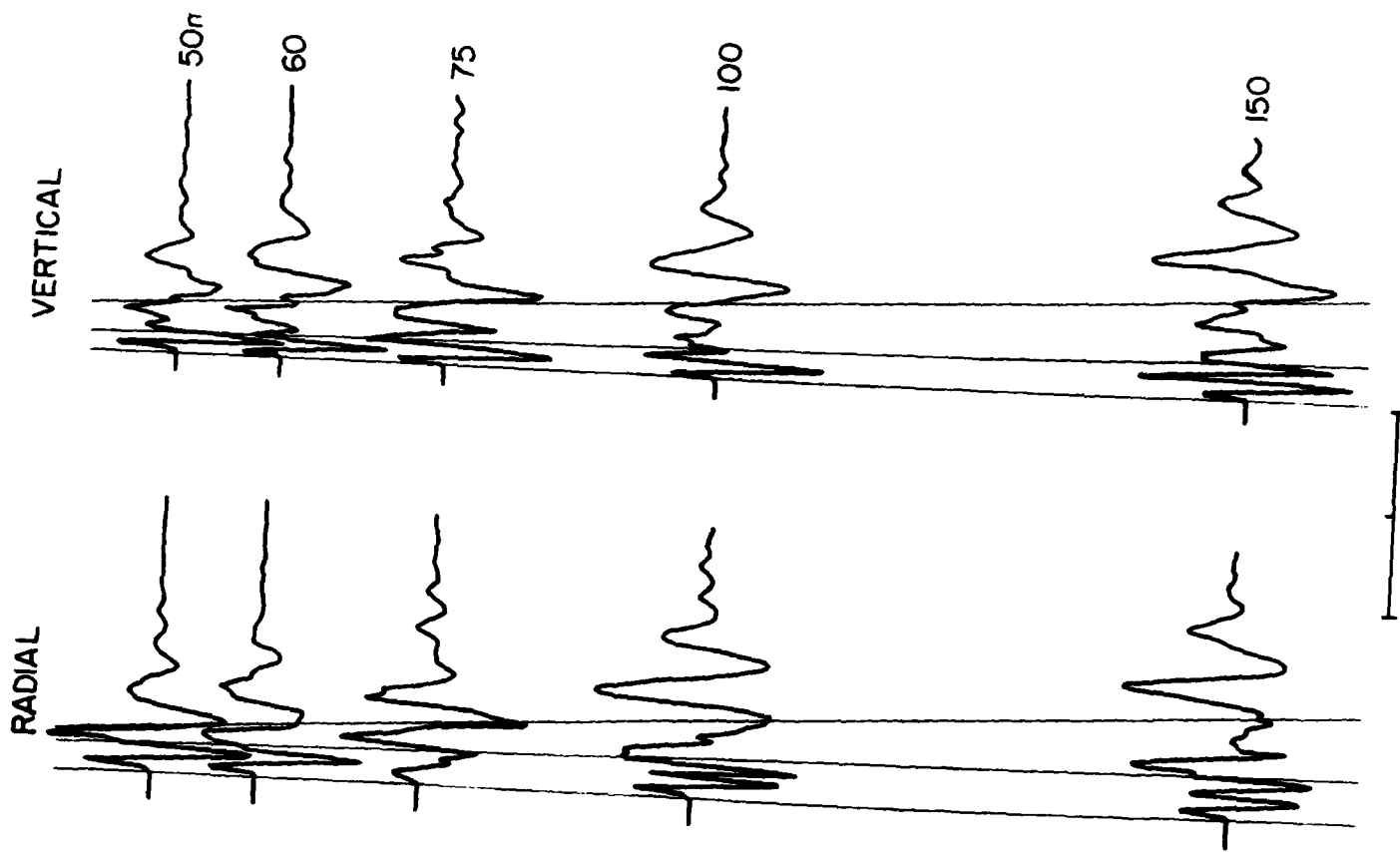


Figure 14

CHEAT R8
SPECTRUM

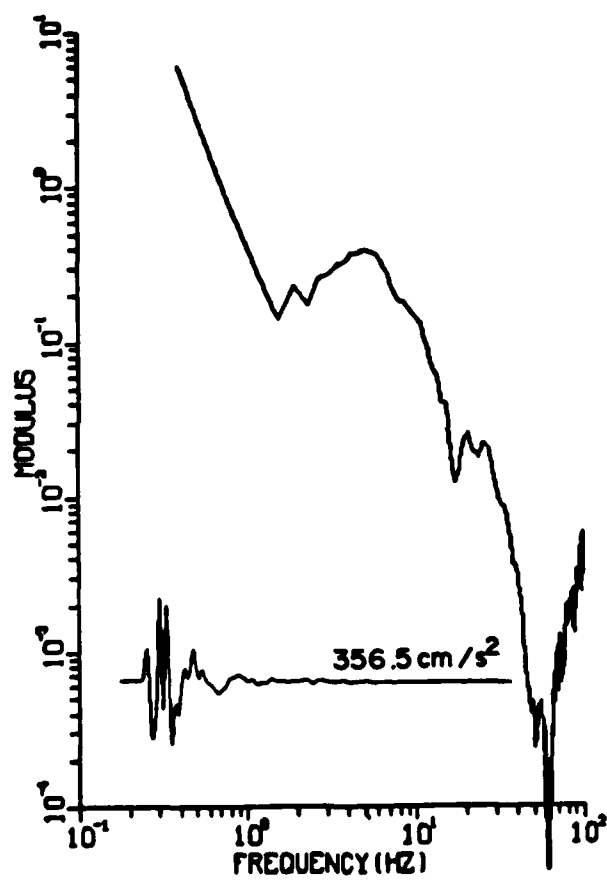


Figure 15

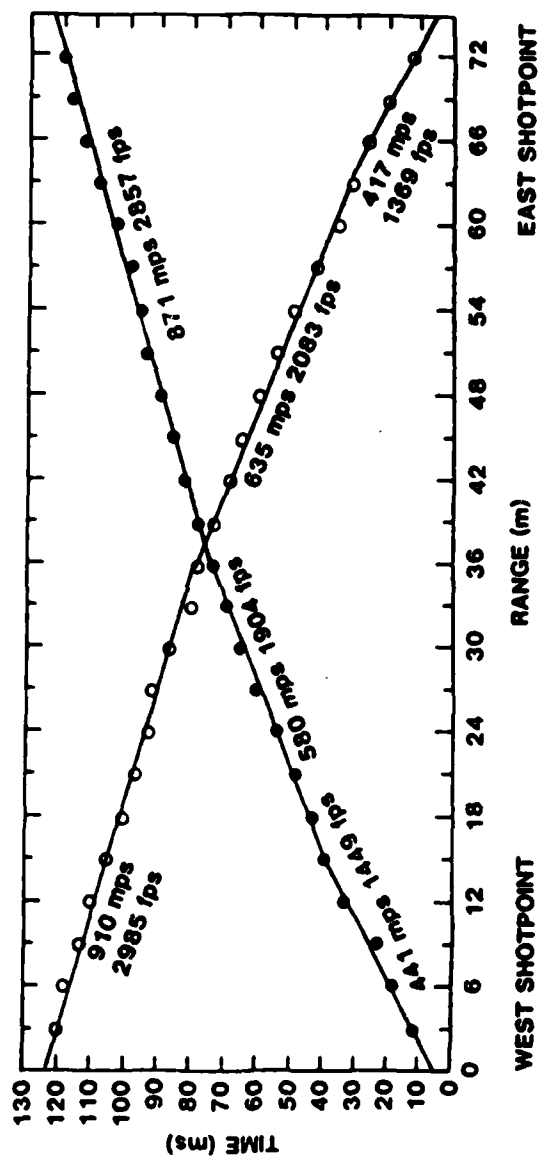


Figure 16a

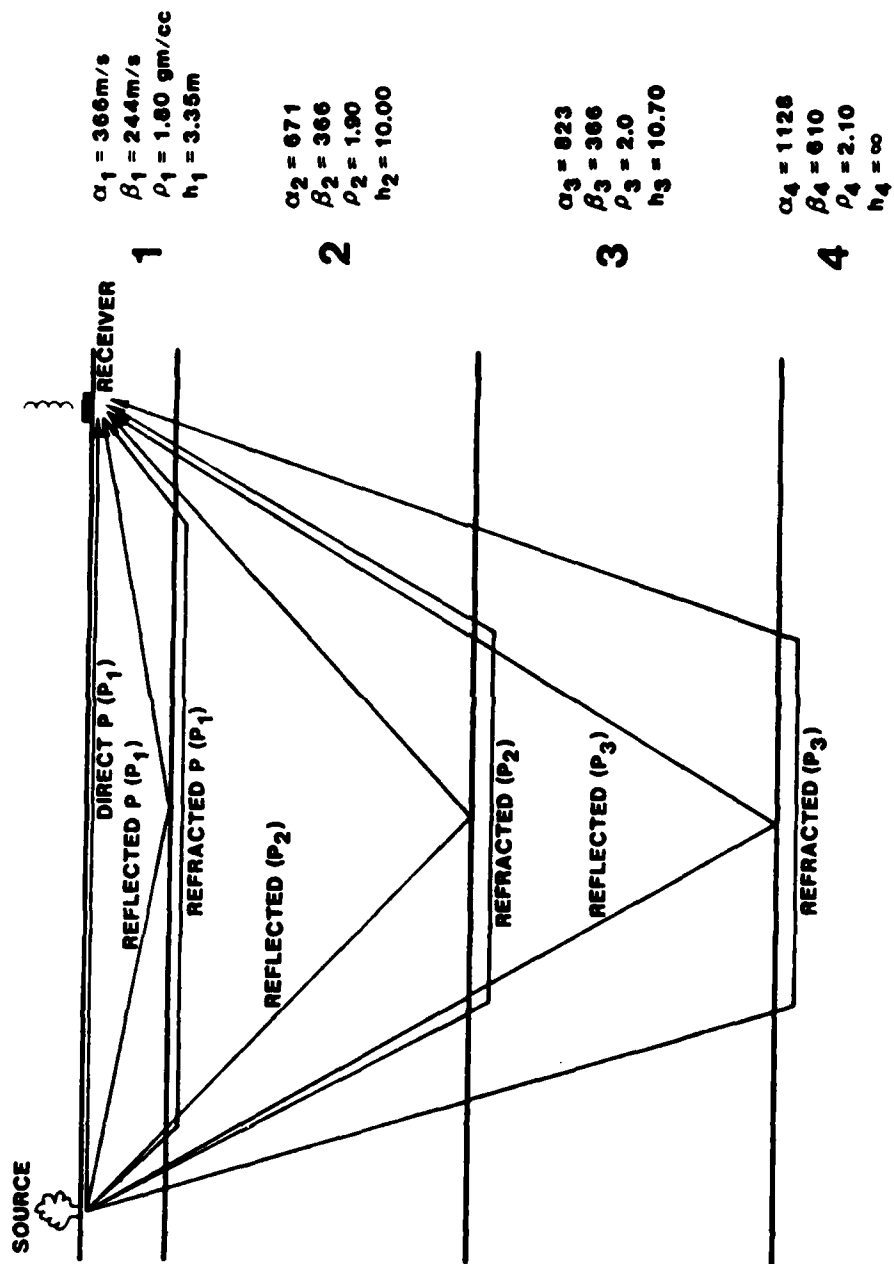


Figure 16b

CHEAT LAYERED VELOCITY MODEL

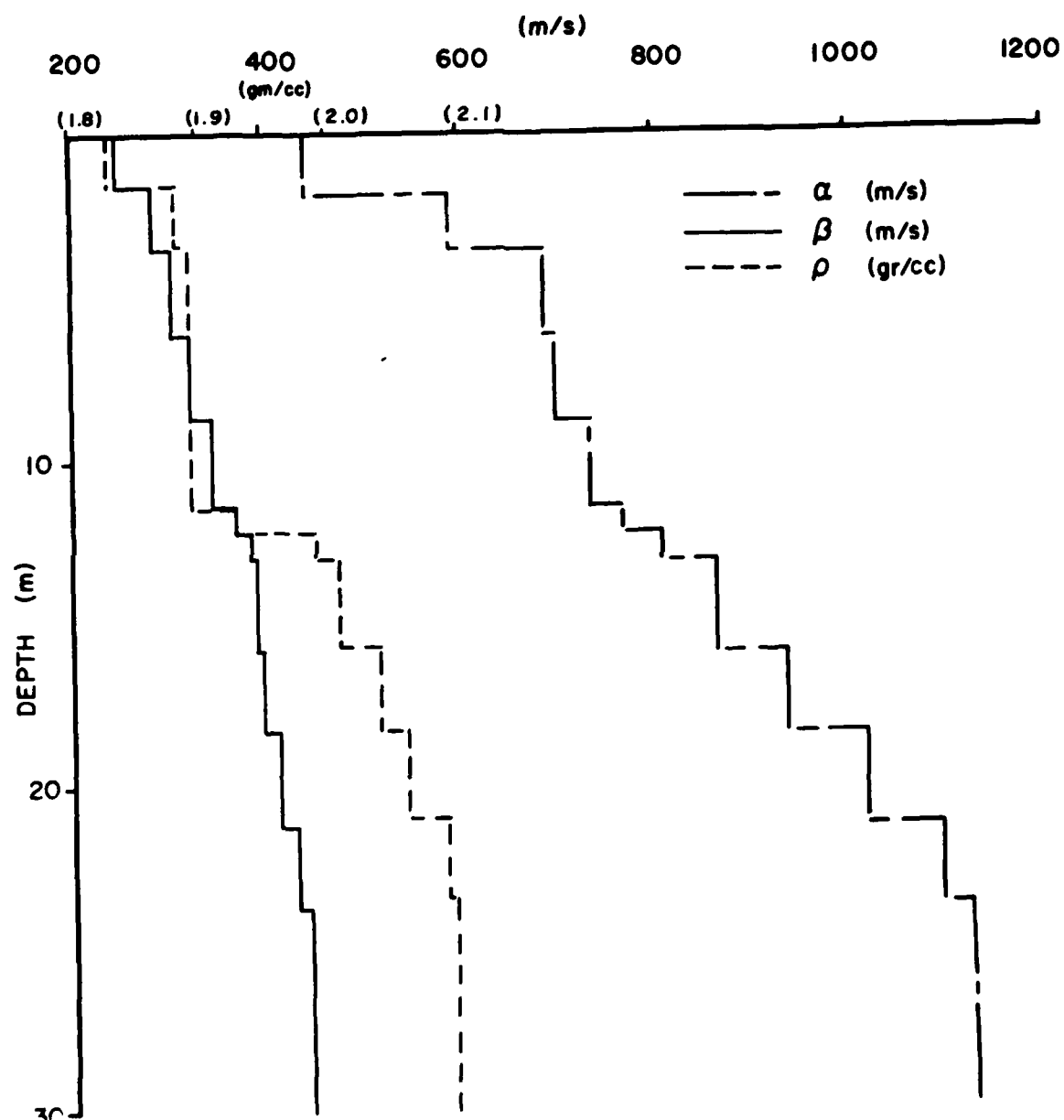


Figure 17

REFLECTIVITY MODEL

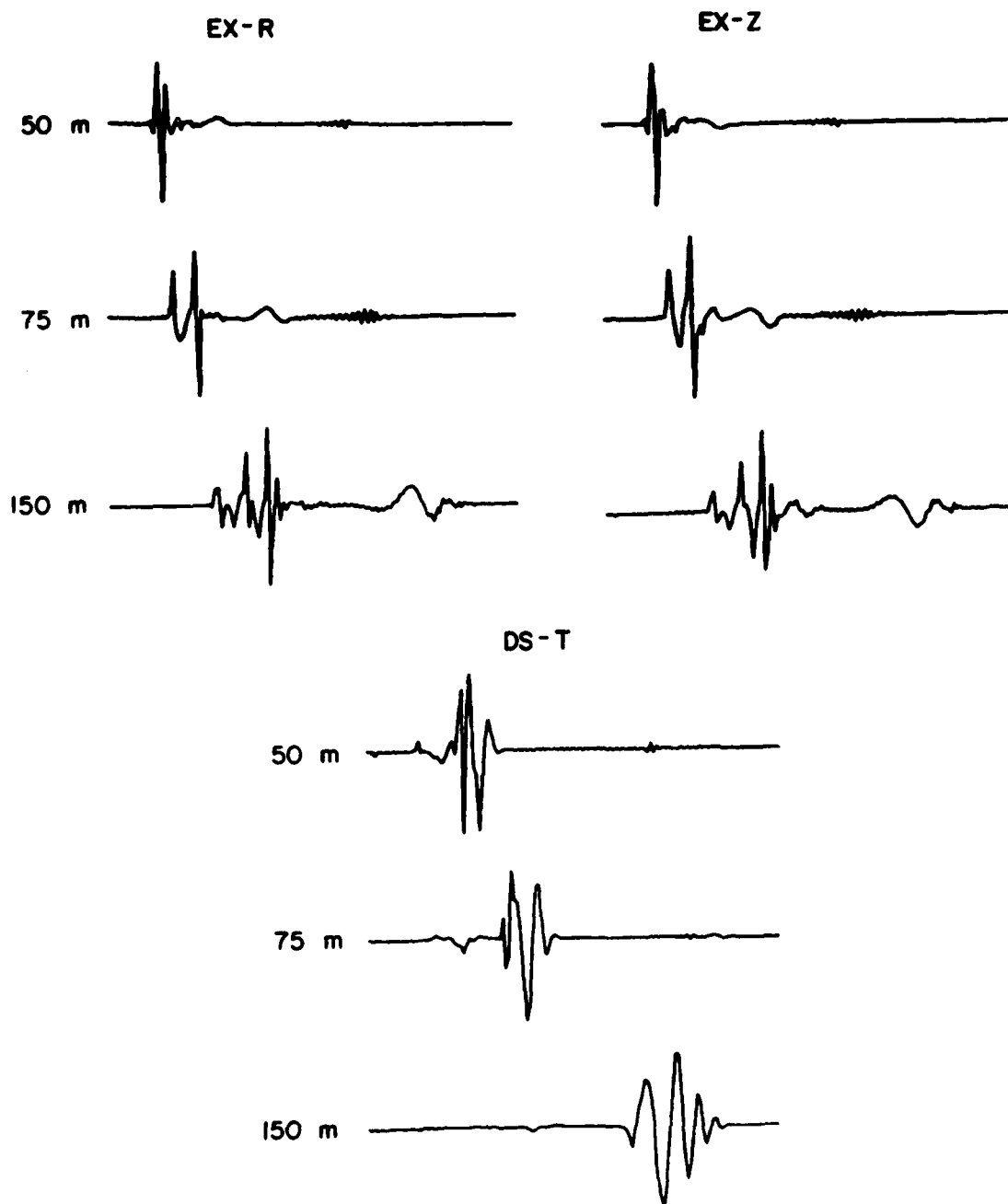


Figure 18

CHEAT FITS STATION 3

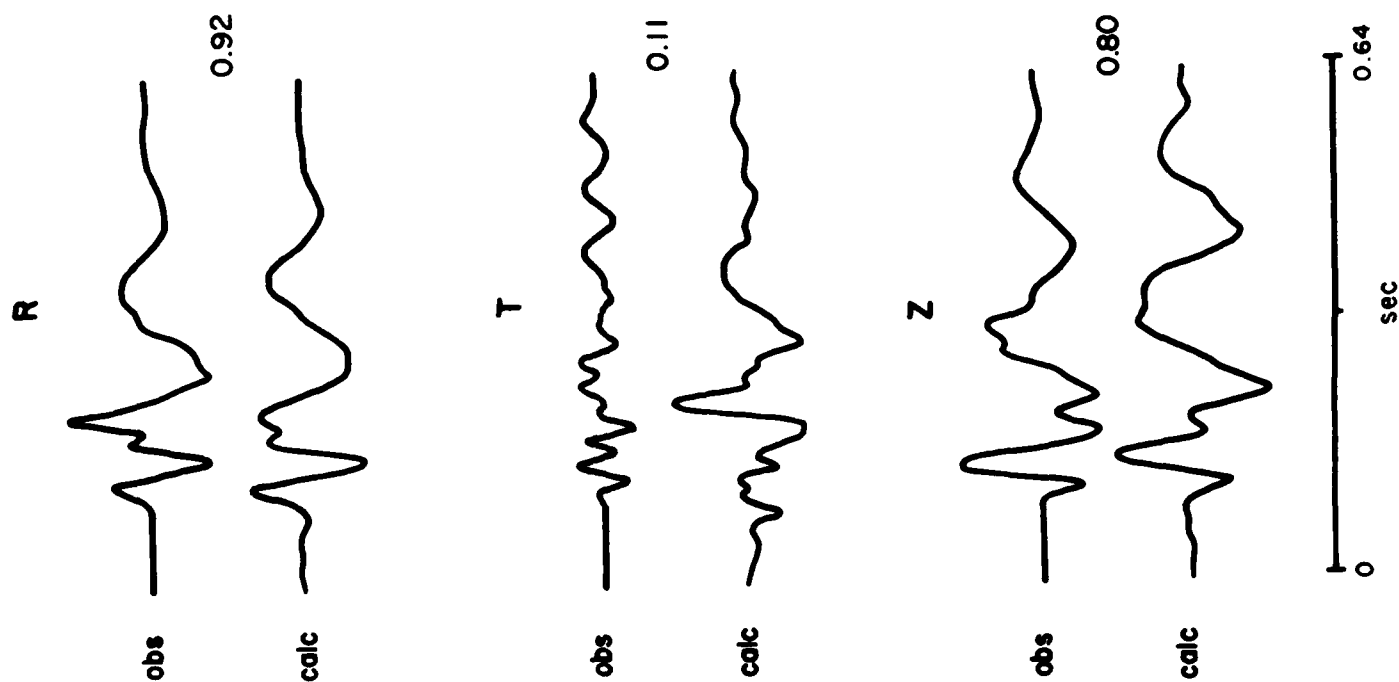


Figure 19

ISOTROPIC MOMENT TENSORS

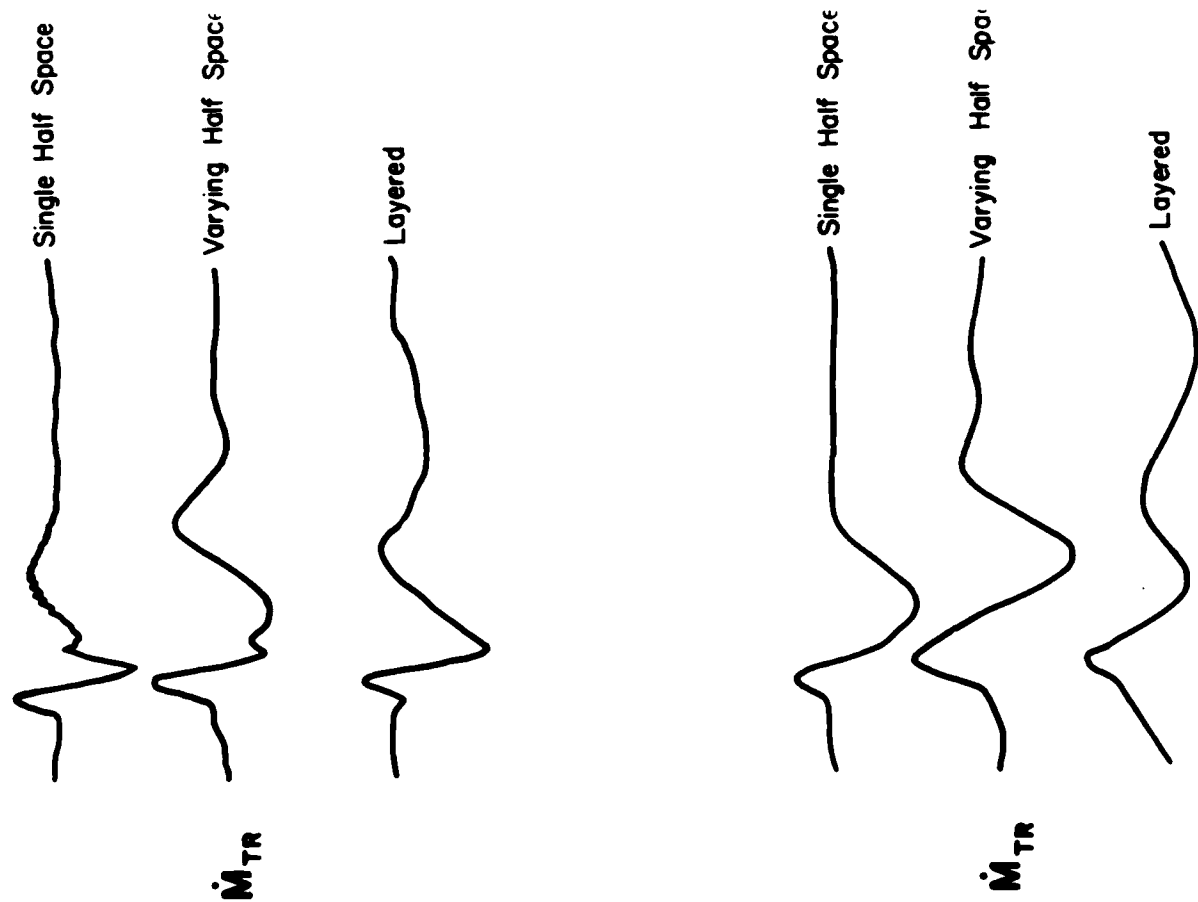


Figure 20

CHEAT $M_{rr}(all)$
SPECTRUM

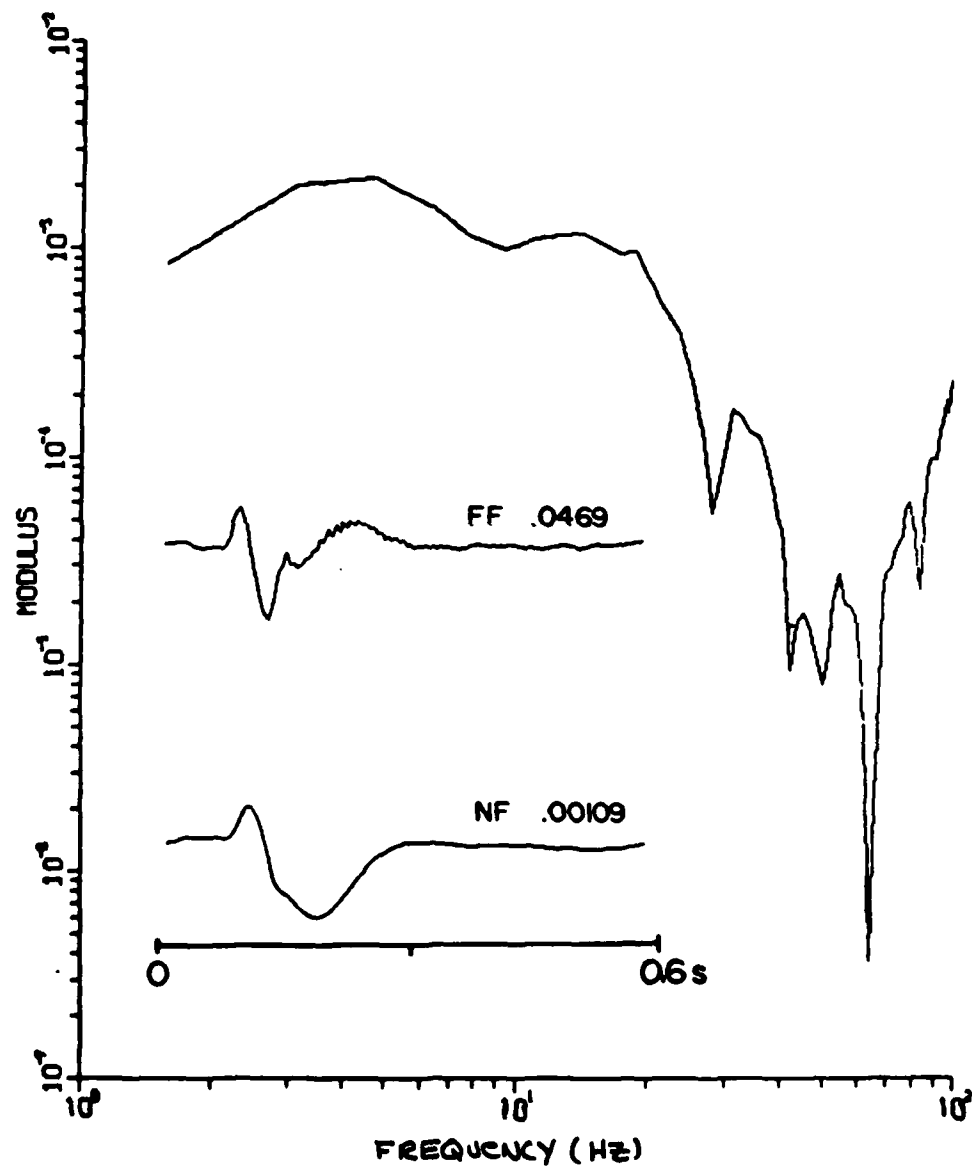


Figure 21

ISOTROPIC SOURCE AND NEAR SOURCE VELOCITY COMPARISON

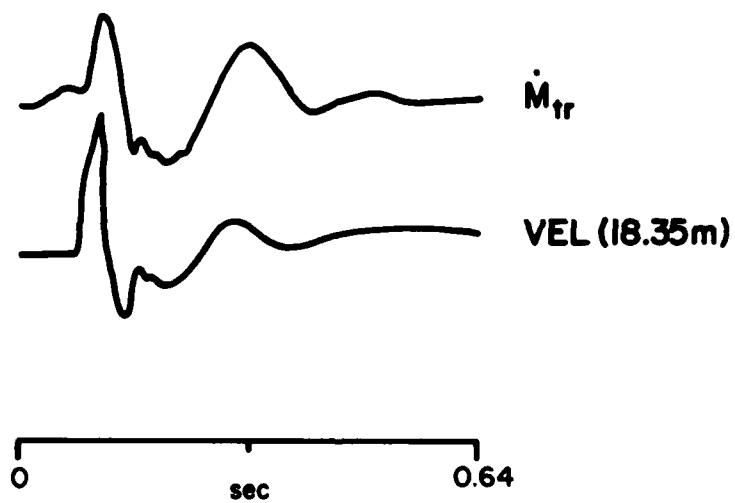


Figure 22

FAR-FIELD MOMENT TENSORS

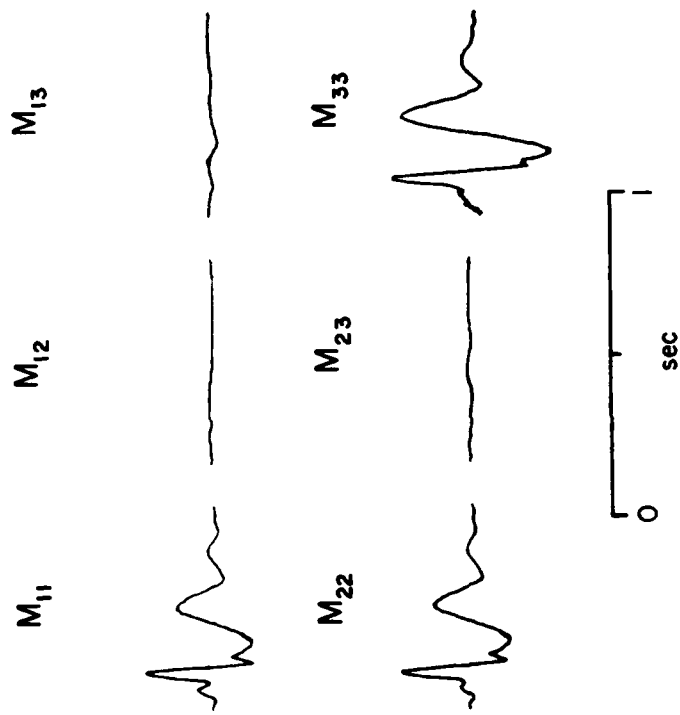


Figure 23a

NEAR-FIELD MOMENT TENSORS

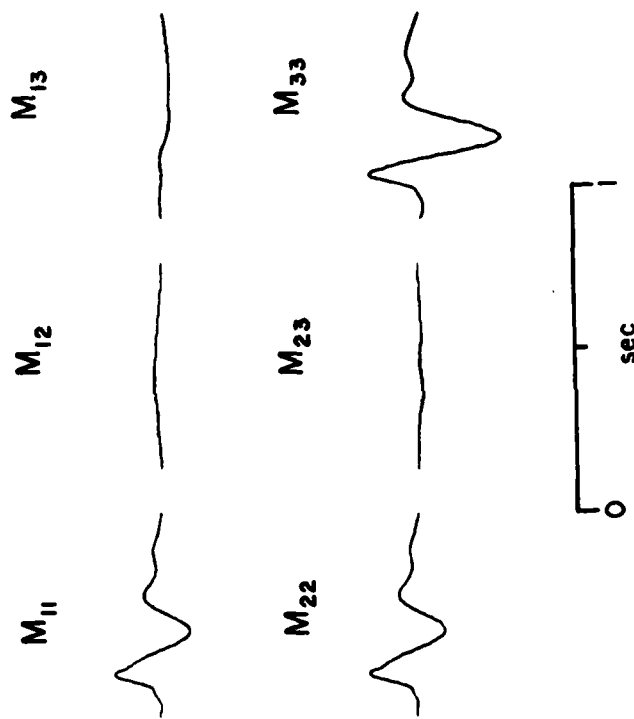
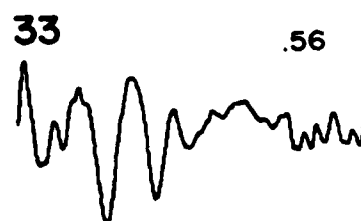
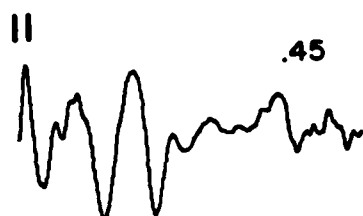


Figure 23b

FARM

M



TR

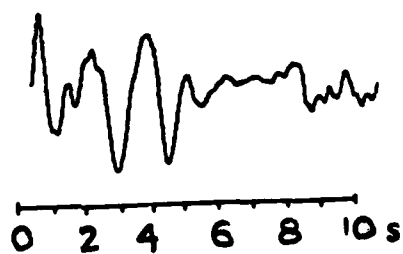


Figure 24

END

FILMED

4-85

DTIC